NASA CONTRACTOR REPORT

NASA CR-2278

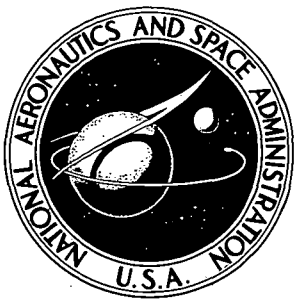

NASA CR-2278

EUTECTIC SUPERALLOYS STRENGTHENED BY δ, Ni_3Cb LAMELLAE AND γ', Ni_3Al PRECIPITATES

by F. D. Lemkey

Prepared by
UNITED AIRCRAFT RESEARCH LABORATORIES
East Hartford, Conn. 06118
for Lewis Research Center

NATIONAL AERONAUTICS AND SPACE ADMINISTRATION • WASHINGTON, D. C. • NOVEMBER 1973

1. Report No.	2. Government Accession No.	3. Recipient's Catalog No.
NASA CR-2278		

4. Title and Subtitle	5. Report Date
EUTECTIC SUPERALLOYS STRENGTHENED BY δ, Ni_3Cb LAMELLAE AND γ', Ni_3Al PRECIPITATES	November 1973
	6. Performing Organization Code

7. Author(s)	8. Performing Organization Report No.
F. D. Lemkey	M911213-15
	10. Work Unit No.

9. Performing Organization Name and Address	11. Contract or Grant No.
United Aircraft Research Laboratories 400 Main Street East Hartford, Connecticut 06118	NAS 3-15562
	13. Type of Report and Period Covered
12. Sponsoring Agency Name and Address	Contractor Report
National Aeronautics and Space Administration Washington, D.C. 20546	14. Sponsoring Agency Code

15. Supplementary Notes

Project Manager, Fredric H. Harf, Materials and Structures Division, NASA Lewis Research Center, Cleveland, Ohio

16. Abstract

By means of a screening and solidification optimization study of certain alloys located on the γ-δ liquidus surface within the Ni-Cb-Cr-Al system, alloys with high temperature properties superior to those of all known superalloys were defined. One alloy, Ni - 19.7 w/o Cb - 6.0 w/o Cr - 2.5 w/o Al, directionally solidified at 3 cm/hr met or exceeded each program goal. A second alloy, Ni - 21.75 w/o Cb - 2.55 w/o Al, although deficient in its inherent oxidation resistance, met the other program goals and combined a remarkable insensitivity of composite microstructure to solidification parameters with excellent low temperature toughness. This investigation demonstrated that useful properties for gas turbine airfoil application have been achieved by reinforcing a strong and tough gamma solid solution matrix containing precipitated gamma prime by a lamellar intermetallic compound Ni_3Cb having greater strength at elevated temperature.

17. Key Words (Suggested by Author(s))	18. Distribution Statement
Eutectics Superalloys Solidification Phase	Unclassified - unlimited

19. Security Classif. (of this report)	20. Security Classif. (of this page)	21. No. of Pages	22. Price*
Unclassified	Unclassified	136	Domestic, $4.50 Foreign, $7.00

* For sale by the National Technical Information Service, Springfield, Virginia 22151

TABLE OF CONTENTS

TABLE OF CONTENTS (Cont'd)

LIST OF TABLES

LIST OF TABLES (Cont'd)

LIST OF ILLUSTRATIONS

LIST OF ILLUSTRATIONS (Cont'd)

LIST OF ILLUSTRATIONS (Cont'd)

LIST OF ILLUSTRATIONS (Cont'd)

LIST OF ILLUSTRATIONS (Cont'd)

SUMMARY

The purpose of this program was to define, by means of alloy screening and iterative optimization, superior high temperature materials with potential for use in advanced gas turbine engines. These new materials were expected to maintain useful high temperature properties above 1200°C (2200°F) and exceed those of available superalloys above 700°C (1300°F). An inherent phase stability and resistance to deterioration under thermal cycling and oxidizing conditions were further required.

Within the quaternary system Ni-Cb-Cr-Al numerous thermodynamically monovariant and bivariant eutectic alloys, located on the γ, nickel solid solution - δ, Ni_3Cb liquidus surface, were identified which permitted the growth of aligned lamellar γ/γ'-δ *in situ* composites. The microstructural and chemical homogeneity of certain γ/γ'-δ alloys were found to be remarkably uniform after directional solidification. After systematic screening, two of the more promising alloys which contained γ', Ni_3Al, precipitates were evaluated in greater detail in a program of tensile, impact, thermal fatigue, and oxidation testing.

One γ/γ'-δ alloy, Ni - 19.7 w/o Cb - 6.0 w/o Cr - 2.5 w/o Al, with a specific gravity of 8.5 was evaluated after directional solidification at a velocity, R, equal to 3 cm/hr and a thermal gradient in the melt, G, of ~300°C/cm. The longitudinal tensile ductility of this alloy measured by elongation and reduction in area met or exceeded five percent over the temperature interval 20-1235°C. Its tensile strength exceeded the strengths of all known superalloys above 815°C and at 1235°C was 210 MN/m^2 (30,000 psi) which exceeded the program goal by 90 MN/m^2 (13,000 psi). Furthermore, its rupture strength surpassed those of advanced nickel superalloys, e.g. NASA-TRW VIA and D.S. MarM200, in the temperature range of 700 to 1200°C. Phase stability and resistance to thermal fatigue cracking and delamination were observed after 3000 thermal exposures between 400°C min/1120°C max in 2.1 minute cycles. Lastly, the oxidation kinetics of this γ/γ'-δ alloy were similar to a Ni - 30 w/o Cr - 2 w/o Al alloy where the rate of oxidation was observed to be controlled by the growth of an external Cr_2O_3 scale.

A second alloy, Ni - 21.75 w/o Cb - 2.55 w/o Al, although deficient in its inherent oxidation resistance, met or exceeded the other program goals and combined a remarkable insensitivity of composite microstructure to solidification parameters (i.e. critical $G/R < 5°C\ hr\ cm^{-2}$) with outstanding low temperature toughness (i.e. notched Charpy energies over twice that of cast superalloys).

This investigation demonstrated that useful properties for gas turbine airfoil application have been achieved by reinforcing a strong and tough gamma solid solution matrix containing precipitated gamma prime by a lamellar intermetallic compound Ni_3Cb having greater strength at elevated temperature. Further improvements in creep and shear strengths are anticipated by quinary additions and heat treatment.

I. INTRODUCTION

The need for better high temperature materials is particularly acute in gas turbines for advanced aircraft. This need results from the significant engine performance advantages which are accomplished by higher turbine inlet temperatures. By increasing the temperature, designers effect a reduction in specific fuel consumption and an increase in thrust per unit weight. In terms of aircraft, these performance advantages might be translated into an air superiority fighter where a lighter, more efficient engine may result in a smaller aircraft with an increased performance capability; into a supersonic transport where a reduced engine weight may represent a large increase in payload; or into a subsonic transport where improved fuel consumption may permit more heavily loaded, long-range operation.

The requirement for better high temperature materials is not only a problem that is to be faced in the coming years but is also today's problem. Engine manufacturers are committed to providing engines with turbine inlet temperatures of at least 1316°C (2400°F) in the near future. Since materials are not available to withstand these temperatures, the first stages of the turbine must be air cooled. Bleeding air from the compressor to cool these parts penalizes the potential performance of the engine. Either reducing the amount of cooling air required or eliminating cooling in stages which were previously cooled is beneficial to the efficiency. Similarly, if simple cooling schemes can be employed, this is favorably reflected in the cost of turbine parts. Thus, increases in the capability of high temperature materials, which might allow these changes, are of considerable value.

Almost all turbine vanes and blades in aircraft engines have and, during the next ten years, will continue to be made of alloys of nickel and cobalt. There is a move directed toward the eventual introduction of more refractory materials in the first turbine stages since such materials would potentially accomplish gains in engine performance that cannot be made with the lower melting alloys. Even if these materials are successfully applied, the nickel and cobalt alloys will still be widely used - perhaps comprising an even larger percentage of the engine structure than in present engines.

In recognition of the current and anticipated requirements for superior high temperature materials, the Materials Laboratory of UARL has directed a substantial research effort in the establishment and evaluation of a technology for producing phase-reinforced nickel and cobalt alloys. From this effort several paths to a new class of materials termed 'Eutectic Superalloys' have been identified. These include *in situ* reinforcement of a nickel or cobalt alloy matrix by either an aligned ductile, semiductile or brittle reinforcing phase. Both lamellar and whisker-like micromorphologies have been evaluated and those systems strengthened by Ni_3Cb lamellae (Refs. 1-4) and by whiskers of MC (Refs. 5-7) or M_7C_3 (Refs. 8-10) type carbides have demonstrated that materials with superior mechanical properties can indeed be developed.

In order to justify and appreciate the suggested procedure of developing high temperature turbine materials by the directional solidification of eutectic alloys, it is appropriate to consider other routes which are being followed or advocated. Aside from the more usual alloy development efforts, a significant approach directed toward improving nickel-based superalloys has been directional solidification to form columnar or single grains. This process was pioneered by P&WA™ and the resulting benefits are considered in recent reviews (Refs. 11,12). Since strengthening remains basically γ' precipitation induced, the materials are limited, however, in temperature capability because of resolutioning of γ'. For example, above 1038°C (1900°F) directionally solidified Mar M-200 is not appreciably stronger than the alloy conventionally cast. Therefore, despite its usefulness, the directionally solidified superalloy approach does not completely satisfy future demands.

By using another strengthening mechanism, that of dispersion hardening by small inert particles such as thoria, a class of materials has been constructed which are potentially important, i.e. TD-Ni-Cr and TD-Co-Cr. These materials have high melting temperatures and may have excellent high temperature strength and static oxidation resistance. To date, both variability in the properties and relatively low strength at intermediate temperatures have limited their usefulness.

The composite approach where high strength fibers are added to a ductile matrix is still another method which has been suggested and used for strengthening nickel, cobalt and columbium alloys. In these artificially constructed materials, deleterious reactions between the reinforcing phase and the matrix during fabrication or subsequent cyclic exposure at elevated temperature is a general and difficult to solve problem. Perhaps the most fully developed systems of this type are the tungsten wire reinforced nickel alloy composites (Ref. 13). Despite the chemical degradation that occurs, these composites have displayed 1093°C (2000°F) creep-rupture properties superior to nickel alloys. Since the reactivity is primarily temperature dependent, higher temperature hastens the degradation. Because of thermodynamic stability considerations, oxides are likely reinforcing candidates for nickel, cobalt and columbium. In the case of alumina fibers in nickel, reaction does occur however (Ref. 14). In columbium containing titanium, reaction is also observed although alumina appears stable in pure columbium at 1204°C (2200°F) (Ref. 15). Although there are many problems anticipated in the composite approach to satisfying high temperature material requirements, it remains an important area for future research.

In comparison with the previously described techniques for obtaining superior high temperature materials, the directionally solidified eutectic approach offers numerous advantages and some disadvantages. Characteristics of eutectics are treated more fully elsewhere and are considered briefly here for comparison. Since these in situ composite structures are generated as a result of an equilibrium reaction, the phases produced are chemically stable with respect to one another. Furthermore, experience has shown that the low energy interfaces, established during the growth,

result in a microstructure with exceptional stability which resists coarsening and spheroidization. Mechanically, as a first approximation, the behavior of these materials can be treated as normal composites. Recently it has been shown, however, that interphase spacing has an important effect on strength. Reducing this spacing, which is accomplished by growing the material at a faster rate, has strengthened the material according to a Hall-Petch relation (Ref. 3). Thus, not only is processing benefited by rate increases but also properties. Included in the disadvantages in the eutectic approach are anisotropic properties (as with other composites), a general inability to vary, randomly, the volume fraction of the phases, and some lack of freedom in selection of interesting systems. These last two disadvantages occur because eutectic or eutectic-like compositions where two or more phases crystallize simultaneously from the melt have been considered. Even within these limitations there are countless alloys which can be selected when one considers ternary and higher order systems for study and development.

The purpose of this investigation was the characterization and optimization of the properties of monovariant and bivariant alloys within the quaternary system Ni-Cb-Cr-Al which permit the production of aligned δ, Ni_3Cb lamellae within a γ, 'nichrome' matrix which contain precipitates of γ', Ni_3Al. These alloys have been identified as being potentially important for application in near-term engines (Ref. 16). From a systematic screening of a number of alloys and the more thorough evaluation of the properties of two alloys selected by the screening experiments, a superior high temperature material was envisioned.

The specific goals of the program were:

- A tensile strength of 120 MN/m^2 (17,000 psi) at 1235°C (2255°F).
- A specific gravity of less than 9.0 (equivalent density 0.325 $lb/in.^3$).
- Rupture strength substantially exceeding that of advanced nickel base superalloys at all temperatures above 700°C (1290°F).
- Ductility, as measured by elongation and reduction in area in tensile tests, of at least 5 percent over the entire temperature range from room temperature to 1235°C (2255°F).
- Phase stability and resistance to thermal fatigue cracking and delamination under conditions of thermal cycling and long exposures at elevated temperatures.
- An inherent resistance to oxidation and high temperature corrosion, although coating of these alloys is considered necessary for use above 900°C (1650°F).

Work was divided into two tasks. The first task included the determination of the directional solidification parameters of selected alloys and the screening by mechanical testing of specimens with acceptable microstructures. The second task included the more detailed evaluation of the mechanical properties of two combinations of alloy and conditions of directional solidification.

II. EXPERIMENTAL PROCEDURES

2.1 Melting and Solidification

Master melts of the various alloys investigated were made in new recrystallized alumina crucibles in a Heraeus vacuum induction melting furnace powered by a 30 kw motor generator and pumped by a 25.4 cm (10 in.) vacuum system. The system was exhausted to approximately 10^{-5} torr (0.001 N/m^2) and then back filled with high purity argon to provide a dynamic 200 liters per hr (~7 cfh) inert cover at atmospheric pressure. Power to the furnace coil was slowly increased until melting of the nickel, chromium and columbium charge material was achieved. Aluminum was then added separately to the melt. Subsequently the melt was held at a constant temperature of ~1400°C (2550°F) for a 15-20 min homogenization period prior to pouring into copper chill molds. The purity of the starting materials used is presented in Table Ia. Impurities detected by atomic absorption analysis by either UARL or the identified vendor are noted.

Each resulting cast alloy bar was usually directionally solidified vertically within a nominally 1.27 cm (1/2 in.) dia 99.7 percent recrystallized alumina cylindrical crucible whose wall thickness was nominally 2 mm. Directional solidification experiments were also performed to evaluate ZrO_2 and BeO as well as various grades and wall thicknesses of Al_2O_3 supplied by a variety of vendors. Vertical controlled solidification (upward moving liquid-solid interface) of the alloys under moderate thermal gradients was accomplished within a dynamic argon atmosphere in one of two identical graphite resistance furnaces. The alumina crucible, either open at both ends or closed at one end, containing the melt was supported on a movable water cooled pedestal as illustrated in Fig. 1. Crucible lowering rates were varied by means of a variable speed motor and a step function gear reducer from 1 to 20 cm/hr. The maximum melt temperatures were approximately 1650°C with the furnace control being accomplished automatically by a Milletron two color (ratio) optical pyrometer whose electronic servo loop monitors a saturable core reactor regulated 35 Kva power supply. The large thermal mass of these resistance furnaces provides the stability required for the linear movement of the liquid-solid interface.

Vertical controlled solidification was also accomplished in a high gradient apparatus described in Ref. 17. In this setup a known mass of alloy typically 200 gms, contained in a both ends open or one end closed cylindrical alumina crucible, is positioned within the induction coil, water spray ring, and constant water level tank as illustrated in Figs. 2,3. With the impinging water spray, melting is accomplished by inductively coupling with the stationary graphite sleeve. Power

Table Ia

Purity of Charge Elements in ppm

	Nickel[1]	Chromium Crystals[2]	Chromium Chunks[3]	Chromium Pellets[4]	Chromium H. P. Flake[5]	Columbium[6]	Aluminum[7]
Al	100	-	160	-	<2	<20	bal.
B	-	-	60	-	-	<1	-
C	-	6	<1000	-	10	35	-
Ca	-	-	-	-	-	<20	-
Cb	-	-	-	-	-	bal.	-
Cd	-	-	-	-	-	<5	-
Cl	-	10	-	-	-	-	-
Co	-	-	-	-	-	<10	-
Cr	-	bal.	bal.	bal.	-	<20	-
Cu	1	-	15	-	2	<40	-
Fe	200	10	1200	<1	<2	<50	2
H	-	-	-	-	<60	2.4	-
Hf	-	-	-	-	-	<50	-
Mg	10	-	-	-	-	<20	2
Mn	-	-	6	-	-	<20	-
Mo	-	-	-	-	-	<20	-
N	-	-	-	-	<30	33	-
Ni	bal.	-	-	-	-	<20	-
O	-	7	-	10	<600	<150	-
Pb	-	-	-	-	<2	<20	-
S	-	2	-	-	<30	-	-
Si	100	-	150	-	<10	<50	-
Sn	-	-	-	-	-	<10	-
Ta	-	-	-	-	-	<110	-
Ti	-	-	-	-	-	<40	-
V	-	-	150	-	-	<20	-
W	<100	-	-	-	-	43	-
Zn	-	2	-	-	-	-	-
Zr	-	-	-	-	-	<100	-

[1]United Mineral & Chemical Corp.
[2]Iodide
[3]Shieldalloy Corp.
[4]Electrolytic
[5]Shieldalloy Corp.
[6]Wah Chang Corp.
[7]Gallard Schlesinger Chemical Mfg. Corp.

GRAPHITE DIRECTIONAL SOLIDIFICATION FURNACE

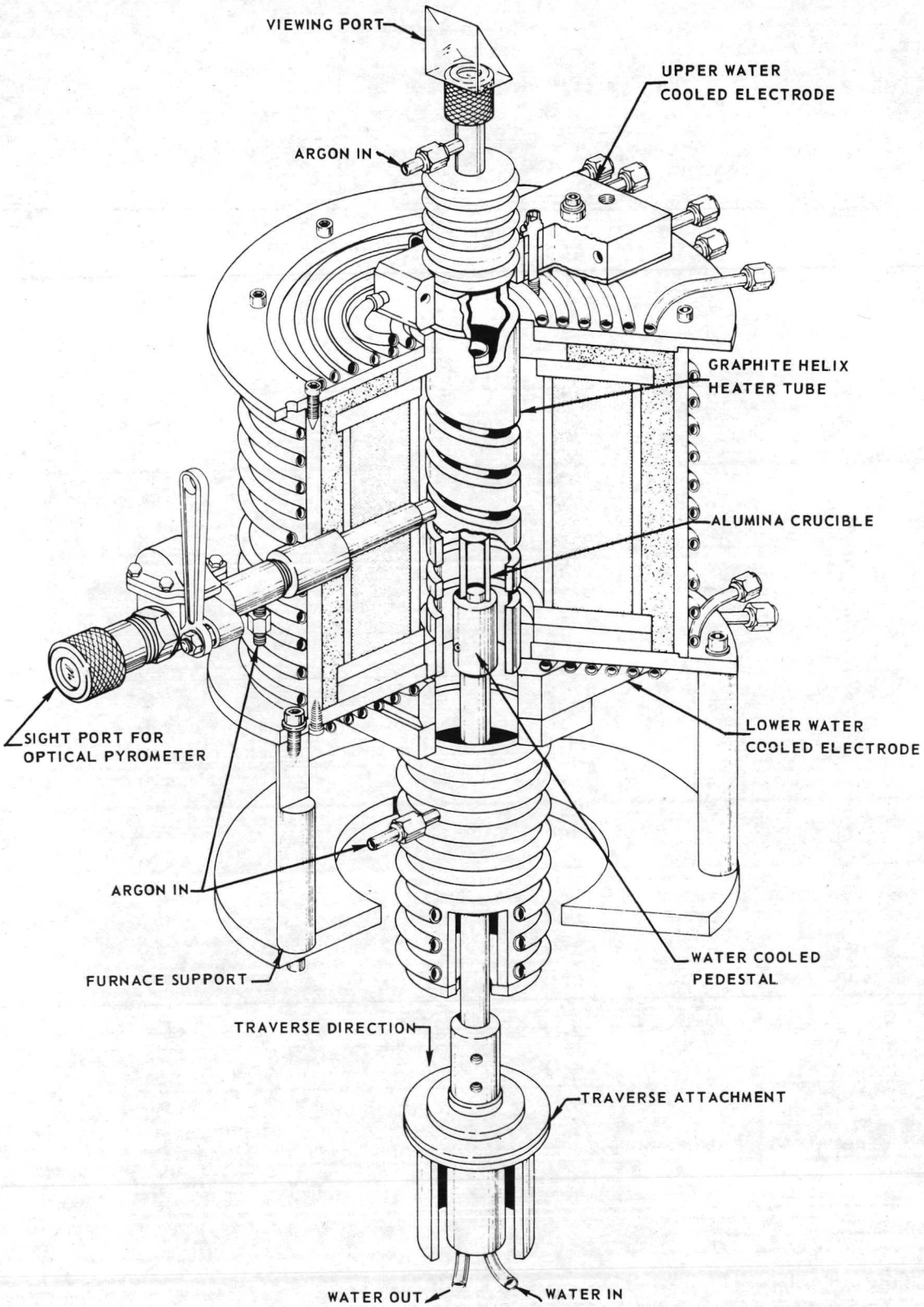

FIGURE 1

HIGH THERMAL GRADIENT DIRECTIONAL SOLIDIFICATION APPARATUS

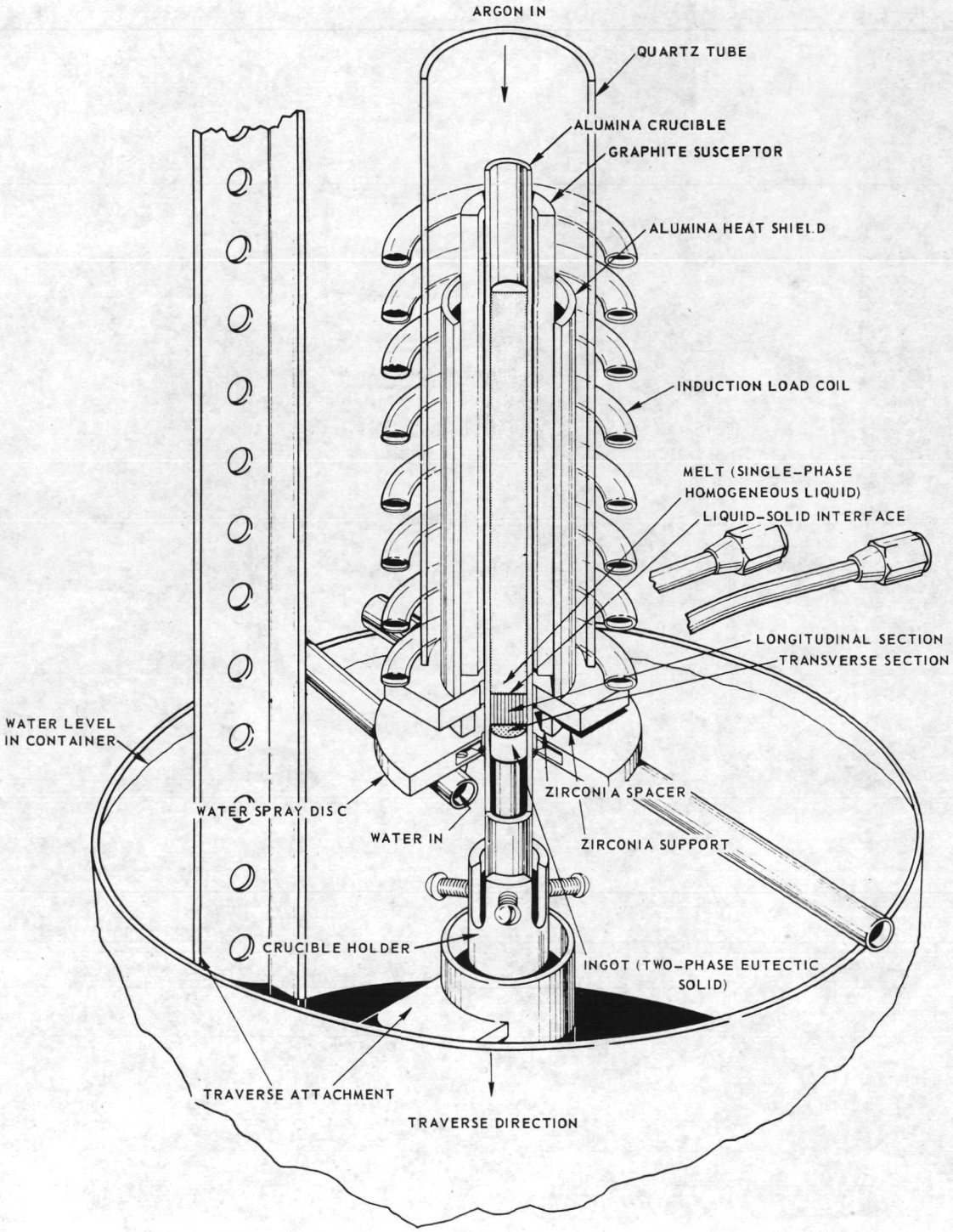

FIGURE 2

HIGH THERMAL GRADIENT DIRECTION SOLIDIFICATION APPARATUS

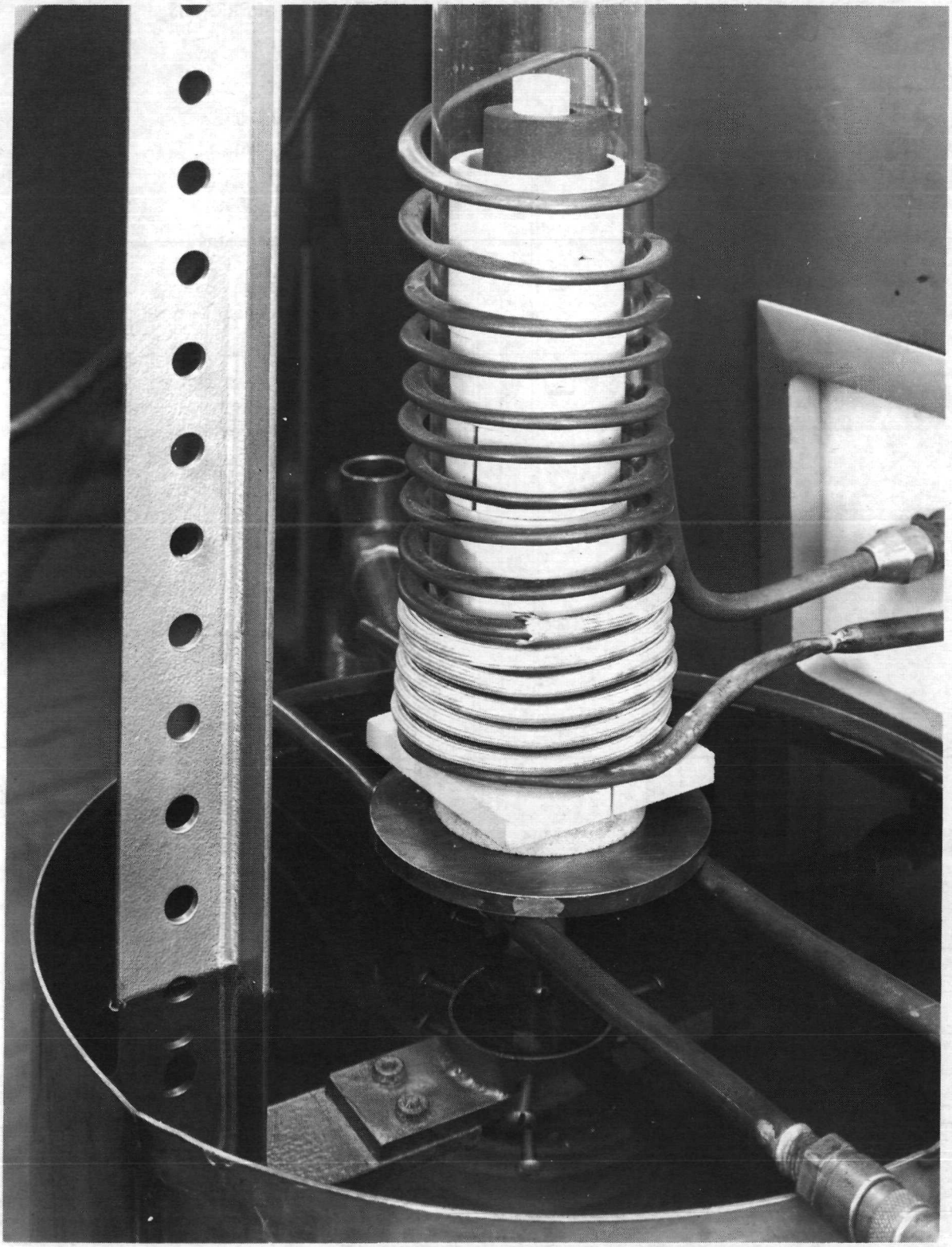

FIGURE 3

requirements are established from empirical trials or experiments instrumented with thermocouples. Controlled freezing commences by the withdrawal of the Al_2O_3 crucible through the water spray ring. In this setup thermal gradients in the liquid of approximately 250-350°C/cm may routinely be achieved. Excluding small end affected regions the rate of freezing is found to be equal to the velocity of crucible withdrawal over the 15 to 25 cms of specimen length dependent on crucible diameter.

The maximum superheat of the melt was monitored by an optical pyrometer and held to approximately 400°C. This technique permitted the containment of the alloys within commercial Al_2O_3 tubes without serious metal-mold reaction and resulted in fully aligned 1.2 cm dia by 18 cm long cylindrical specimens. Some vertical cracking of the oxide tubes resulted from the severe thermal shock of the water spray. However, complete loss of the melt or vertical lines of severe local oxidation from cracks occurred in less than 10 percent of the total experiments after experience was gained. During the second task of the contract a total of forty directionally solidified specimens were prepared without run-out failures.

2.2 Differential Thermal Analysis

The liquidus and solidus temperatures of certain alloys in the system Ni-Cb-Cr-Al were determined using a differential thermal analysis apparatus (Ref. 4). Heating and cooling of the sample was accomplished in argon at a rate of 3°C/min. The platinum vs platinum-10 percent rhodium thermocouple used was calibrated against a pure silver standard and the accuracy of the temperatures measured was within $\pm$ 2°C. The liquidus temperature was normally determined during cooling and the solidus during heating from the respective exothermic and endothermic inflections of the temperature-differential temperature traces.

2.3 Density Determinations

The density of certain Ni-Cb-Cr-Al alloys were measured by determining the weight per unit volume for ground cylinders and weighing the sample in air and in toluene at room temperature.

$$\text{Density} = \frac{\text{weight in air}}{\text{weight in air - weight in toluene}} \times \rho_{\text{toluene}}$$

2.4 Chemical Analyses

Wet chemical analyses were performed on specimens taken from the steady state growth area of a directionally solidified bar. The sample was dissolved in a nitric acid-hydrofluoric acid solution and fumed with sulfuric acid. After dissolution Cb was precipitated with cupferron. The precipitate was ignited and dissolved by fusion with potassium pyrosulfate. The Cb was then hydrolyzed and the precipitate ignited

and weighed as Cb_2O_5. The filtrate from the hydrolysis and the cupferron precipitation were combined and evaporated to destroy the excess cupferron. After diluting to a convenient volume, a sample was taken for each Ni, Al, and Cr analysis procedure. Chromium was determined by a ferrous sulfate permanganate titration after persulfate oxidation to a chromate. Nickel was precipitated as the glyoximate. Finally, after a mercury cathodic electrolysis to remove nickel and chromium, aluminum was determined by E.D.T.A. titration.

As wet chemical analysis is a tedious and expensive destructive process, the use of X-ray fluorescence analysis was employed as an alternative nondestructive and less expensive technique. Under a separate program (Ref. 18), the X-ray fluorescence (XRF) intensities of Co, Ni, Fe, Mo, Zr, V, Al, Ti, Cr, Nb, W, and Ta in approximately seventy-five analyzed samples were recorded. These samples included Ni-base alloys obtained from the National Bureau of Standards, Carpenter Technology, and those previously analyzed by wet chemical means for NASA at UARL. A least mean square fit of intensities versus concentration was obtained using a multi-element regression program on a PDP-6 time share computer. After obtaining the sample XRF's intensities, they are entered into the program to obtain the calculated concentration.

X-ray fluorescence analyses at one-half inch intervals were performed over the entire length of d.s. (Ni - 19.7 w/o Cb - 6.0 w/o Cr - 2.5 w/o Al) and (Ni - 21.75 w/o Cb - 2.55 w/o Al) alloy bars. A 0.95 cm (3/8 in.) dia window was used in recording the X-ray fluorescence intensities. Measurements were made by translating a typically 15.2 cm (6 in.) long specimen with a ground longitudinal flat under the window at 1.27 cm (1/2 in.) intervals.

2.5 Tensile Testing

Tensile specimens were ground from unidirectionally solidified ingots oriented in such a way that the load would be applied parallel to the growth direction. Tensile tests of 1.27 cm (0.5 in.) gage length and 0.36 cm (0.140 in.) diameter samples were conducted in accordance with ASTM specification E21-69 (Ref. 19) from room temperature to 1235°C (2200°F) in air using a Tinius-Olsen four screw machine at strain rates of 0.01 min^{-1} (room temperature) and 0.05 min^{-1} (elevated temperatures). Temperature, controlled to within $\pm$ 3°C, was monitored during each test. Strain was measured at room temperature with two element averaging strain gages positioned 180° apart and by total crosshead deflection as measured by an LVDT extensometer at elevated temperature. Ultimate strain and reduction in area values were made from measurements of the gage length and area before and after testing.

Measurements of the offset yield and elastic modulus at elevated temperatures of 750, 815, 870, 927, 1000, 1050, 1100, 1150, 1200, and 1235°C were made using specimens (Fig. 4) containing ridges defining the 1.27 cm (0.5 in.) gage length which permitted direct strain measurements using 304 stainless steel extension rods coupled to a pair of averaging LVDT extensometers.

TENSION TEST SPECIMEN

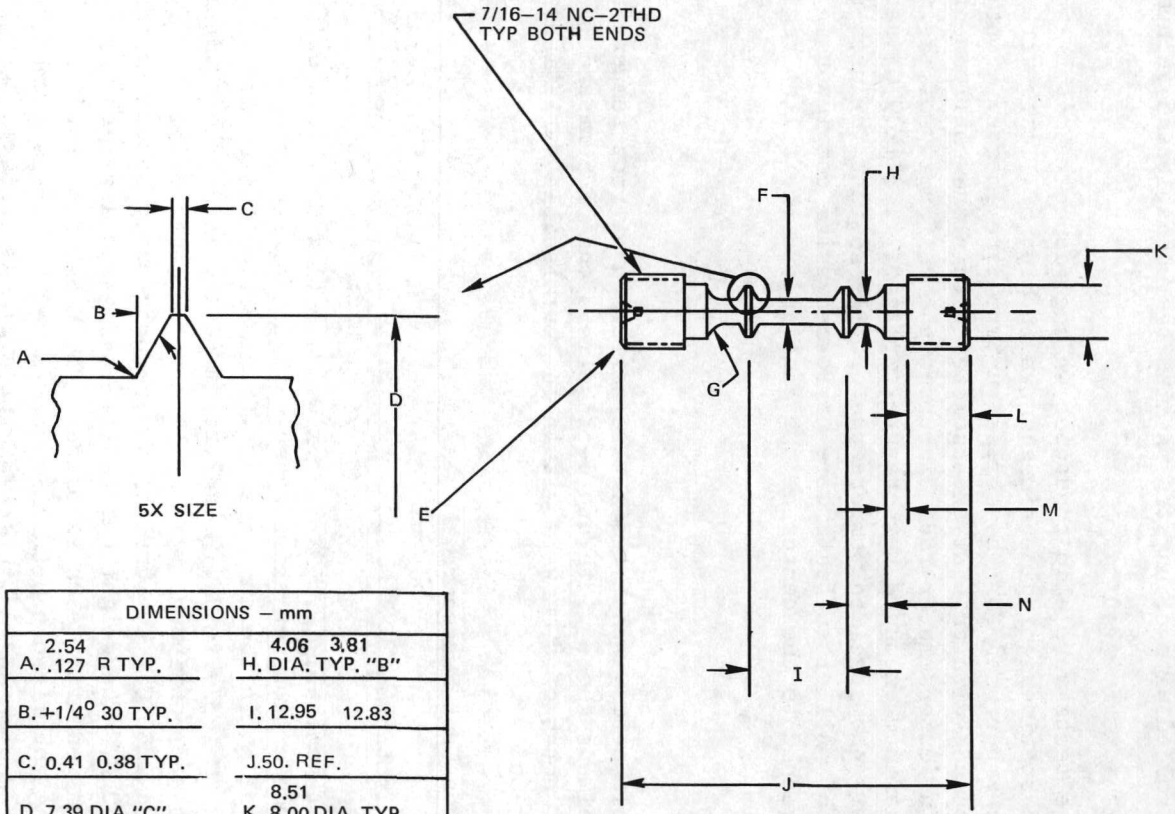

DIMENSIONS – mm	
A. 2.54 .127 R TYP.	H. 4.06 3.81 DIA. TYP. "B"
B. +1/4° 30 TYP.	I. 12.95 12.83
C. 0.41 0.38 TYP.	J. 50. REF.
D. 7.39 DIA "C"	K. 8.51 8.00 DIA. TYP.
E. 0.76 x 45° TYP	L. 9.78 9.27 TYP.
F. 3.58 3.53 "A" dia	M. 2.16 1.65 TYP.
G. 3.18 R (MIN) TYP.	N. 7.75 7.24 TYP.

DIMENSIONS – INCHES	
A. 0.10 0.005 R. TYP.	H. 0.160 0.150 DIA. TYP "B"
B. + 1/4° 30 TYP.	I. 0.510 0.505
C. 0.016 0.015 TYP.	J. 2. REF.
D. 0.291 DIA. "C"	K. 0.335 0.315 DIA. TYP
E. 0.030 x 45° TYP	L. 0.385 0.365 TYP.
F. 0.141 0.139 "A" DIA.	M. 0.085 0.065 TYP.
G. 0.125 R. (MIN) TYP.	N. 0.305 0.285 TYP.

FIGURE 4

2.6 Stress Rupture and Creep Rupture Testing

Stress rupture tests were performed at 1149°C (2100°F) in vacuum. These tests were performed in accordance with ASTM E139-69 as applicable, with specimens of gage diameter 0.28 cm (0.110 in.) and gage length 1.27 cm (0.50 in.) with 5/16-18 threaded ends. A redesign of the stress rupture and creep specimens from one with 1.27 cm (0.50 in.) long, 0.32 cm (0.125 in.) diameter gage and 1/4-20-NC3 threaded end was necessitated from thread shear failures observed after prolonged times under load at 1149°C (2100°F). Crosshead extension was measured during the test and elongation and reduction of area were measured on the fractured halves. Tests were conducted in a furnace as shown in Fig. 5, which consists of a chrome plated stainless steel vacuum chamber. Heating was accomplished with a tantalum resistance furnace. Temperature was controlled with a tungsten rhenium thermocouple and vacuum to 10^{-6} torr was standard.

Creep rupture tests were also conducted in accordance with ASTM specifications E139-69 on ridged specimens of dimensions shown in Fig. 6. Tests were performed in the same vacuum chamber used for the stress rupture experiments. Continuous creep measurements were made with an LVDT extensometer within the environment. Because the presence of the extensometer rods disrupted the uniformity of the temperature gradient at the maximum exposure temperature employed, i.e. 1200°C, radiation baffling was added to modify the specimen temperature profile so that failures occurred within the gage length. All creep tests were performed using continuously recording thermocouples attached to the center of the gage and to the fillet region near the top threaded end.

2.7 Impact

Charpy (simple beam) impact tests were performed at room temperature on notched subsize test specimens whose width and depth dimensions of 5 mm and 10 mm and dimension to bottom of notch of 8 mm were within the permissible variations of ASTM specification E23-66.

2.8 Oxidation Test Procedure

2.8.1 Isothermal

Test coupons, nominally 2.54 x 1.27 x 0.13 cm (1 x 0.5 x 0.050 in.), were ground and lapped with 600 grit paper and cleaned with trichloroethylene. The long dimension of the coupon lay in the eutectic growth direction. Separate coupons were contained in ~1.9 cm (~3/4 in.) O.D. x 2.86 cm (1 1/8 in.) high cylindrical alumina crucibles and exposed continuously in still air for times of 5, 50, 200 and 500 hrs at 1000, 1100, and 1200°C. The crucibles were previously heated to constant weight for 24 hrs at 1250°C. The weight change (including spall weight) and the spall weight were determined after each exposure. The depletion zone thickness was determined by measuring the microstructurally unaffected thickness normal to the largest faces of the test coupon and computing on the basis of one side. Changes in

VACUUM CREEP RUPTURE TESTER

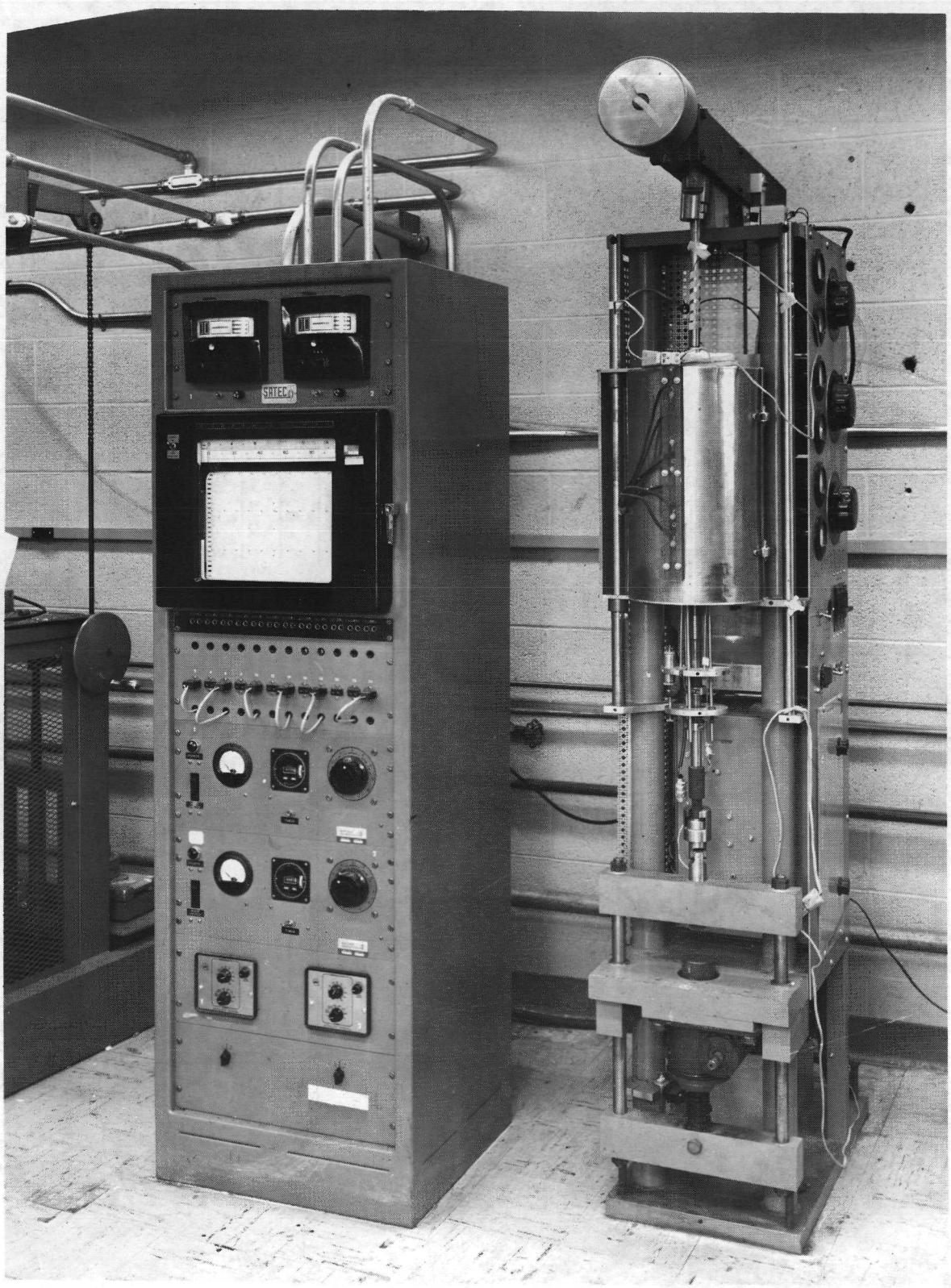

FIGURE 5

CREEP TEST SPECIMEN

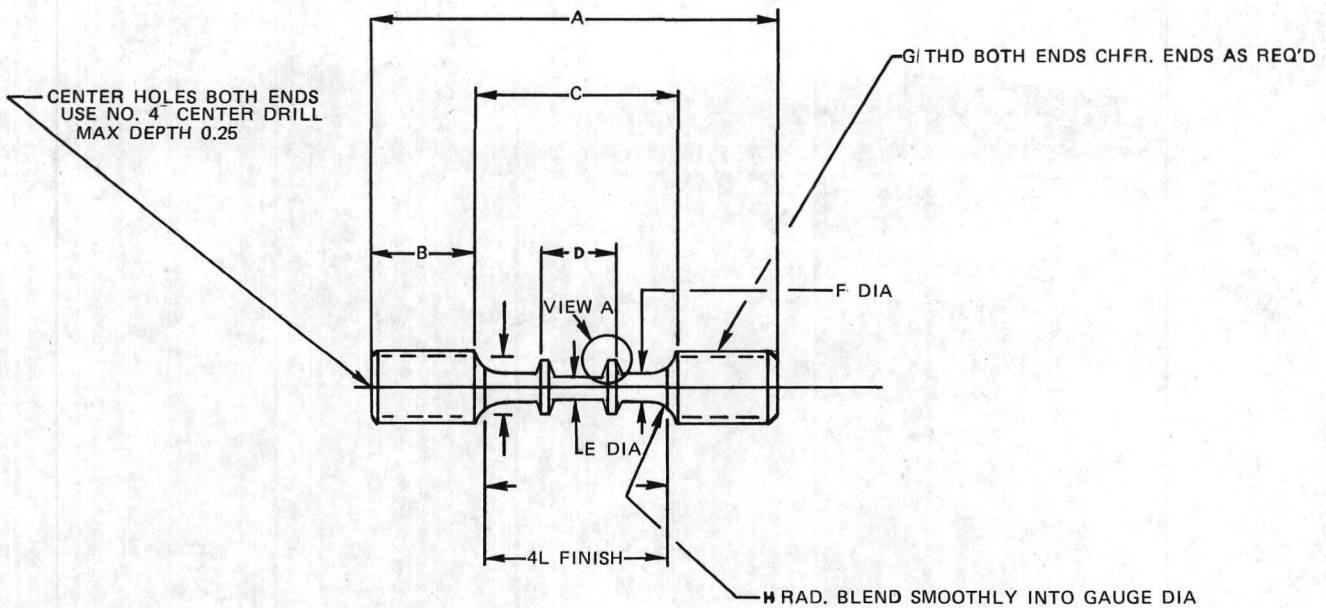

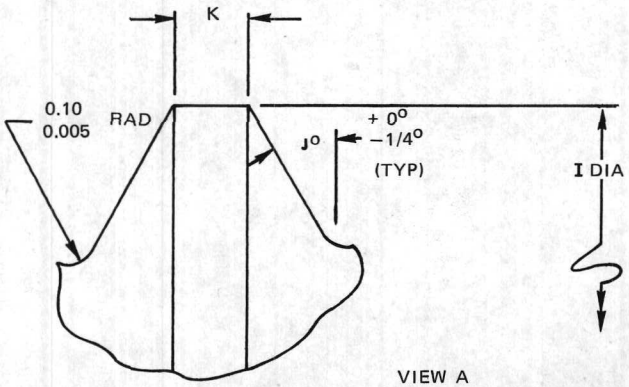

NO UNDERCUTTING PERMITTED BLEND SMOOTHLY

NOTE:
1. IDENTIFY ONE END BY NUMBER

SPECIMEN DIMENSIONS – mm		SPECIMEN DIMENSIONS – INCHES	
A. 57.15	H. 5.08	A. 2.250	H. 0.200
B. 12.7	I. 4.41	B. 0.500	I. 0.1735
C. 31.75	J. $30^{\circ}\ ^{+0^{\circ}}_{-1/4^{\circ}}$	C. 1.250	J. $30^{\circ}\ ^{+0^{\circ}}_{-1/4^{\circ}}$
D. 12.7	K. 0.40	D. 0.500	K. 0.0155
E. 2.78		E. 0.1100	
F. 3.18		F. 0.1250	
G. 5/16–18–NC–3		G. 5/16–18–NC–3	
ALL DIMENSIONS ± 0.013		ALL DIMENSIONS ± 0.0005	

FIGURE 6

each sample's total thickness were measured microstructurally on mounted and polished cross sections as well as by micrometer after each exposure. Microstructure stability, scale adhesion and oxide penetration paths were observed and recorded.

2.8.2 Cyclic

Test coupons were prepared as above and contained in alumina crucibles with loosely fitting Al_2O_3 covers. The specimens were fitted in the crucible so as to freely expose the surfaces to air. One set of samples of each material investigated was exposed for a total of 24 hrs in still air at 1100°C. After every hour of exposure the samples were allowed to air cool to room temperature for approximately one hour and then returned to test temperature. The specimens were weighed after every four hours of exposure and examined visually. The oxide penetration change in metal thickness and adhesion were recorded. In a similar manner another set of samples was exposed for a total of 100 hrs in still air at 1100°C. After every hour of exposure these samples were allowed to air cool for approximately one hour and returned to test temperature. The specimens were weighed after every ten hours of exposure and examined as above. Each specimen was cross sectioned perpendicular to the long dimension of the sample mounted, polished and etched to measure alloy depletion zone thickness, oxide penetration and the thickness and adhesion of the scale as was the case for isothermally exposed samples.

III. RESULTS AND DISCUSSION

3.1 Alloy Studies

3.1.1 Background

It is now known that certain eutectic alloys respond to unidirectional solidification techniques to produce useful phase aligned microduplex structures. Previous studies (Refs. 1,20) have identified the pseudobinary eutectic, γ' Ni_3Al - δ Ni_3Cb, as the strongest nickel base alloy known. However, improvements in low temperature ductility and oxidation resistance would benefit its utility as a structural turbine component. Substitution of chromium as a quaternary alloying element to γ'-δ has been attempted but its low solubility in both intermetallics did not permit its addition to the necessary beneficial level (Ref. 2). Decreasing the volume fraction of δ from 0.44 to 0.32 by directional solidification of hypo-eutectic γ'-δ compositions permitted a gain in the room temperature fracture strain from ~0.7 to ~2.0 percent (Ref. 3) but required too stringent growth control to merit its further development (Ref. 4).

Based on these studies and the observations which had been made of the high ductility available in the γ Ni - δ Ni_3Cb system (Ref. 21), a path of investigation was chosen which has been very rewarding. Since both chromium and aluminum were known to be soluble in nickel, a study of the alloys in the nickel-rich corner of the Ni-Cb-Cr-Al quaternary system was undertaken. Our initial work showed that aligned, in situ composites could indeed be produced from numerous bivariant eutectic compositions (Ref. 16). The objective of this study therefore was to define, by means of screening and optimization of Ni-Cb-Cr-Al alloys exhibiting eutectic behavior, a superior high temperature material.

3.1.2 Phase Equilibria

The compositions in the quaternary system, Ni-Al-Cb-Cr, to which this study was directed are those solidifying according to the bivariant eutectic reaction. These compositions may be geometrically defined as those residing on the liquidus surface wherein two solid phases separate from the liquid upon freezing. This thermodynamically bivariant surface wherein the three phase equilibria of the type $L \rightleftarrows \gamma + \delta$ occurs is shown in Fig. 7 which illustrates a polythermal projection of the nickel-columbium-chromium-aluminum quaternary diagram. The shaded surface represents the loci of the compositions which were optimized in this program. This surface is bounded in the pertinent ternary systems by monovariant eutectic troughs which in the Ni-Cr-Cb system extend between the binary eutectic Ni-Ni_3Cb and the ternary eutectic Ni-Ni_3Cb-$CbCr_2$ and which in the Ni-Al-Cb system extend between the binary eutectic Ni-Ni_3Cb and the ternary eutectic Ni-Ni_3Al-Ni_3Cb.

Alloys whose compositions are identified in Table Ib were prepared to define more precisely the two boundary monovariant eutectic troughs and also the bivariant eutectic surface. Because of the difficulty in geometrically presenting these compositions residing in phase diagrams which are not planar figures but spatial bodies without the aid of anaglyphs (Ref. 23), the liquidus surface and 1200°C isothermal sections of the pertinent ternary systems were constructed upon the surfaces of an equilateral tetrahedron, Fig. 8. The edges of this tetrahedron represent the six binary systems Ni-Ni_3Cb, Ni-Ni_3Al, Ni-'Ni_3Cr', Ni_3Al-Ni_3Cb, Ni_3Al-'Ni_3Cr', and Ni_3Cb-'Ni_3Cr', and the apices represent the components Ni, 'Ni_3Cr', Ni_3Al and Ni_3Cb. The triangular faces represent the four ternary systems and finally the interior of the tetrahedron represents the quaternary system Ni-'Ni_3Cr'-Ni_3Al-Ni_3Cb. For convenience, only the alloys from Table Ib, whose compositions reside on the ternary surfaces, are plotted.

From the shape and size of the phase fields it can be seen that there is restricted solubility of Cr and Al in δ Ni_3Cb. The γ solid solution phase field in contrast is extensive, and with decreasing temperature a drastic reduction of the γ field size occurs from 1200 to 800°C (Ref. 24). Thus, there is opportunity for precipitation of both γ', Ni_3Al, and γ'', the latter phase a tetragonal form of Ni_3Cb (Ref. 25).

POLYTHERMAL PROJECTION SHOWING BIVARIANT EUTECTIC SURFACE WHEREIN $L \rightleftharpoons \gamma + \delta$

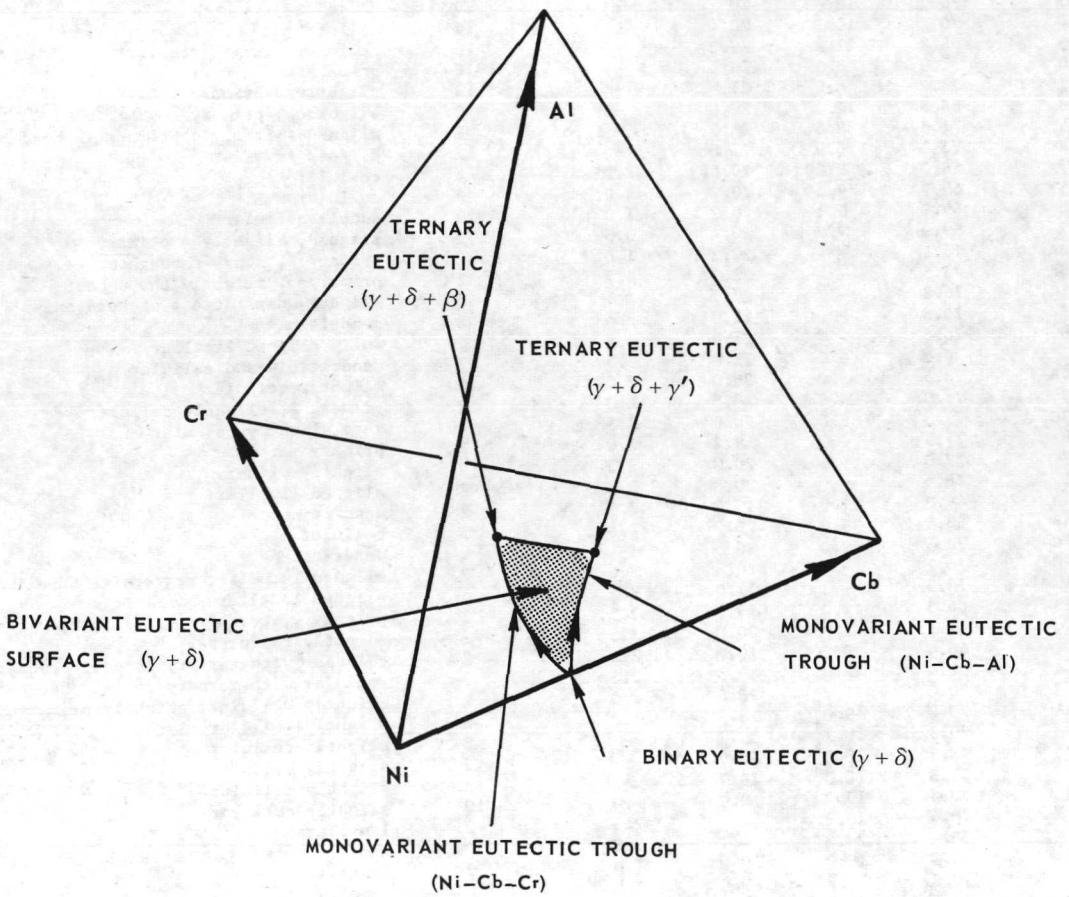

FIGURE 7

Table Ib

Summary of Directional Solidification Experiments

Specimen No.	Aim Composition wt/o Ni	wt/o Cr	wt/o Cb	wt/o Al	Freezing Velocity cm/hr	Microstructure
A71-311	69	12	19	-	20	aligned lamellar, primary γ, Ni
A71-312	69	12	19	-	10	aligned lamellar, primary γ, Ni
A71-314	69	12	19	-	2	aligned lamellar
A71-318	71	9	20	-	20	cellular, primary γ, Ni
A71-319	71	9	20	-	2	aligned lamellar
A71-320	71	9	20	-	10	slightly cellular
A71-321	73	6	21	-	10	aligned lamellar
A71-322	73	6	21	-	20	aligned lamellar
A71-323	73	6	21	-	2	aligned lamellar
A71-341	70	10	20	-	10	cellular
A71-344	70	10	20	-	10	cellular
A71-349	68.8	11.2	20.0	-	10	cellular, slightly primary in δ
A71-350	71.0	8.5	20.5	-	10	primary in δ
A71-351	73.0	6.0	21.0	-	10	slightly δ primary
A71-353	68.8	11.2	20.0	-	2	aligned, δ primary
A71-355	71.0	8.5	20.5	-	2	aligned slightly δ primary in head end
A71-364	73.0	6.0	21.0	-	2	aligned lamellar
A71-197	68.03	9.20	20.56	2.21	2	cellular
A71-245	69.7	9.1	20.2	1.0	2	cellular
A71-258	69.7	9.1	20.2	1.0	10	deeply cellular
A71-277	69.9	9.2	20.4	0.5	2	aligned, slightly δ primary
A71-508A	76.1	-	22.3	1.6	2	primary δ, heavy throughout
A71-508B	75.5	-	22.3	2.2	2	primary δ, slightly throughout
A71-508C	76.8	-	22.1	1.1	2	slightly dendritic δ at head only
A71-535	75.6	-	22.0	2.4	2	dendritic δ
A71-546	76.5	-	21.0	2.5	2	fully aligned lamellar
A71-567	70.5	6.0	21.0	2.5	2	dendritic δ and cellular
A71-589A	72.5	5.0	20.0	2.5	2	slightly cellular
A71-589B	73.0	4.0	20.5	2.5	2	primary δ, slightly cellular
A71-589C	71.5	6.0	20.0	2.5	2	very slightly cellular
A71-636	77.5	-	19.7	2.8	2	primary γ
A71-639	72.0	5.5	20.0	2.5	5	slightly primary γ
A71-651	76.4	-	20.8	2.8	2	aligned lamellar
A71-664A	66.0	12.0	19.5	2.5	2	dendritic δ
A71-664B	68.5	9.0	20.0	2.5	2	cellular
A71-664C	70.5	9.0	20.5	-	2	dendritic δ
A71-689B	76.2	-	20.8	3.0	2	aligned lamellar, segregates to aligned ternary
A71-695	76.5	-	21.0	2.5	5	aligned lamellar
A71-711B	66.5	12.0	19.0	2.5	2	primary γ, ternary in cell boundaries
A71-711C	71.5	6.0	20.0	2.5	2	slightly cellular
A71-730	68.4	9.2	20.2	2.2	2	cellular with ternary in cell boundaries
A71-745A	66.0	12.0	19.5	2.5	2	cellular with ternary in cell boundaries
A71-745B	70.0	9.0	20.0	1.0	2	slightly cellular, slightly primary in δ
A72-026A	70.3	9.0	19.7	1.0	2	slightly cellular
A72-030	70.3	10.1[1]	19.7	-	2	slightly cellular
A72-037	70.3	10.0[2]	19.7	-	2	slightly cellular
A72-043	70.3	10.0[3]	19.7	-	2	slightly cellular
A72-080	70.3	19.7	9.0	1.0	10	slightly cellular
A72-083	76.4	20.8	-	2.8	2	lamellar
A72-085	76.4	20.8	-	2.8	2	lamellar
A72-097	70.3	19.7	9.0	1.0	2	lamellar
A72-140	70.5	19.5	9.0	1.0	2	lamellar
A72-148	71.5	20.0	6.0	2.5	5	lamellar

[1]Iodide 99.9995 (A69-714)
[2]Electrolytic 99.98 (A67-822)
[3]Spectrographic 99.999 (A67-549 and A71-670)

Table Ib (Cont'd)

Specimen No.	Aim Composition wt/o Ni	wt/o Cr	wt/o Cb	wt/o Al	Freezing Velocity cm/hr	Microstructure
A72-187	70.5	9.0	19.5	1.0	2	lamellar
-197	71.5	6.0	20.0	2.5	2	lamellar
-202	71.5	6.0	20.0	2.5	2	lamellar
-208	71.5	6.0	20.0	2.5	2	lamellar
-212	70.3	10.0	19.7	-	2	lamellar with Al_2O_3
-229	71.5	6.0	20.0	2.5	2	lamellar
-234	70.5	9.0	19.5	1.0	2	lamellar
-235	71.8	6.0	19.7	2.5	3	lamellar
-566	71.7	6.0	19.8	2.5	2	lamellar
-570	71.7	6.0	19.8	2.5	2	lamellar
-597	71.8	6.0	19.7	2.5	3	lamellar
-599	↓	↓	↓	↓	↓	↓
-604						
-613						
-617						
-621						
-627						
-628						
-631						
-634						
-636						
-659						
-664						
-668						
-670						
-673						
-675						
-682						
-684						
-687	71.8	6.0	19.7	2.5	3	lamellar
-506	76.5	-	21.0	2.5	2.0	lamellar
-325	76.5	-	21.0	2.5	5.0	lamellar
-536	76.5	-	21.0	2.5	5-15	no banding
-543	76.5	-	21.0	2.5	15	dendritic γ
-572	76.4	-	20.8	2.8	5-15	increasing dendritic γ
-577	76.25	-	21.25	2.5	5-15	increasing dendritic γ after 10 cm/hr
-596	76.0	-	21.5	2.5	8.0	run out
-603	76.5	-	21.0	2.5	10.0	dendritic γ
-623	76.0	-	21.5	2.5	10.0	lamellar
-608	76.0	-	21.5	2.5	8.0	slightly primary δ
-625	76.4	-	20.8	2.8	7.5	lamellar
-640	75.5	-	22.0	2.5	20.0	dendritic δ
-657	75.75	-	21.75	2.5	25-28.8	very slight dendritic δ
-663	76.0	-	21.5	2.5	25.0	lamellar
-669	75.83	-	21.67	2.5	38.4	very slight dendritic γ
-678	75.5	-	22.0	2.5	38.0	dendritic δ
-679	75.5	-	22.0	2.5	50.5	very slight dendritic δ
-690	75.5	-	22.0	2.5	75	very slight dendritic γ
-692	75.7	-	21.8	2.5	50	lamellar
-694	75.3	-	22.2	2.5	100	primary γ
-768	75.7	-	21.75	2.55	38	lamellar
-769	75.7	-	21.75	2.55	38	lamellar
-771	75.7	-	21.75	2.55	38	lamellar
-788	75.7	-	21.75	2.55	38	lamellar
-790	75.7	-	21.75	2.55	38	lamellar

Table Ib (Cont'd)

Specimen No.	Aim Composition wt/o Ni	wt/o Cr	wt/o Cb	wt/o Al	Freezing Velocity cm/hr	Microstructure
A72-800	75.7	-	21.75	2.55	38	lamellar
-807	↓	↓	↓	↓	↓	↓
-808						
-809						
-810						
-811						
-814						
-815						
-816						
-817						
-818						
-819						
-820						
-826						
-827						
-829						
-831						
-832						
-836	75.7	-	21.75	2.55	38	lamellar

THE LIQUIDUS SURFACE AND 1200°C PHASE FIELDS IN THE NICKEL RICH CORNER OF THE Ni–Cb–Cr–Al DIAGRAM

(REFS. 30,31)

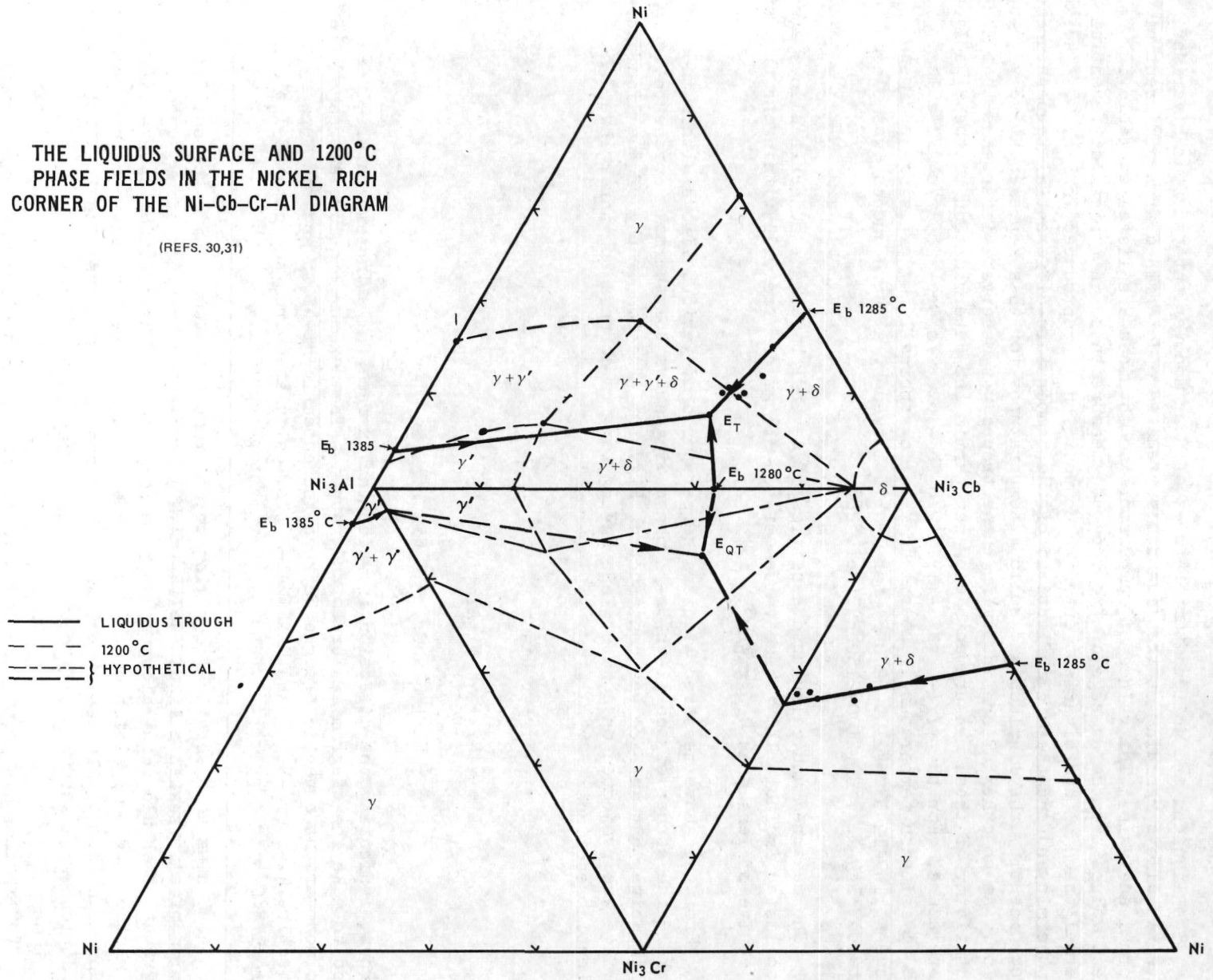

FIGURE 8

The liquidus and solidus temperatures of four monovariant and four bivariant eutectic alloys residing on the liquidus surface were determined from differential thermal analysis. The values of temperature so obtained are listed in Table II. These values are the average of two separate measurements. A typical differential thermal trace of one bivariant eutectic composition is reproduced in Fig. 9. The exothermic and endothermic inflections of the temperature-differential temperature trace identify the liquidus and solidus temperatures for this representative γ/γ'-δ alloy. As no other discontinuity in these traces was observed, it appears that the sensitivity of these measurements does not permit the determination of the γ' solvus temperature. For the γ/γ'-δ (Ni - 19.7 w/o Cb - 6.0 w/o Cr - 2.5 w/o Al) alloy, the γ' solution temperature, determined metallographically by exposing specimens between 1149-1245°C (2100-2270°F) for 1 hr followed by a rapid quench, was placed between 1149-1177°C (2100-2150°F) (Ref. 28).

The measured and calculated densities of several bivariant eutectic alloys are also listed in Table II. These values of 8.5-8.7 gm/cm^3 are well within the program objective of less than 9.0 gm/cm^3.

From the above measured liquidus temperatures of various alloys within the nickel rich corner of the Ni-Cb-Cr-Al phase diagram, a polythermal representation of the bivariant surface was constructed, Fig. 10. The topography of the liquidus surface was projected on a base plane having for its corners the three invariant eutectic reactions:

$$L \rightarrow \gamma\ Ni + \delta\ Ni_3Cb$$

$$L \rightarrow \gamma\ Ni + \gamma'\ Ni_3Al + \delta\ Ni_3Cb$$

$$L \rightarrow \gamma\ Ni + \beta\ CbCr_2 + \delta\ Ni_3Cb.$$

Arrows, indicating the direction in which the surface falls in temperature, were used to make the diagram easier to understand. The maximum liquidus slopes of the two monovariant eutectic troughs between the eutectic Ni-Ni_3Cb and the ternary eutectics Ni-$CbCr_2$-Ni_3Cb and Ni-Ni_3Al-Ni_3Cb, calculated from the data of Table II, were 1.8°C/weight percent Cr and 2.5°C/weight percent Al.

According to theoretical equilibrium considerations concerning the solidification of alloys with a liquid-solid (mushy) temperature range (Ref. 29), noticeable segregation should occur along a 20-25 cm long ingot. The question then arises as to whether the composition of the monovariant and bivariant eutectic alloys produced under high thermal gradient, variable molten zone length, directional solidification conditions will substantially change from one end to the other.

To examine this point, the variation in composition along the length of two directionally solidified γ/γ'-δ alloys was determined at positions approximately 1.2 cm apart by X-ray fluorescence. The charge composition of the two alloys were

Table II

Melting Temperatures and Densities of Ni-Cb-Cr-Al Alloys

Identification Specimen No.	Composition w/o Ni	Cb	Cr	Al	ρ* gm/cm^3	ρ gm/cm^3	Liquidus Temp. °C	Solidus Temp. °C
A70-590	77.6	22.4	--	--	8.99	--	1278	1278
Ni-Ni_3Cb(Ref.26)	76.5	23.5	--	--	8.99	8.8(est)	1270	1270
Ni-Ni_3Cb(Ref.27)	--	--	---	--	--	--	1285	1285
A71-302	73.0	21.0	6.0	--	8.86	--	1278	1263
A71-341-01	70.0	20.0	10.0	--	8.78	--	1263	1251
A72-956	68.5	19.5	12.0	--	8.74	--	1256	1242
A71-691C(Ref.4)	76.1	20.7	--	3.2	8.57	--	1276	1270
A72-961	76.5	21.0	--	2.5	8.60	--	1274	1272
A71-711C	71.5	20.0	6.0	2.5	8.49	8.58	1260	1242
A72-911-04	71.8	19.7	6.0	2.5	8.49	--	1257	1244
A71-744	70.0	20.0	9.0	1.0	8.65	8.69	1260	1242
A71-664A	68.5	20.0	9.0	2.5	8.44	8.51	1247	1220
A71-730	68.4	20.2	9.2	2.2	8.48	8.55	1243	1216

*Calculated by method of F. D. Hull 'Estimating Alloy Densities', Metal Progress, 96, (1969) p 139. Information supplied by F. Harf, NASA Lewis Research Center.

DIFFERENTIAL THERMAL ANALYSIS TRACE
OF 71.5 w/o Ni, 20.0 w/o Cb, 6.0 w/o Cr, 2.5 w/o Al

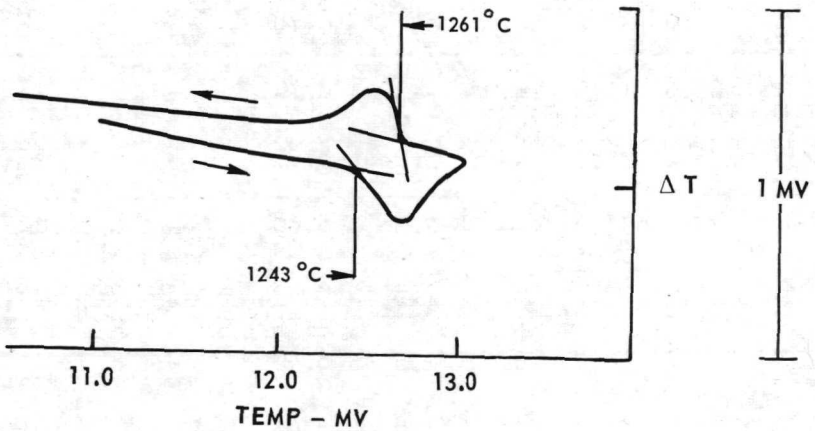

FIGURE 9

POLYTHERMAL REPRESENTATION OF THE BIVARIANT SURFACE, $L \rightarrow \gamma + \delta$, WITHIN THE QUATERNARY SYSTEM Ni–Cb Cr–Al

(ARROWS INDICATE DIRECTION IN WHICH SURFACE FALLS IN TEMPERATURE)

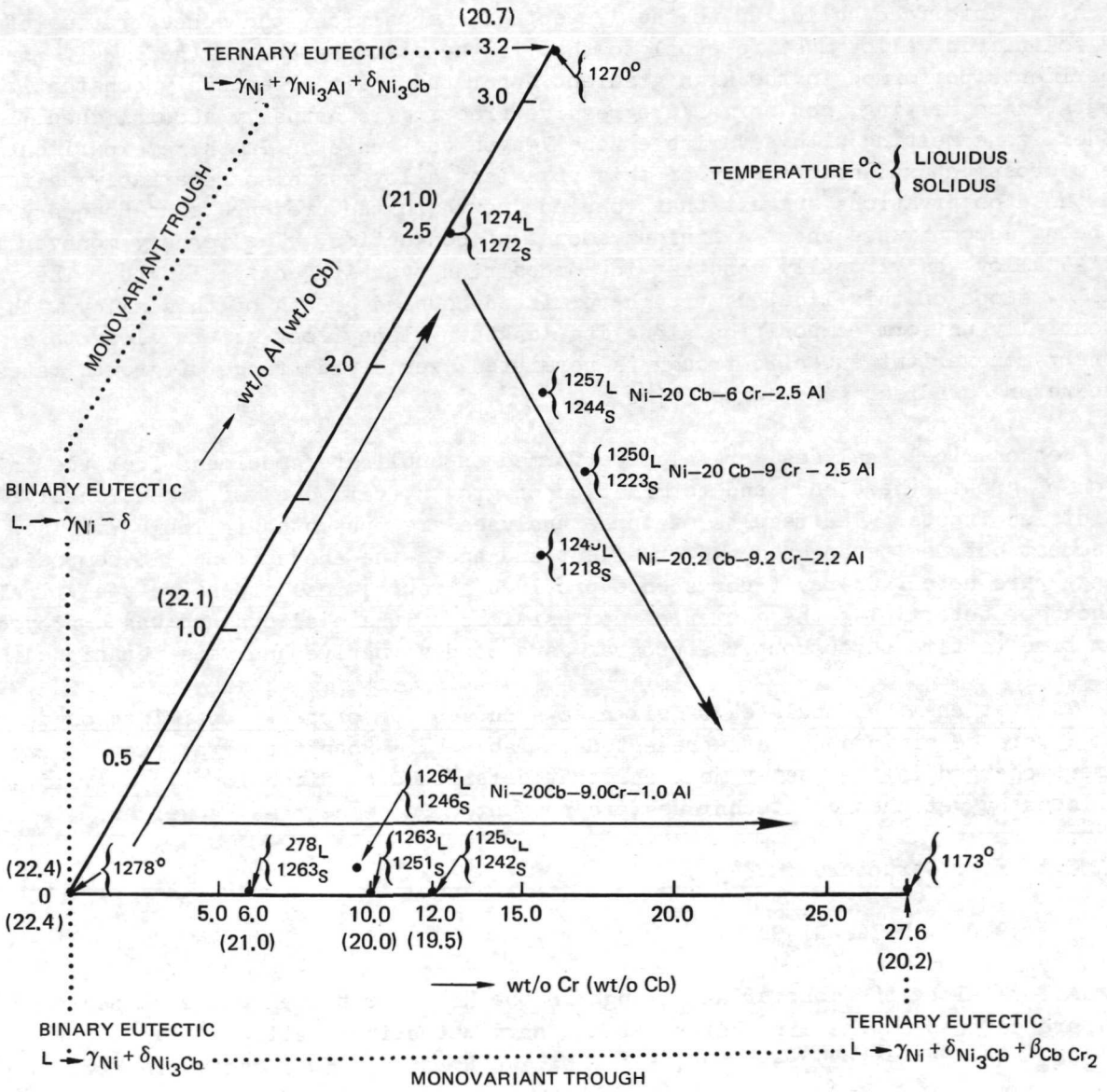

FIGURE 10

Ni - 19.7 w/o Cb - 6.0 w/o Cr - 2.5 w/o Al, specimen A72-488 and Ni - 21.75 w/o Cb - 2.55 w/o Al, specimen A72-818. These specimens were directionally solidified at 3 and 38 cm/hr respectively in the high gradient-solidification apparatus. The result of the XRF analyses are presented in Tables III and IV and graphically in Figs. 11 and 12. A slight but continuous increase in chromium and aluminum content was observed with distance for the bivariant quaternary γ/γ'-δ alloy. This expected result arises from the fact that both elements act to continuously lower the melting point of this alloy system as seen in Fig. 10. The three phase space beneath the liquidus surface for this alloy and the separation between the liquidus and solidus temperature, although small in magnitude, leads to detectable variations in composition along the sample. One way to eliminate such concentration variations is to pass a small molten zone along the specimen. After a short transient region during which the interface builds up to the 'eutectic' composition, the concentration of the solidifying alloy must be equal to that in the starting charge (Ref. 34). In the experiments performed in the high gradient apparatus, neither entirely constant zone length, zone melting, nor normal/progressive freezing is actually accomplished. Rather, zone melting with a variable zone length was achieved in these experiments. The microstructural homogeneity of this bivariant alloy was also remarkably uniform and these observations suggest that coupled growth in the presence of a boundary layer is being accomplished under a minimum amount of convection. The ternary monovariant γ/γ'-δ alloy was virtually constant in composition over its entire length. The shallow slope of this liquidus trough permitted coupled growth of this alloy with essentially uniform composition along its length. Plane front growth along this ternary monovariant eutectic trough is permitted over a wide range of growth rates, temperature gradients and composition.

Wet chemical analyses were also performed on duplicate specimens from the iniation of growth (head end) and termination of growth (tail end) of directionally solidified ingots. The results of these analyses are presented in Table V. The agreement between techniques was excellent and again the above trends in composition change were noted. X-ray fluorescence provided a rapid, less expensive analytical method for determining the elemental compositions of these alloys and was employed from time to time throughout the program as a nondestructive analysis technique (Ref. 18).

The wet chemical analyses of six alloys chosen for property optimization during Task I were determined and are presented in Table VI. Both the percentage of each element charged in the master melt and that determined on directionally solidified specimens by wet chemical techniques are presented in percentage by weight.

3.2 Microstructure

3.2.1 Ni,Cr-Ni_3Cb

Alloys along the monovariant trough in the Ni-Cb-Cr system whose composition loci are defined as the line between the binary eutectic reaction, $E_b \rightarrow \gamma$ Ni + δ Ni_3Cb, and the ternary reaction, $E \rightarrow \gamma$ Ni + δ Ni_3Cb + ε $NbCr_2$ shown in Figs. 7

Table III

X-ray Fluorescence Analysis of A72-627,
Nominal Composition Ni-19.7 w/o Cb-6.0 w/o Cr-2.5 w/o Al

Position Identification	w/o Ni	w/o Cb	w/o Cr	w/o Al
A72-627 A	71.43 max.	19.55	5.68	3.80
	71.35 min.	19.49	5.46	3.40
A72-627 B	72.13	19.75	5.86	2.64
	72.07	19.25	5.82	2.56
A72-627 C	72.15	19.81	5.72	2.76
	71.51	19.61	5.68	2.74
A72-627 D	72.58	19.88	5.81	2.64
	72.44	19.66	5.67	2.40
A72-627 E	72.10	19.72	5.77	2.67
	72.02	19.60	5.77	2.53
A72-627 F	70.74	19.62	5.96	2.54
	70.66	19.44	5.80	2.50
A72-627 G	71.73	19.77	5.90	2.50
	71.33	19.43	5.80	2.96
A72-627 H	72.31	19.82	6.63	2.65
	72.01	19.00	5.91	2.41
A72-627 I	71.74	19.80	6.06	2.81
	70.66	19.66	5.94	2.47
A72-627 J	72.07	20.14	5.98	2.65
	71.85	20.02	5.96	2.49
A72-627 K	71.95	20.06	6.00	2.68
	71.55	19.26	6.00	2.62
A72-627 L	71.12	20.04	6.09	2.82
	70.44	19.90	5.99	2.76
A72-627 M	70.17	19.93	6.27	3.12
	68.83	19.43	6.23	2.78

Table IV

X-ray Fluorescence Analysis of A72-818,
Nominal Composition Ni-21.75 w/o Cb-2.55 w/o Al

Position Identification	w/o Ni	w/o Cb	w/o Al
A72-818 A	74.81 max.	22.64	2.78
	74.69 min.	22.60	2.58
A72-818 B	74.89	22.63	2.76
	74.55	22.57	2.60
A72-818 C	74.62	22.72	2.73
	74.58	22.66	2.69
A72-818 D	74.77	22.67	2.73
	74.59	22.59	2.65
A72-818 E	74.67	22.61	2.85
	74.59	22.57	2.71
A72-818 F	74.76	22.69	2.71
	74.58	22.63	2.63
A72-818 G	74.73	22.63	2.85
	74.67	22.59	2.53
A72-818 H	74.59	22.62	2.86
	74.53	22.62	2.78
A72-818 I	74.81	22.66	2.79
	74.45	22.56	2.73
A72-818 J	74.58	22.64	2.91
	74.46	22.62	2.79
A72-818 K	74.68	22.68	2.87
	74.48	22.62	2.67
A72-818 L	74.81	22.71	2.82
	74.35	22.57	2.74

COMPOSITIONAL VARIATION ALONG LENGTH OF $\gamma/\gamma'-\delta$ (Ni – 19.7 w/o Cb – 6.0 w/o Cr – 2.5w/o Al)
1.2 CM BAR SPECIMEN DIRECTIONALLY SOLIDIFIED AT 3cm/hr (HIGH GRADIENT).

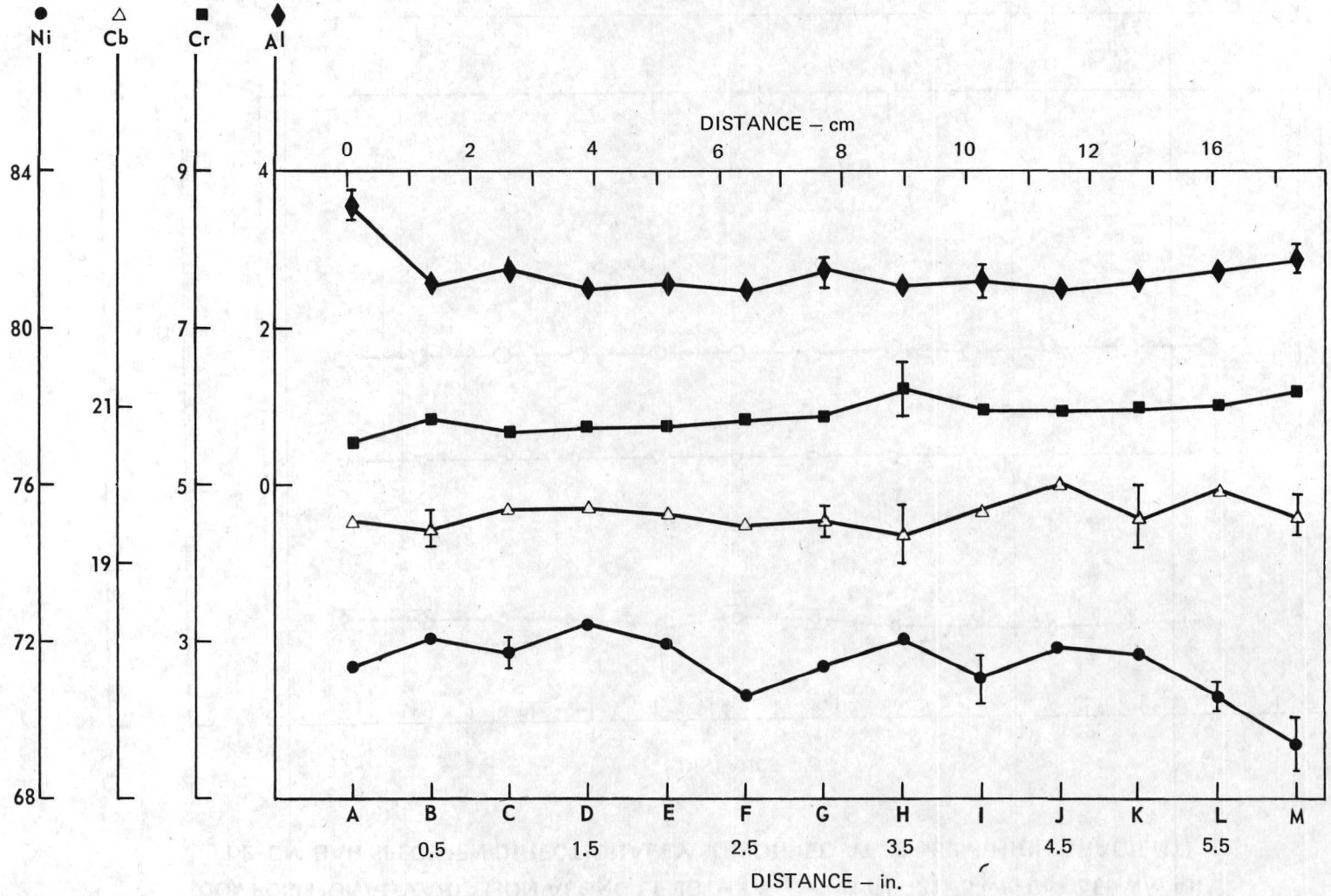

FIGURE 11

COMPOSITIONAL VARIATION ALONG LENGTH OF $\gamma/\gamma' - \delta$ (Ni–21.75 w/o Cb–2.55 w/o Al)
1.2 CM BAR SPECIMEN DIRECTIONALLY SOLIDIFIED AT 38 cm/hr (HIGH GRADIENT)

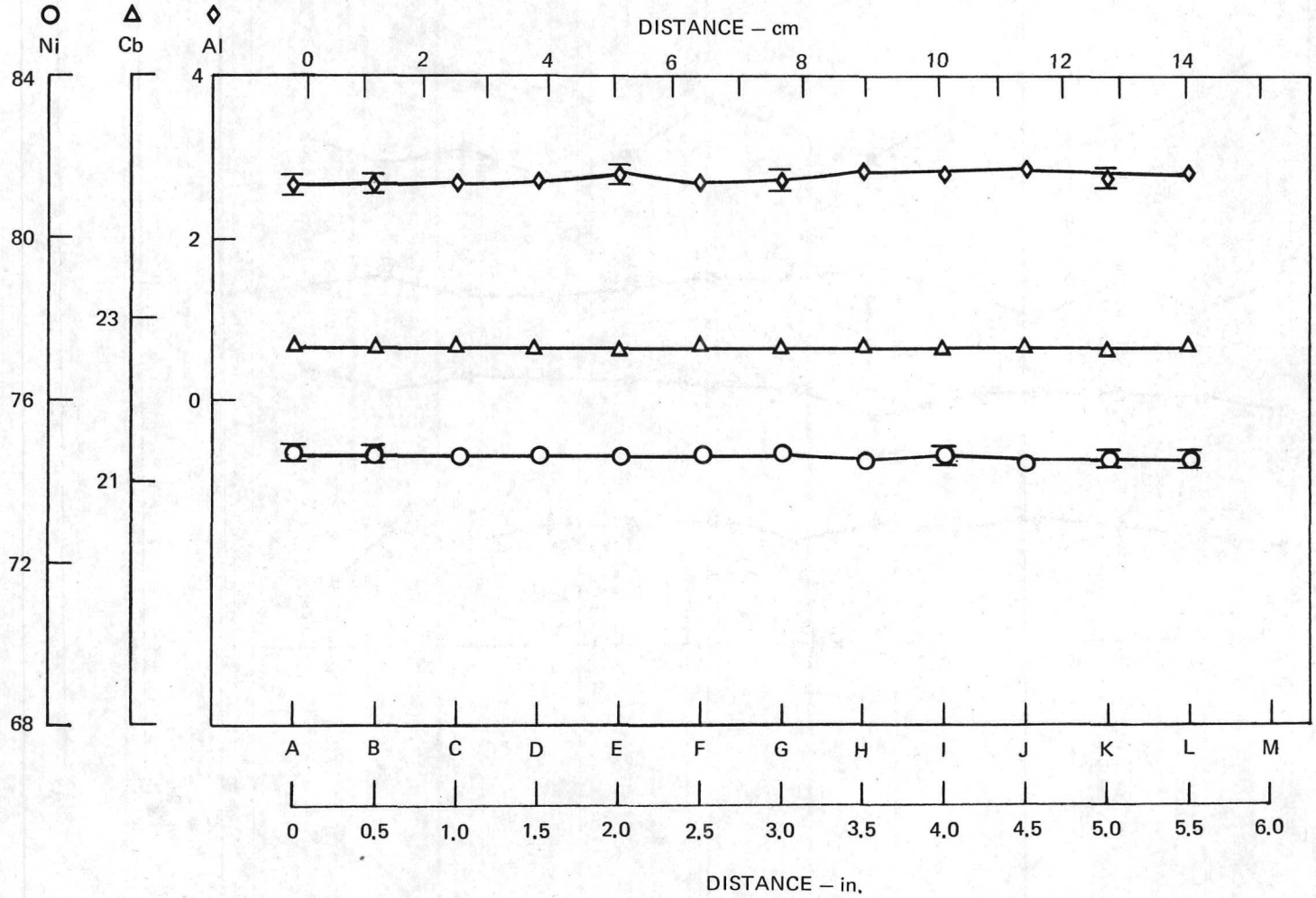

FIGURE 12

Table V

Wet Chemical and X-ray Fluorescence Analyses of the Head and Tail Ends of Directionally Solidified Specimen, A72-488 (71.8 w/o Ni-19.7 w/o Cb-6.0 w/o Cr-2.5 w/o Al)

Wet Chemical Analyses:

Identification		Ni w/o	Cb w/o	Cr w/o	Al w/o	Total w/o
A72-488 H		72.16	19.82	5.89	2.44	100.31
" duplicate		71.45	19.83	5.86	2.42	99.56
	Avg.	71.81	19.82	5.88	2.43	99.94
A72-488 T		71.22	20.01	5.94	2.75	99.92
" duplicate		71.72	20.13	6.07	2.59	100.51
	Avg.	71.47	20.07	6.00	2.67	100.21

X-ray Fluorescence Analyses:

A72-488 H		72.34	19.69	5.91	2.35	100.29
" duplicate		72.29	20.03	5.91	2.26	100.49
	Avg.	72.31	19.86	5.91	2.31	100.39
A72-488 T		71.39	20.10	6.11	2.41	100.01
" duplicate		71.88	19.91	5.90	2.41	100.10
	Avg.	71.64	20.00	6.00	2.41	100.05

Table VI

Chemical Analyses of Directionally Solidified Ni,Cr-Ni_3Cb (Ni)/(Ni_3Al)-Ni_3Cb and (Ni,Cr)/(Ni_3Al)-Ni_3Cb

Specimen No.		Ni w/o	Cb w/o	Cr w/o	Al w/o	Total w/o
A71-351	charged	73.0	21.0	6.0	--	100.00
	analyzed	73.0	21.0	5.97	--	99.97
A71-766	charged	70.3	19.7	10.0	--	100.00
	analyzed	70.1	19.6	9.96	--	99.66
A71-695	charged	76.5	21.0	--	2.5	100.00
	analyzed	76.8	20.9	--	2.5	100.20
A71-651	charged	76.4	20.8	--	2.8	100.00
	analyzed	76.1	20.8	--	2.82	99.72
A71-711C	charged	71.5	20.0	6.0	2.5	100.00
	analyzed	71.5	19.2	5.92	2.54	99.16
A71-766B	charged	70.3	19.7	9.0	1.0	100.00
	analyzed	70.5	19.5	8.79	0.96	99.75

and 10 were first prepared. Trough compositions were estimated from the work of Cbeyhnkob and Pan (Ref. 30) and refined by the iterative steps illustrated in Fig. 13. In the event an alloy grew dendritically or with a cellular interface, compositional and/or solidification parameters, i.e. ratio of gradient to solidification rate (G/R), were adjusted to locate, by microstructural response, alloys which produced aligned biphase composite microstructure. The aligned biphase microstructures of three monovariant eutectic alloys are shown in Fig. 14. In alloys of these compositions the chromium content within the matrix varied from zero to 35 percent by weight. The volume percentage δ Ni_3Cb was found to increase with increasing chromium content from ~32 percent by volume for zero percent chromium (i.e. γ-δ binary eutectic) to ~39 and ~43 percent for monovariant eutectic alloys containing 6 and 10 w/o Cr respectively. The Ni,Cr-Ni_3Cb monovariant alloys with increasing Cr content required a higher thermal gradient in the liquid for growth with a planar L/S interface because of its increased melting range (liquidus-solidus, ΔT). For example, even with a high purity Ni - 20 w/o Cb - 10 w/o Cr alloy, cellular microstructure was produced at R = 2 cm/hr, G $\simeq$ 70°C/cm. Growth of these alloys at such rates thus required the attainment of plane front conditions in a high gradient (i.e. 250-350°C/cm) apparatus, Figs. 2 and 3. During these experiments an alumina-melt reaction was encountered which entrained an undesirable dendritic Al_2O_3 base phase within the aligned composite microstructure and grain boundaries. This reaction was minimized by decreasing superheat and increasing the freezing velocity but both changes lowered the G/R ratio which was undesirable for plane front growth. Remarkably the presence of this third phase did not break down the advancing planar liquid solid interface; however, its presence was detrimental to the mechanical properties of the material. A microbeam probe investigation of the composition of the dendritic third phase indicated it was primarily Al_2O_3. The quantitative electron microbeam probe analysis of this phase formed within the monovariant specimen of nominal composition Ni - 21.0 w/o Cb - 6.0 w/o Cr is presented in Table VII. The observed vertical phase segregation was believed to be associated with the change in liquid composition from dissolution of Al_2O_3 leading to oxide precipitation and density segregation.

No metal-mold reactions were observed in directional solidification experiments using BeO crucibles even at a maximum superheat of 400°C. This solution to the above described problem had two distinct disadvantages - these being the toxicity and expense of BeO. Fortunately, as will be described below, all the Ni-Cr-Cb alloys containing over 1 w/o aluminum were compatible with Al_2O_3. Successful containment of each alloy, even for prolonged periods of contact, i.e. solidification rates below 2 cm/hr, at superheats in excess of 400°C with 99.95 percent Al_2O_3 crucibles was achieved.

3.2.2 Ni,Al-Ni_3Cb

Alloys along the monovariant trough in the Ni-Al-Cb system whose composition loci are defined as the line between the binary eutectic reaction, $E_b \rightarrow \gamma$ Ni + δ Ni_3Cb, and the ternary reaction, $E \rightarrow \gamma$ Ni + δ Ni_3Cb + γ' Ni_3Al shown in Figs. 7

ITERATION FOR MICROSTRUCTURAL IMPROVEMENT
OF Ni–Cr–Cb–Al EUTECTIC ALLOYS

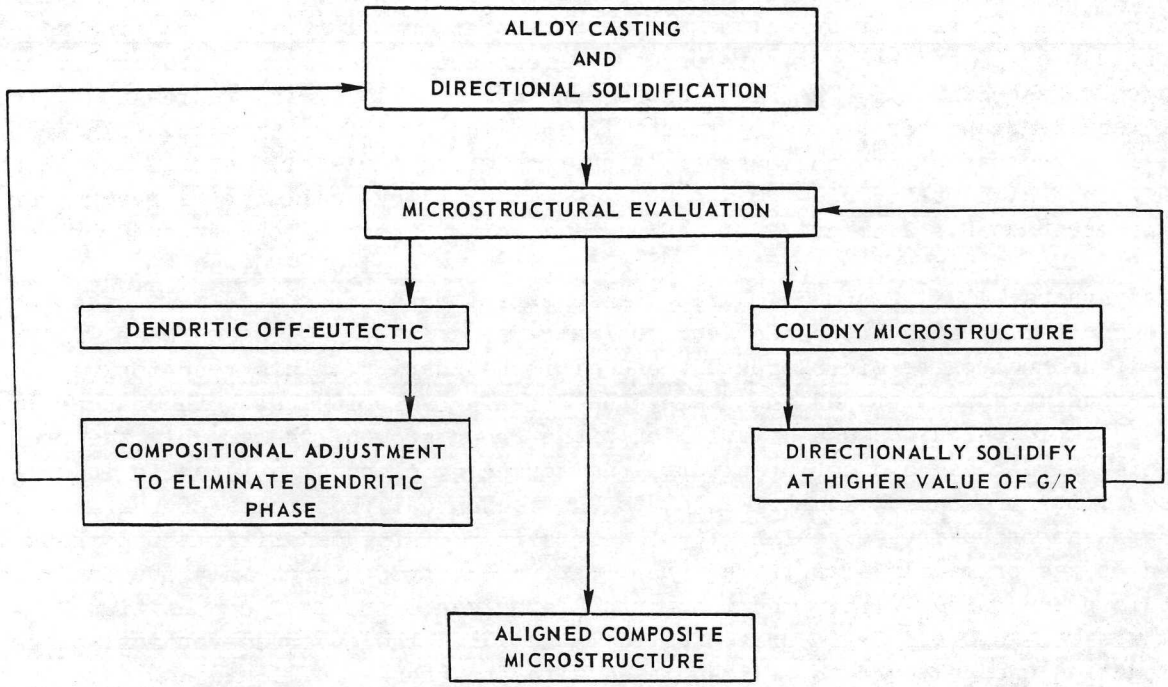

FIGURE 13

LONGITUDINAL SECTIONS OF DIRECTIONALLY SOLIDIFIED MONOVARIANT EUTECTIC COMPOSITIONS BETWEEN γ – NICHROME AND δ – Ni_3Cb

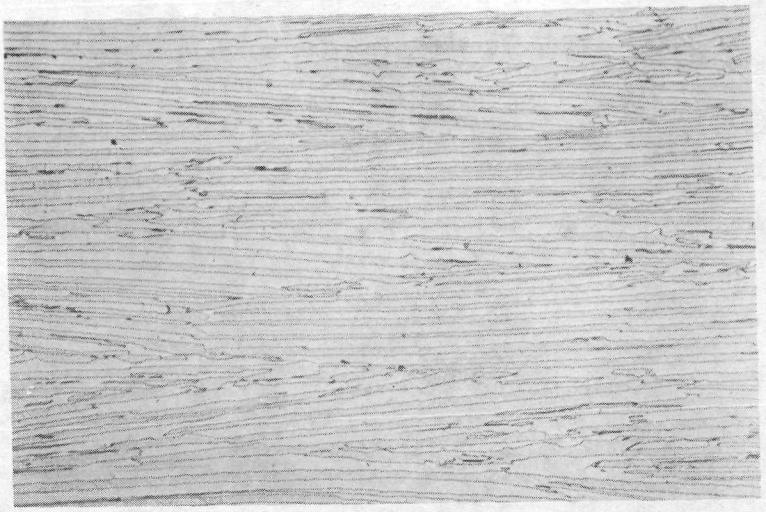

A71–297C
73 Ni, 21 Cb, 6 Cr
X200

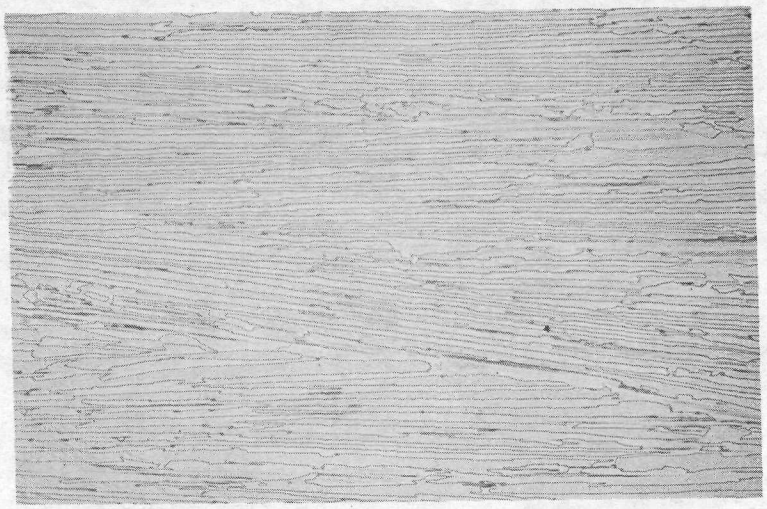

A71–109C
71 Ni, 20 Cb, 9 Cr
X200

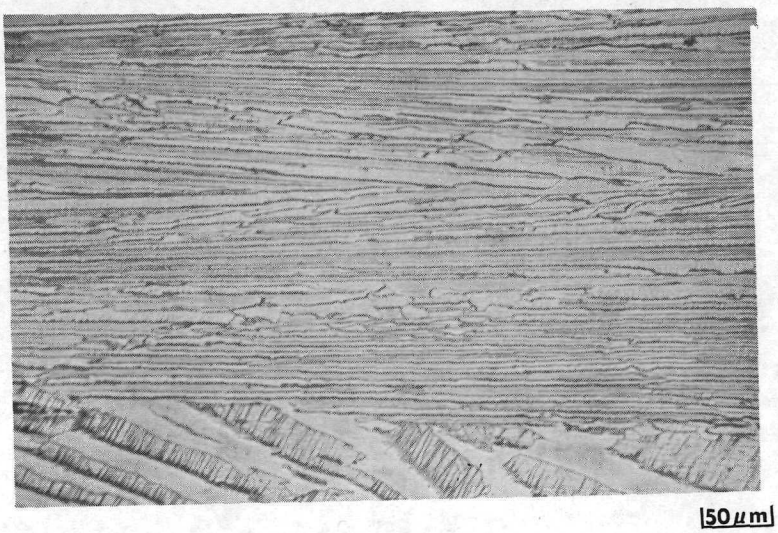

A71–297B
69 Ni, 19 Cb, 12 Cr
X200

50 μm

FIGURE 14

Table VII

Microbeam Probe Analysis of Ni,Cr-Ni_3Cb Alloy
Containing Mold Reaction Product

	Composition, Weight Percent				
	Al	Cb	Ni	Cr	O
Overall Composition	0.15	19.5	72.7	6.9	--
Dendritic Third Phase	38.7	4.0	4.7	8.4	44.3*
γ/γ' Matrix of Eutectic	0.74	21.4	71.5	6.9	--

*determined by difference

and 10 were next produced. Trough compositions were first estimated from the 1200°C (2192°F) isothermal section of the pseudoternary Ni-Ni_3Al-Ni_3Cb by J. Cisse and R. G. Davies (Ref. 31) and refined by the iterative steps discussed above. The aligned biphase microstructures of three monovariant eutectic alloys in this system are shown in Fig. 15. In these alloys the amount of aluminum soluble in the γ nickel matrix varies from 0-4 percent by weight. An important result of this variable aluminum content is the change in the volume percentage γ', Ni_3Al precipitate, i.e. 0 - >50 percent, which forms in the solid state after solidification. The γ' in such alloys has been previously found to be extremely stable due to the low γ-γ' lattice mismatch and to be very hard, i.e. up to 400 dpm (Ref. 31). Aligned microstructures in the low gradient apparatus were produced with comparative ease along this monovariant trough, as the liquidus slope from the binary eutectic between Ni and Ni_3Cb to the ternary eutectic between Ni, Ni_3Cb and Ni_3Al is very shallow (Fig. 10).

All the Ni,Al-Ni_3Cb monovariant eutectic alloys, i.e. 1.0-3.0 w/o Al, froze with a planar interface even at the lowest thermal gradients studied and produced well aligned lamellar microstructures. Fig. 16. For these alloys, no one of which possesses a melting range greater than 5 degrees Celsius, the critical value of G/R is ~5°C hr cm^{-2}. With respect to the foundryman's endeavor to control microstructure in a complex shape, this property is a highly desirable one.

Since improvements in the yield and creep strength of δ Ni_3Cb reinforced γ' Ni_3Al were shown to be derived from increases in solidification velocity (Ref. 2), experiments investigating the range of coupled growth in the monovariant Ni,Al-Ni_3Cb system were performed. The results of these experiments are presented in Table VIII and Fig. 17. Previous studies of binary eutectic structures (Refs. 32-34) have indicated that coupled eutectic growth is favored over a large range of compositions when the ratio of thermal gradient in the liquid ahead of the freezing interface to the freezing velocity, G/R, is high. Thus when primary γ dendrites were observed together with aligned lamellae in the microstructures of the Ni - 21.0 w/o Cb - 2.5 w/o Al alloy, directionally solidified at multiple rates between 5 and 15 cm/hr (see Table VIII), skewed coupled growth was indicated. A plot of the microstructurally determined dendrite-aligned monovariant eutectic transition is presented in Fig. 18. As shown in Ref. 35, the conditions for eutectic stability only approximate a simple dependence on the ratio, G/R, for high values of G. In the present experiments the thermal gradient was kept at approximately 300°C/cm by control of the maximum superheat in the high gradient growth apparatus and only the freezing velocity was varied. A smaller composition envelope for coupled growth was observed in comparison to those generated for the simple binary eutectics Al-$CuAl_2$ (Ref. 33) and Pb-Sn (Refs. 32-34). The reason for this phenomenon is obscure at present but it may be associated with an appreciable kinetic undercooling behavior of the δ Ni_3Cb phase. Observations of δ Ni_3Cb dendrites in the present investigation have indicated that this phase forms from a faceted growth interface and has a strong tendency to grow in the [100] direction.

LONGITUDINAL SECTIONS OF DIRECTIONALLY SOLIDIFIED MONOVARIANT EUTECTIC COMPOSITIONS BETWEEN γ (Ni,Al) AND δ (Ni_3 Cb)

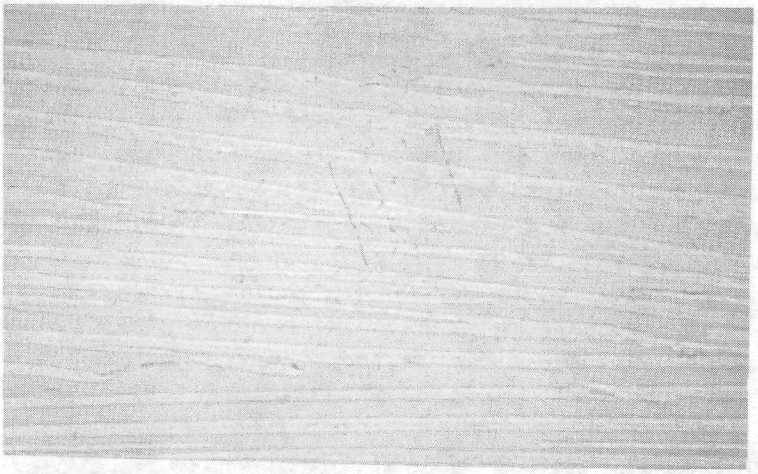

A71 – 508C
Ni, 22.1 Cb, 1.1 Al
X500

A71 – 508A
Ni, 22.3 Cb, 1.6 Al
X500

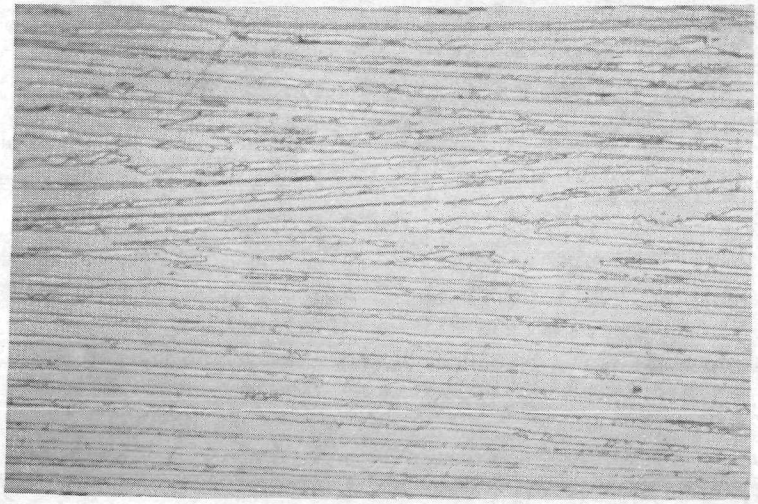

A71 – 535
Ni,22 Cb, 2.4 Al
X500

FIGURE 15

TRANSVERSE MICROSTRUCTURE OF DIRECTIONALLY SOLIDIFIED $\gamma/\gamma'-\delta$
(Ni–20.8 w/o Cb–2.8 w/o Al) R = 2 cm/hr, $G_L \sim 70^\circ$ C/cm

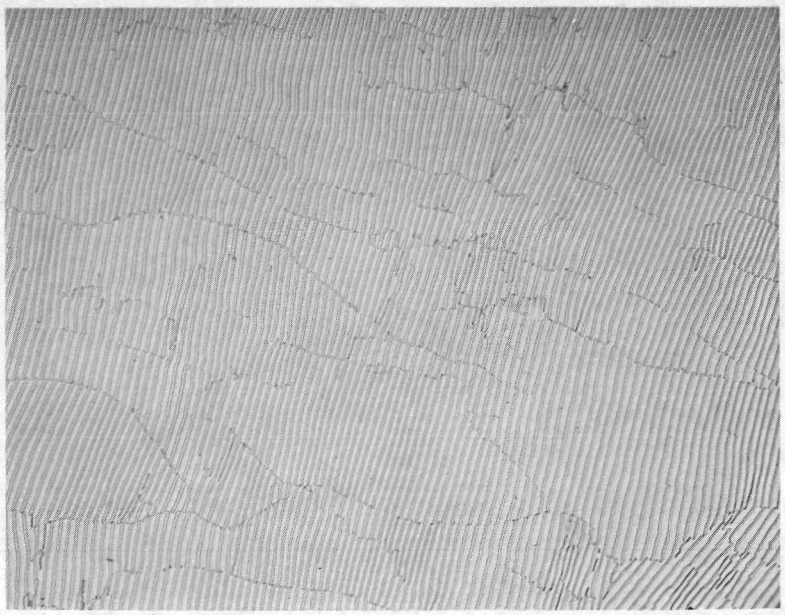

50μm

FIGURE 16

Table VIII

Summary of Freezing Velocity Effects on the Microstructure and Composition of γ/γ'-δ, Nominally Ni - 21.0 w/o Cb - 2.5 w/o Al

Specimen Number	Composition (w/o)	D.S.* Furnace	Freezing Rate (cm/hr)	$R^{-1/2}$ $(cm/sec)^{-1/2}$	λ (μm)	Microstructure Comments
A72-506	Ni 21.0Cb-2.5Al	L.G.	2.0	42.4	$5.8^{+.7}_{-.6}$	3.17 cm (1 1/4 in.) dia Al_2O_3 crucible**, aligned lamellar
A72-325	Ni 21.0Cb-2.5Al	H.G.	5.0	26.8	$3.1^{+.3}_{-.4}$	aligned lamellar
A72-536	Ni 21.0Cb-2.5Al	L.G.	5-15	26.8-15.5	---	no bands
A72-543	Ni 21.0Cb-2.5Al	L.G.	15.0	15.5	---	dendritic γ/γ'
A72-561	Ni 21.5Cb-2.5Al	L.G.	5-15	26.8-15.5	---	rerun: A72-596
A72-572	Ni 20.8Cb-2.8Al	L.G.	5-15	26.8-15.5	---	increasing primary γ/γ', no bands
A72-577	Ni 21.25Cb-2.5Al	L.G.	5-15	26.8-15.5	---	increasing primary after 10 cm/hr, banded
A72-596	Ni 21.5Cb-2.5Al	L.G.	8.0	21.3	---	lost charge, run out
A72-603	Ni 21.0Cb-2.5Al	H.G.	10.0	19.0	---	primary γ/γ'
A72-623	Ni 21.5Cb-2.5Al	H.G.	10.0	19.0	$2.6^{+.4}_{-.7}$	aligned lamellar
A72-608	Ni 21.5Cb-2.5Al	L.G.	8.0	21.3	---	slightly primary in δ
A72-625	Ni 20.8Cb-2.8Al	H.G.	7.5	21.9	---	aligned lamellar
A72-640	Ni 22.0Cb-2.5Al	H.G.	20.0	13.4	---	slightly primary in δ
A72-657	Ni 21.75Cb-2.5Al	H.G.	25-28.8	12.0	$1.6^{+.1}_{-.1}$	very slightly primary in δ

Table VIII (cont'd)

Specimen Number	Composition (w/o)	D.S. Furnace	Freezing Rate (cm/hr)	$R^{-1/2}$ $(cm/sec)^{-1/2}$	λ (μm)	Microstructure Comments
A72-663	Ni 21.5Cb-2.5Al	H.G.	25.0	12.0	---	aligned lamellar
A72-669	Ni 21.67Cb-2.5Al	H.G.	38.4	9.7	$1.2^{+.4}_{-.1}$	very slightly primary in γ/γ'
A72-678	Ni 22.0Cb-2.5Al	H.G.	38.0	9.74	---	primary δ
A72-679	Ni 22.0Cb-2.5Al	H.G.	50.5	8.4	$1.0^{+.1}_{-.2}$	very slightly primary in δ
A72-690	Ni 22.0Cb-2.5Al	H.G.	75.0	6.9	$0.88^{+.06}_{-.05}$	very slightly primary in γ/γ'
A72-692	Ni 21.8Cb-2.5Al	H.G.	50.0	8.5	---	aligned lamellar
A72-694	Ni 22.2Cb-2.5Al	H.G.	100.0	6.0	$0.78^{+.16}_{-.15}$	slightly primary in γ/γ'

*(L.G.) low thermal gradient ~70°C/cm, (H.G.) high thermal gradient ~300°C/cm

**All other experiments in 0.95 cm (3/8 in.) dia Al_2O_3 crucibles

TRANSVERSE MICROSTRUCTURES OF $\gamma/\gamma' - \delta$ MONOVARIANT EUTECTIC ALLOYS AS A FUNCTION OF FREEZING VELOCITY

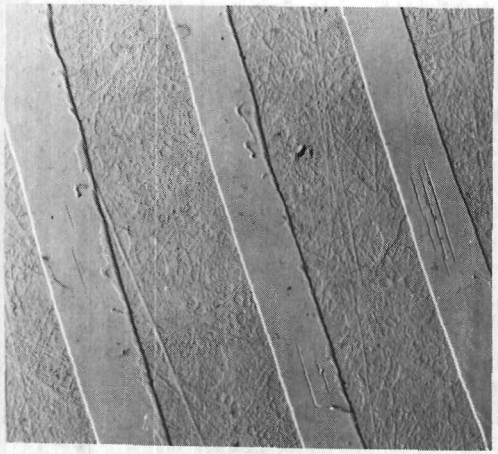

A72–506, 2 cm/hr 2 μm

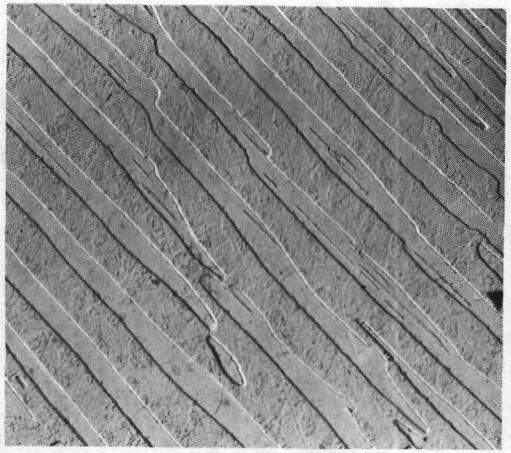

A72–663, 25 cm/hr 2 μm

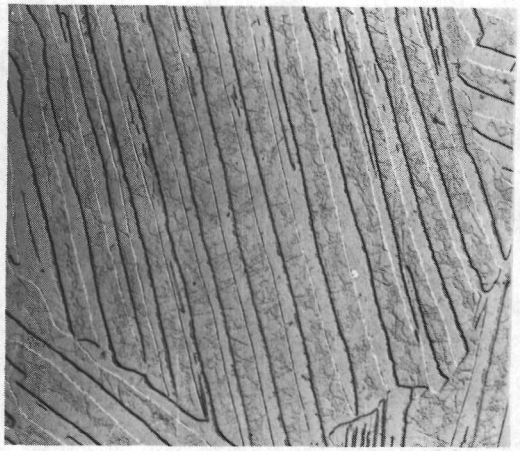

A72–669, 38.4 cm/hr 2 μm

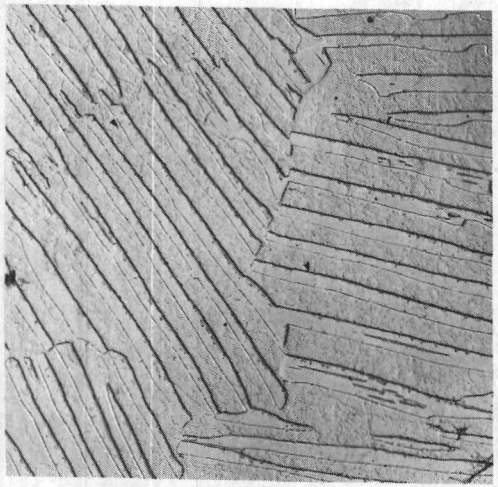

A72–679, 50.5 cm/hr 2 μm

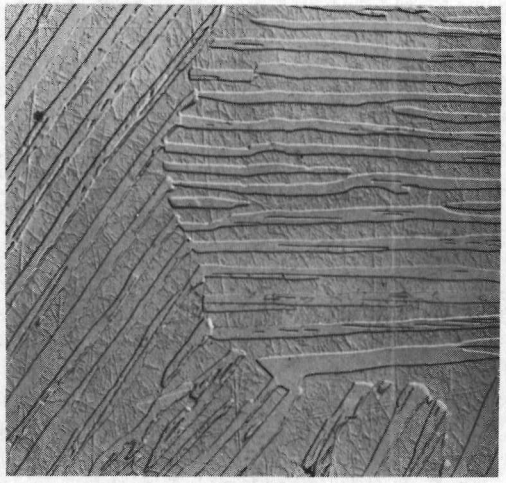

A72–690, 75.0 cm/hr 2 μm

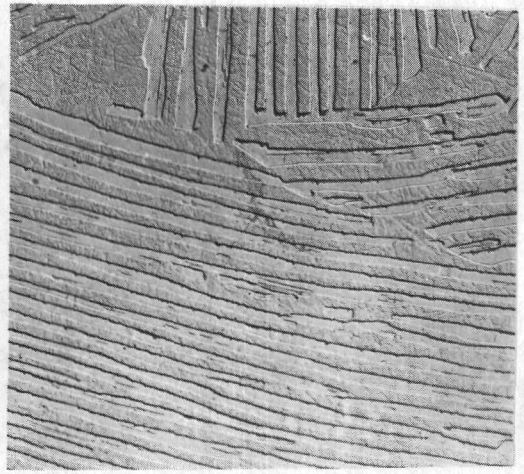

A72–694, 100 cm/hr 2 μm

FIGURE 17

PLOT OF THE DENDRITE–MONOVARIANT EUTECTIC TRANSITION FOR THE $Ni/Ni_3Al–Ni_3Cb$ ($\gamma/\gamma'-\delta$) SYSTEM AT 2.5% Al

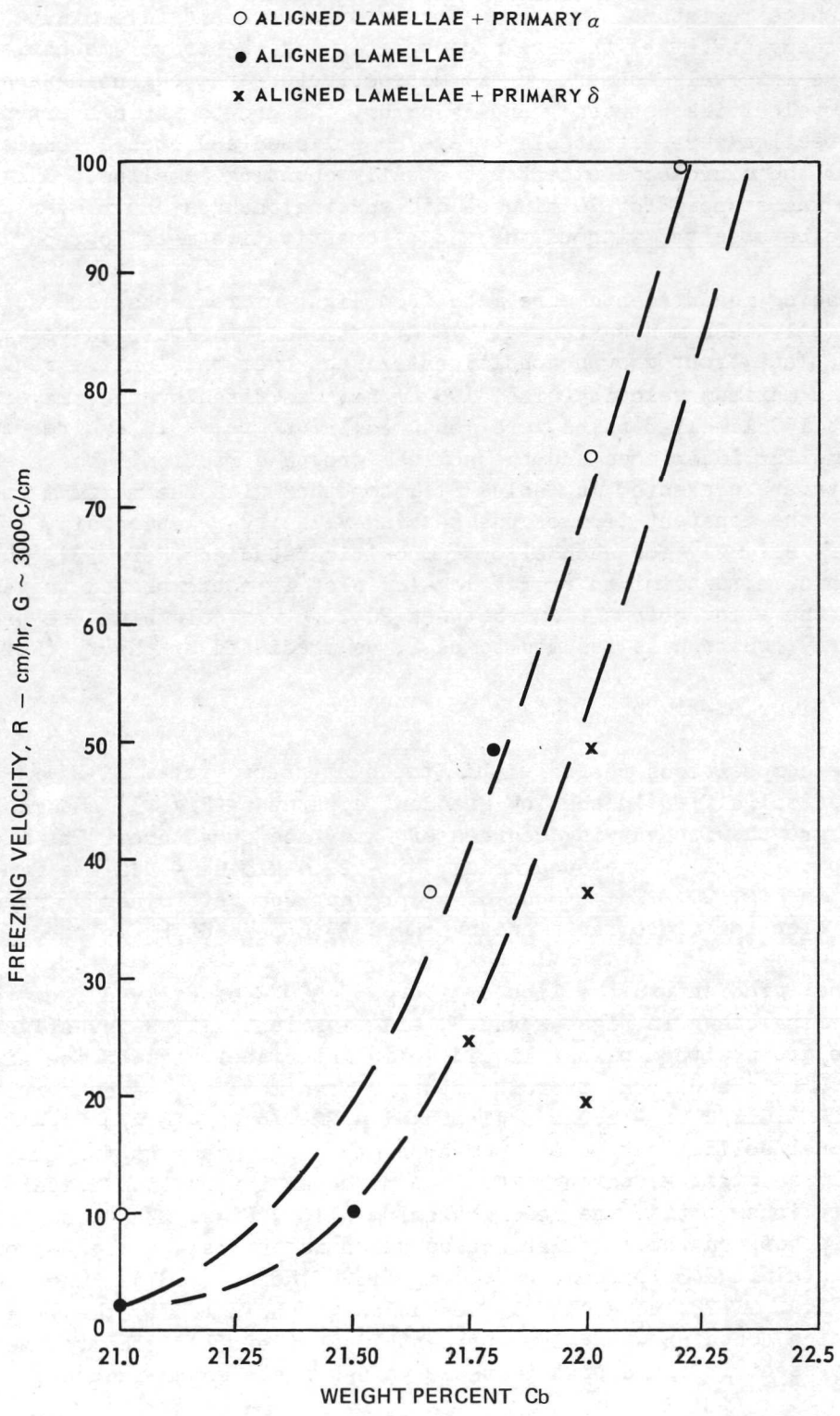

FIGURE 18

It was also surprising to note that banding (defined as an interlamellar spacing change) could not easily be induced in directional solidification experiments in the low gradient graphite resistance furnace. For example, one and five minute perturbations to the steady state growth were made by stopping the travel mechanism at six predetermined time intervals to mark on the microstructure the beginning and end of various freezing velocities between 5 and 15 cm/hr. No growth striae perpendicular to the growth direction were detectable by eye on polished and etched longitudinal surfaces or under the microscope except by actually counting lamellae. Only when the travel mechanism was stopped for 10 minutes did spacing changes occur over a sufficient distance to be observed without the aid of quantitative metallography.

Lamellar spacing measurements were made from light micrographs (1000X) and electron micrographs of Ni,Al-Ni_3Cb monovariant alloys directionally solidified between 2-100 cm/hr. Essentially plane front growth conditions existed over this entire range of growth velocities and the maximum velocity, i.e. 100 cm/hr, was fixed by the traversing mechanism. About 150 lamellar pairs were measured in subgrains in a direction at right angles to the lamellar interfaces and the nominal growth direction. The averages of these measurements are presented in Table VIII, together with the maximum and minimum values. Although the constant term of the spacing-velocity relationship, $\lambda^n R$ = constant, may vary slightly for each alloy composition studied (Ref. 33), the slope of the relationship, n, determined from a log-log plot is not expected to vary. Thus, the data for all the alloy compositions between 20-22.5 w/o columbium are presented together in Fig. 19, where n is assumed to be 2, as predicted by theory (Ref. 36).

3.2.3 Ni,Cr,Al-Ni_3Cb

Alloys whose compositions reside within the quaternary system Ni-Ni_3Al-Ni_3Cb-'Ni_3Cr' were first solidified in the low gradient apparatus (Fig. 1) and resulted in cellular coupled growth with varying degrees of interface curvature. The microstructure within a typical cell of one such alloy, Ni - 20.5 w/o Cb - 9.2 w/o Cr - 2.21 w/o Al, is shown in Fig. 20. The amount of γ' present was determined by areal analysis on four electron micrographs and averaged 35.6 percent by volume.

Using a higher gradient in the liquid, i.e. 250-350°C/cm derived from the use of a water spray ring shown in Figs. 2 and 3, all bivariant alloys investigated, Table I, could be grown with a planar liquid solid interface provided the growth rate was appropriate. The plane front microstructure of two more γ/γ'-δ quaternary alloys, Ni - 19.7 w/o Cb - 9.0 w/o Cr - 1.0 w/o Al and Ni - 20 w/o Cb - 6 w/o Cr - 2.5 w/o Al after directional solidification at 2 cm/hr in the high gradient furnace, are shown respectively in Figs. 21 through 24. One notes an interesting comparison for the transverse sections in that the lower chromium alloy, Figs. 23-24, has less regular interfaces between the lamellar phases which is typical of the γ-δ eutectic microstructure containing ~32 percent by volume Ni_3Cb (Refs. 22,37). The high chromium alloy, Figs. 21-22, more closely resembles morphologically the γ'-δ eutectic microstructure which contains ~44 volume percent Ni_3Cb (Ref. 1). The volume percentage δ Ni_3Cb present in these bivariant alloys was again determined by lineal

INTERLAMELLAR SPACING OF $\gamma/\gamma' - \delta$; (Ni–21.0–22.2 w/o Cb 2.5 w/o Al)
AS A FUNCTION OF FREEZING RATE

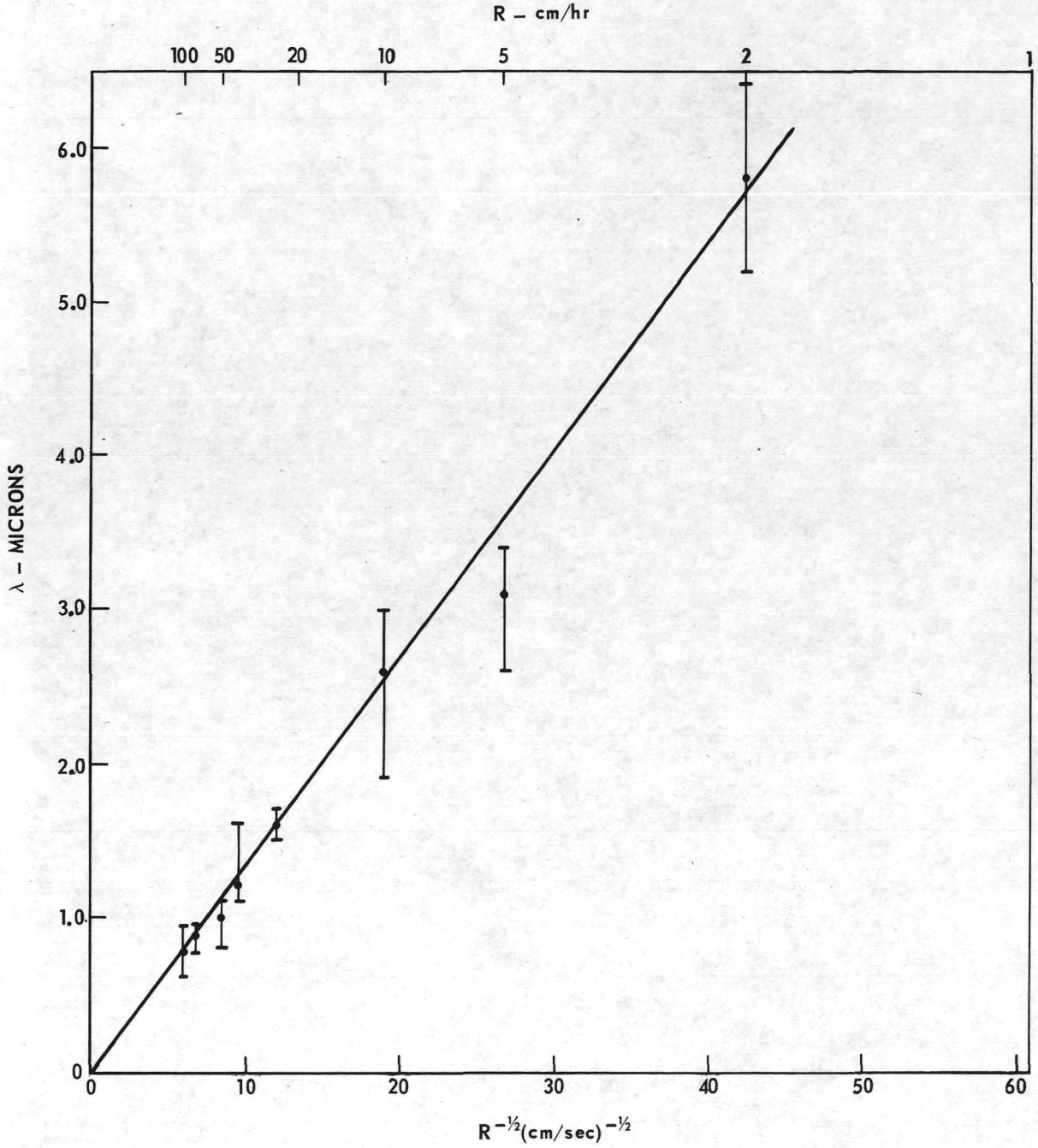

FIGURE 19

Ni_3 Al (γ') PRECIPITATION HARDENED, NICHROME (γ) – Ni_3 Cb (δ) EUTECTIC

Ni –20.5 Cb–9.2 Cr–2.2 Al

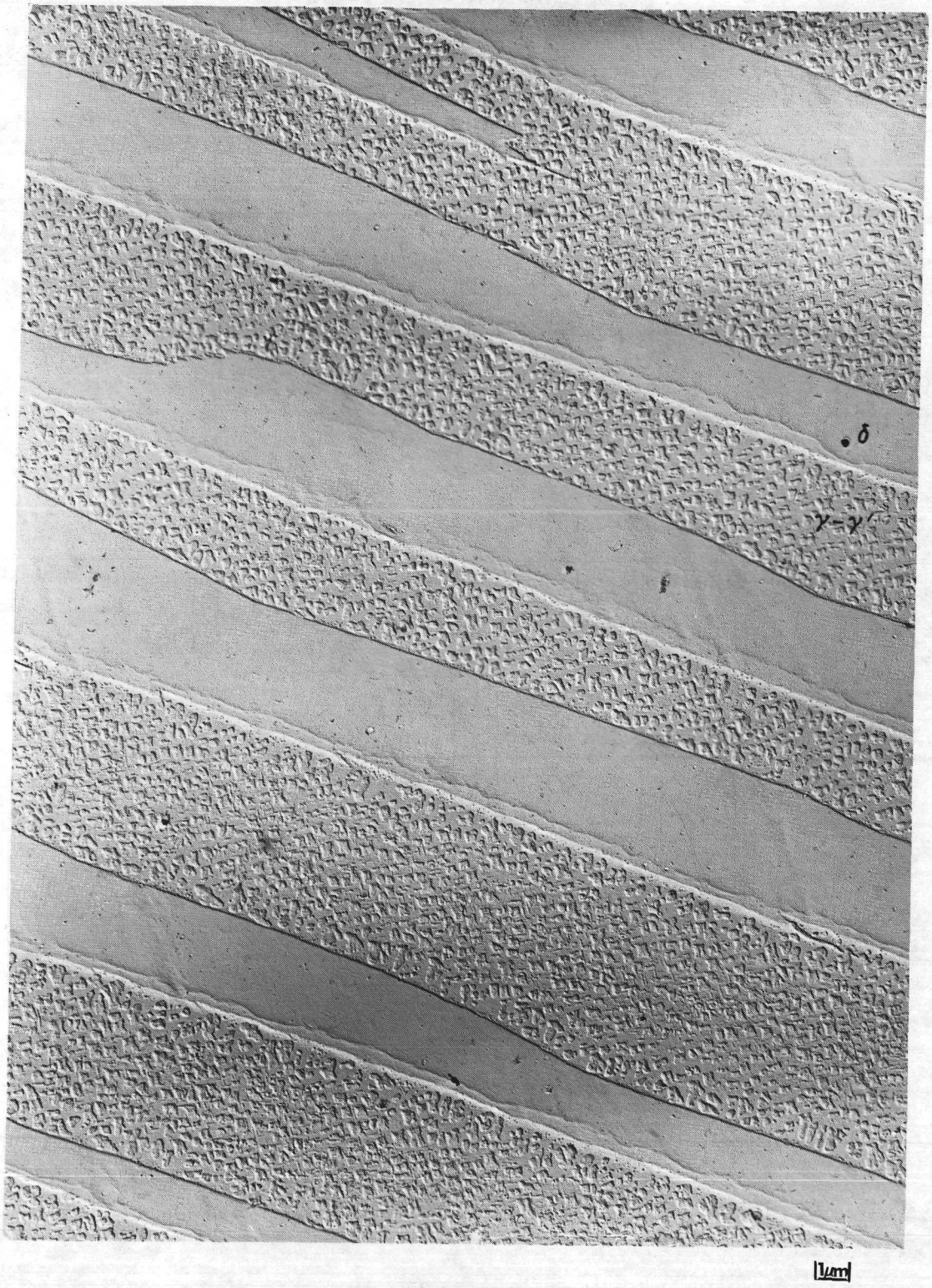

FIGURE 20

MICROSTRUCTURE OF THE D.S. BIVARIANT $\gamma/\gamma' - \delta$ EUTECTIC (Ni 70.3 w/o, Cb 19.7 w/o, Cr 9.0 w/o, Al 1.0 w/o)

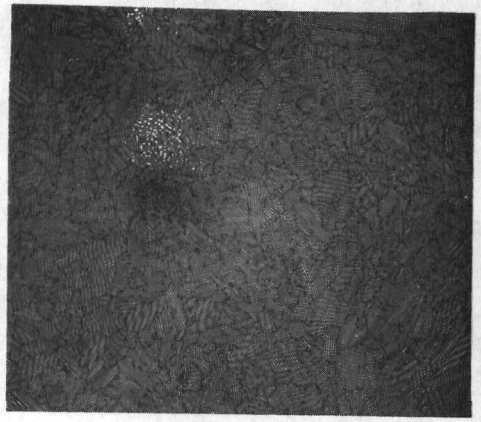

100μm

TRANSVERSE

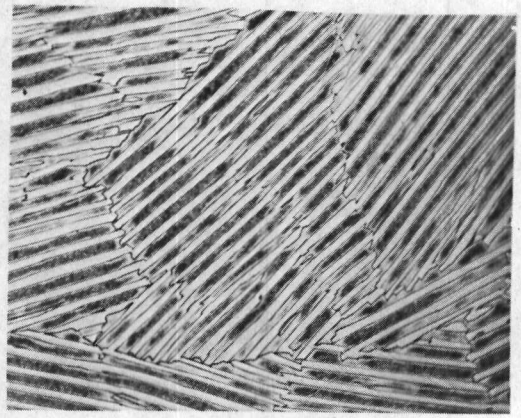

10μm

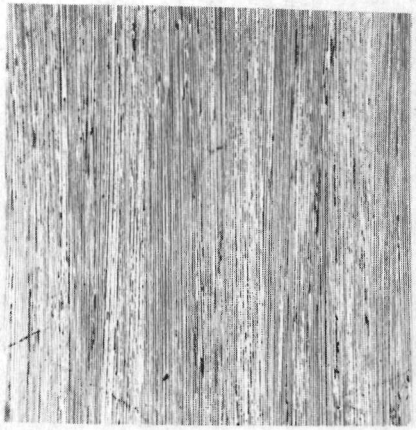

100μm

LONGITUDINAL

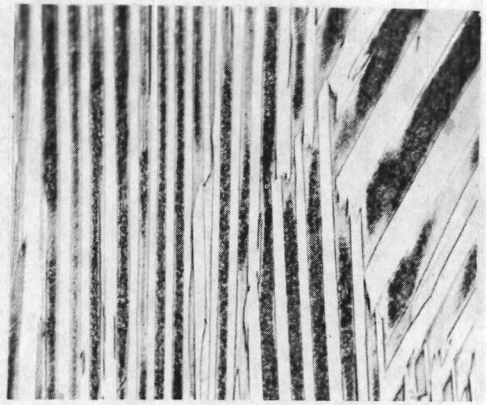

10μm

FIGURE 21

REPLICA OF ($\gamma'\gamma''$) PRECIPITATION HARDENED, γ NICHROME – δ Ni_3Cb

Ni – 19.7 Cb – 9.0 Cr – 1.0 Al (A72 – 097)

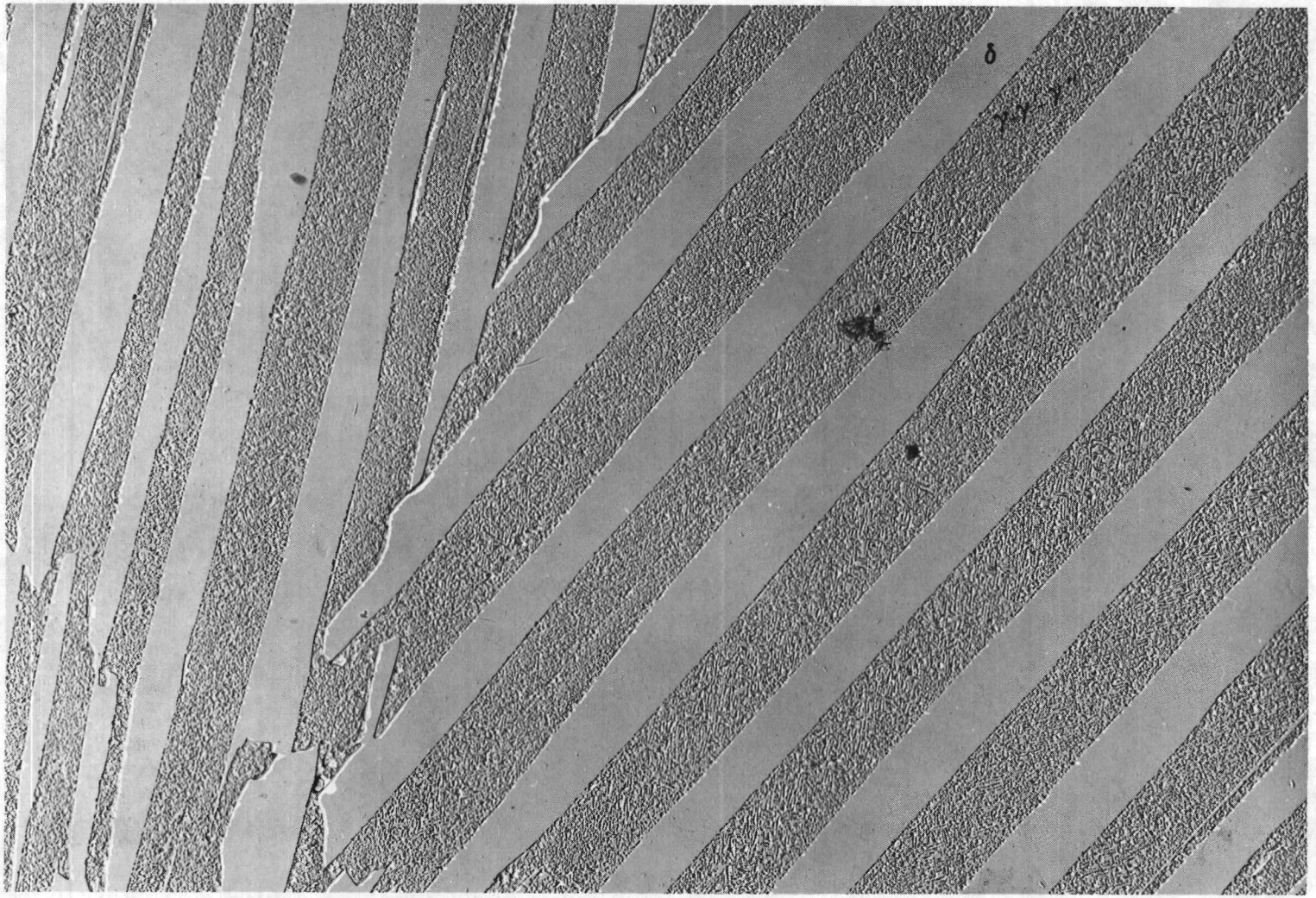

FIGURE 22

MICROSTRUCTURE OF THE D. S. BIVARIANT $\gamma,\gamma'-\delta$ EUTECTIC
Ni 71.5 w/o, Cb 20.0 w/o, Cr 6.0 w/o, Al 2.5 w/o

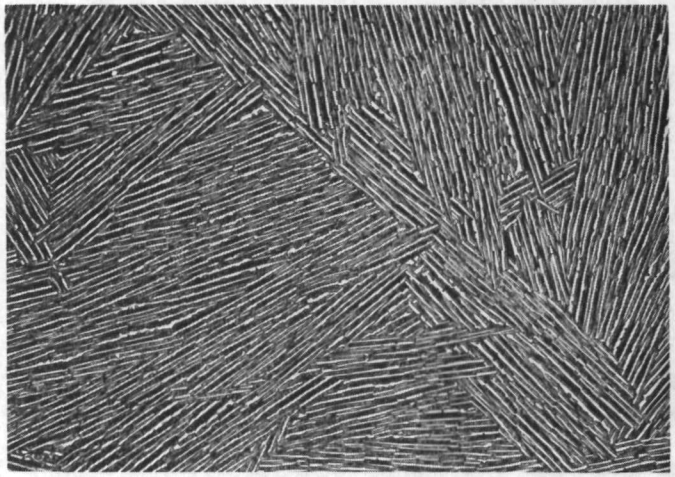

50μm

TRANSVERSE

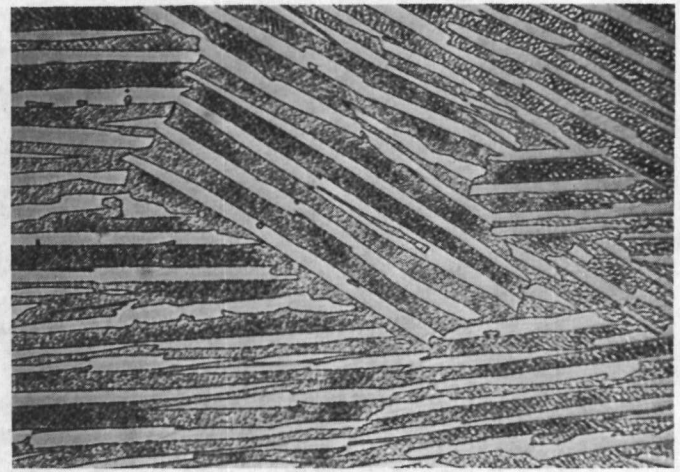

10μm

100μm

LONGITUDINAL

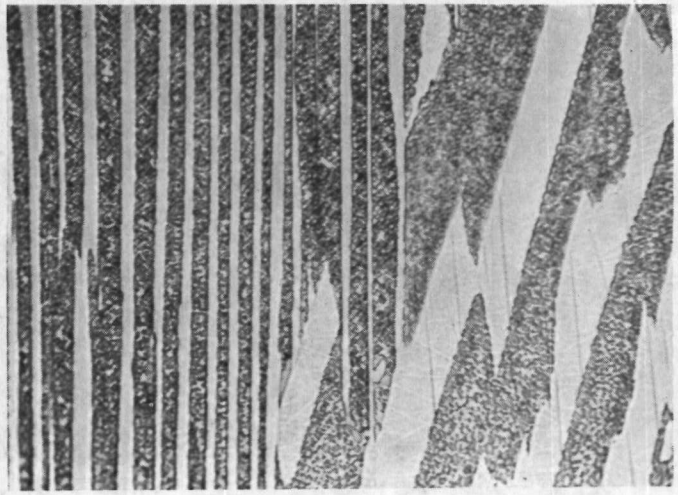

10μm

FIGURE 23

REPLICA OF ($\gamma'\gamma''$) PRECIPITATION HARDENED, γ NICHROME – δ Ni_3Cb

Ni – 20.0 Cb – 6.0 Cr – 2.5 Al (A72 – 197 – OM)

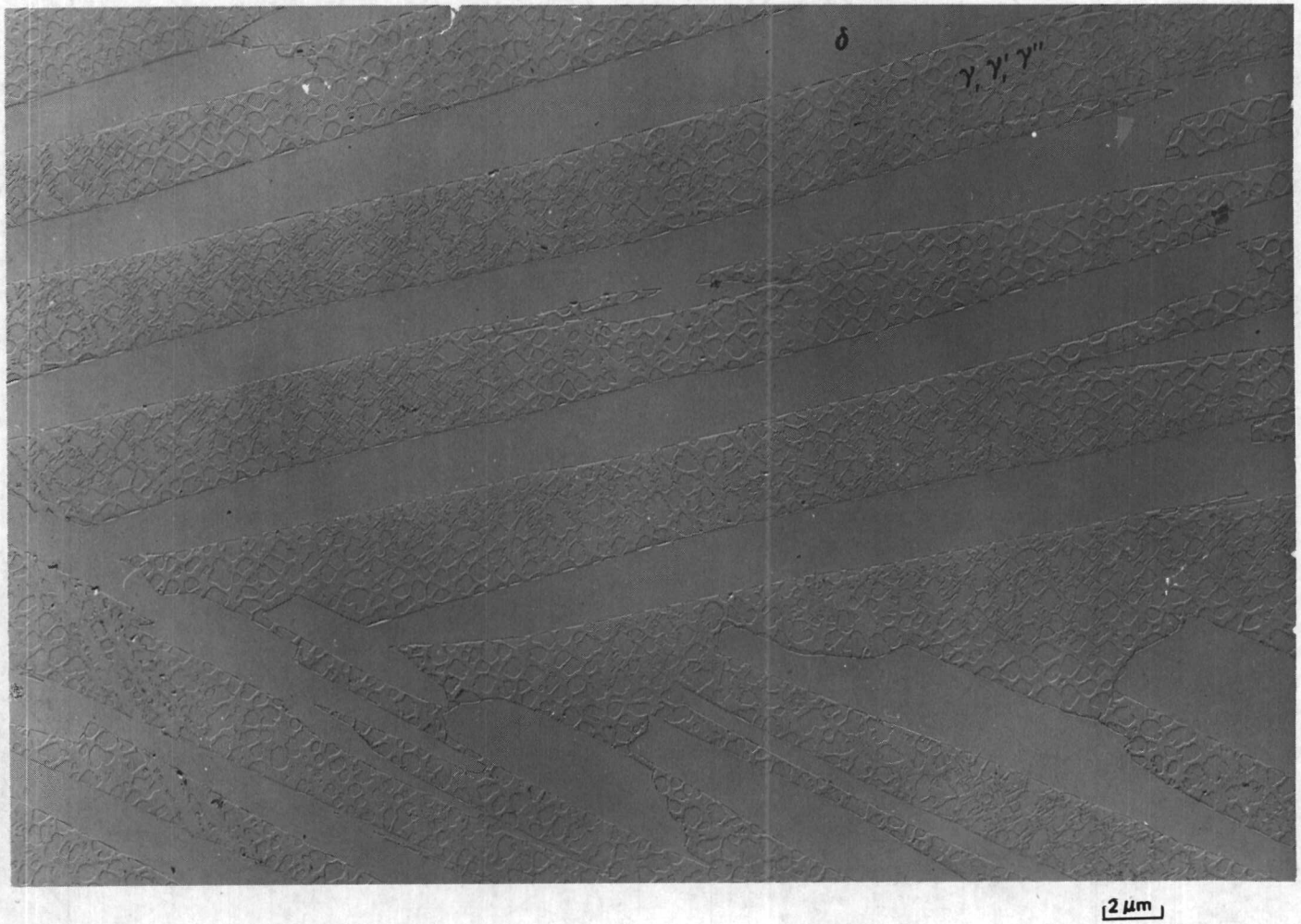

FIGURE 24

analysis of electron photomicrographs of plastic replicas from transverse sections. The Ni - 19.7 w/o Cb - 9.0 w/o Cr - 1.0 w/o Al alloy averaged 42.5 percent by volume δ while the Ni - 20.0 w/o Cb - 6.0 w/o Cr - 2.5 w/o Al alloy averaged 37.3 volume percent δ. Both alloys contained both gobular γ', Ni_3Al precipitates and what morphologically appears to be lath-like γ'' b.c.t. Ni_3Cb precipitates (Ref. 25) within the γ nichrome lamellar matrix. The lath-like phase resides parallel to the {100} and {110} planes of γ.

As will be discussed later in the mechanical behavior section, a slight reduction in columbium content was made to the Ni - 20.0 w/o Cb - 6.0 w/o Cr - 2.5 w/o Al alloy to provide improved low temperature ductility. This resulted in the γ/γ'-δ alloy composition: Ni - 19.7 w/o Cb - 6.0 w/o Cr - 2.5 w/o Al. A specimen of this composition was directionally solidified at 0.9 cm/hr and examined by high resolution microscopy. The percentage δ Ni_3Cb was found to be approximately 33. Some δ platelets forming a Widmanstätten structure near eutectic grain boundaries were observed as well as disc-like γ'' and gobular γ' type precipitates. This suggests ways the system has of reducing the columbium supersaturation. Slow δ thickening kinetics appear to limit the thickness of the δ phase which under equilibrium might be expected to occupy over 50 percent of the volume.

From the above measurements of volume percent δ, the composition of the γ/γ' matrix was calculated from the lever principle assuming negligible solubility of chromium in δ. The composition of the γ/γ' matrix thus computed was Ni, 12.4 w/o Cb, 9.1 w/o Cr, and 3.4 w/o Al. Additionally an alloy whose matrix lamellae would contain approximately 16 w/o Cr and 3 w/o Al was computed. This alloy, Ni - 19.5 w/o Cb - 10.5 w/o Cr - 2.0 w/o Al, may possess improved oxidation resistance by virtue of its ability to form a large amount of Al_2O_3.

3.3 γ/γ'-δ Grain Growth and Orientation

The γ/γ'-δ eutectic composites grown from the melt in this program contained various microstructural imperfections, e.g. subgrains and lamellar faults - the structure and suspected origins of which have been treated in some detail in Ref. 38. One interesting observation noted for all the γ/γ'-δ alloy compositions directionally solidified in the high gradient apparatus was the absence of competitive grain growth. A montage of the 1.27 cm (1/2 in.) transverse sections of the γ/γ'-δ alloy, Ni - 19.7 w/o Cb - 6.0 w/o Cr - 2.5 w/o Al, illuminated in a manner to illustrate the changes in grain orientation along the 20 cm of growth, is shown in Fig. 25. Microstructural examination shows the presence of no larger eutectic grains at the end of growth than those present after the first centimeter. Evidence was obtained on three different γ/γ'-δ compositions that indicated one preferred crystallographic relationship between the phases is developed.

MONTAGE MACRO GRAIN STRUCTURES OF $\gamma/\gamma' - \delta$ (Ni – 19.7 w/o Cb – 6.0 w/o Cr – 2.5 w/o Al)
TRANSVERSE TO GROWTH
(DISTANCE FROM NUCLEATION)

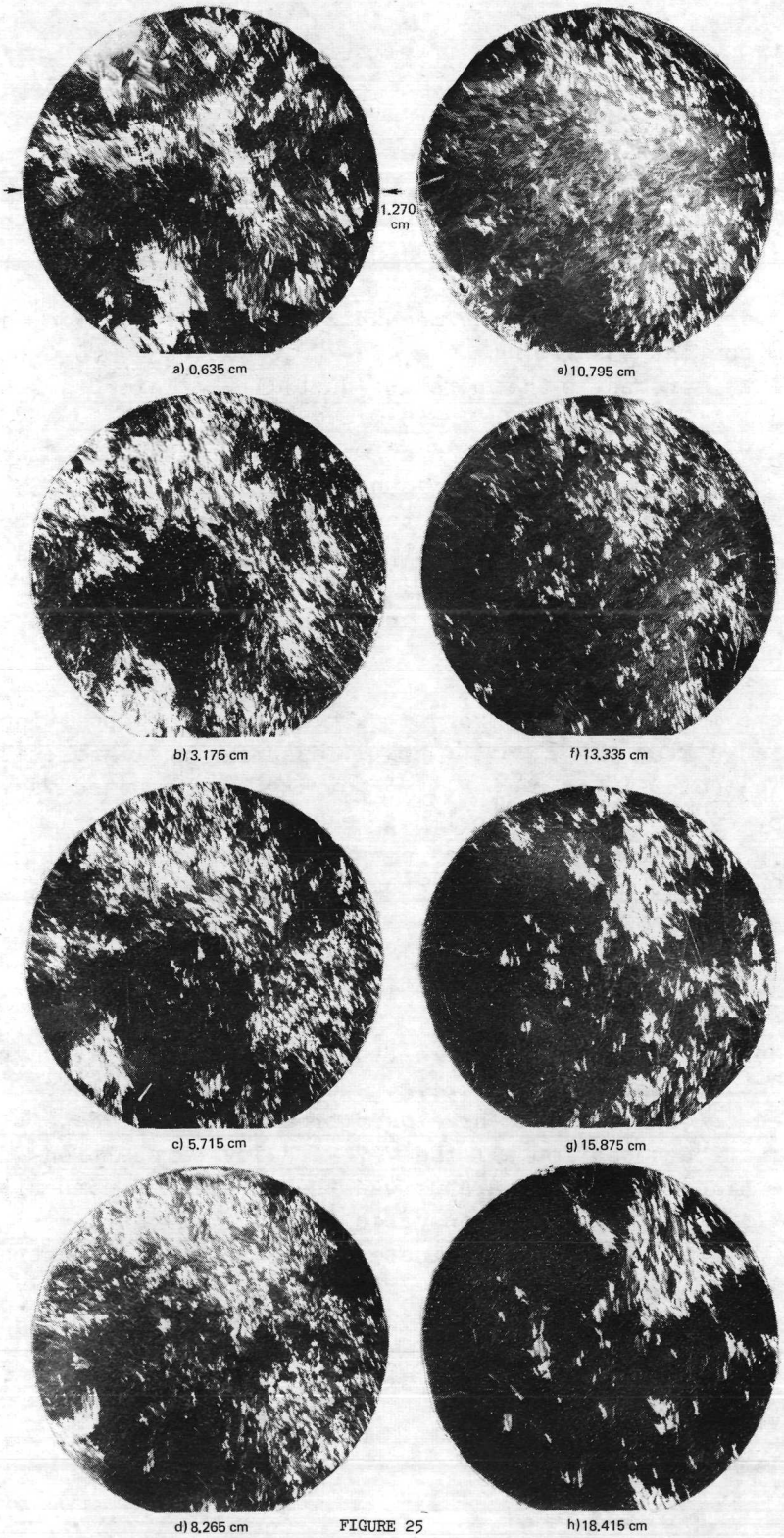

FIGURE 25

A thin foil of Ni - 20.0 w/o Cb - 5.5 w/o Cr - 2.5 w/o Al prepared perpendicular to the growth direction is shown in Fig. 26. Selected area diffraction performed on the eutectic phases singularly and together as shown in Fig. 26 indicated the preferred growth direction was $[1\bar{1}0]\gamma \| [100]_\delta$. The interface plane was parallel to $(111)\gamma$ and $(010)_\delta$. This relationship confirms that previously found (Refs. 1,22,41, 42,43) for both the γ-δ and γ'-δ eutectics and indicates that the cleavage plane of δ and one primary slip plane in γ will be parallel to the stress axis of specimens tested parallel to growth. Splitting of the γ/γ' diffraction spots indicate that a difference in lattice parameter exists for these phases of the Ni - 20.0 w/o Cb - 5.5 w/o Cr - 2.5 w/o Al alloy, the lattice parameter of the γ phase being slightly larger.

3.4 Mechanical Behavior

3.4.1 Background

Previous studies of the γ Ni - δ Ni_3Cb (Refs. 21,22,41) and the γ' Ni_3Al - δ Ni_3Cb (Refs. 1-5) eutectics produced with a lamellar microstructure indicated that the matrix phase γ or γ' was strengthened by the presence of soluble columbium, and the δ Ni_3Cb present as 32 and 44 volume percent of the respective eutectic structures served to reinforce the matrix in a composite sense. Twinning in the δ which leads to fracture was initiated by slip in the γ and γ' phases of these systems. The γ' Ni_3Al - δ Ni_3Cb pseudobinary eutectic becomes considerably stronger as the lamellar spacing decreases, and in fact, both the yield and the tensile strength from room temperature to 1093°C (2000°F) are adequately described by a Hall-Petch correlation (Ref. 2). The γ Ni - δ Ni_3Cb binary eutectic exhibited approximately an order of magnitude greater ductility at room temperature, i.e. >10 percent, than has been observed for lamellar composites of equivalent percentage reinforcement with the exception of the Ni-NiBe eutectic (Ref. 44).

3.4.2 Tensile Properties

Six alloys from the γ-δ lamellar 'eutectic' family were first chosen for tensile stress-elongation characterization between room temperature and 1204°C (2200°F). These alloys listed below in percentage by weight were directionally solidified in the high gradient apparatus except for the Ni,Al-Ni_3Cb alloys #3 and #4 which were produced in the low gradient apparatus:

#1 Ni - 21.0 Cb - 6.0 Cr
#2 Ni - 20.0 Cb - 10.0 Cr
#3 Ni - 21.0 Cb - 2.5 Al
#4 Ni - 20.8 Cb - 2.8 Al
#5 Ni - 20.0 Cb - 6.0 Cr - 2.5 Al
#6 Ni - 19.7 Cb - 9.0 Cr - 1.0 Al

TRANSVERSE SECTION OF γ (Ni, Cr)/γ' Ni_3Al – δ, Ni_3Cb

(72.0 w/o Ni, 20.0 w/o Cb, 5.5 w/o Cr, 2.5 w/o Al)

FIGURE 26

The results of these tensile tests are presented in Table IX. A series of stress elongation curves describing the tensile behavior of each of these alloys at temperatures to 1204°C are shown in Figs. 27-32. As strain was measured in most cases by total crosshead deflection during this initial task of mechanical property screening, the observed values of the elastic modulus were lower than the true values.

3.4.2.1 Room Temperature Tensile Behavior

The room temperature tensile ductility of δ Ni_3Cb reinforced gamma nickel-chromium and gamma/gamma prime matrices contrasted sharply. While only a small degree of plasticity (<2 percent) was observed in the deformation of Ni,Cr-Ni_3Cb specimens (Figs. 27,28), considerable ductility, i.e. up to 30 percent, was exhibited by specimens of Ni,Ni_3Al-Ni_3Cb (Figs. 29,30). This behavior was attributed in part to the differing amounts of aligned δ Ni_3Cb present in each alloy as each matrix individually exhibits considerable tensile elongation. The volume percentage δ in the former alloys was between 39-43 while that of the latter was approximately 33. Assuming that the growth directions of the phases and their crystallographic relationships were identical, as has previously been shown for all analogous δ Ni_3Cb reinforced alloys, the same cooperative twinning and slip mode of coupled deformation of the interpenetrating orthorhombic and f.c.c. phases (Refs. 41,45) would be expected for both these monovariant eutectic alloys. It had indeed also been observed (Refs. 1-4) that the strain to failure of the γ'-δ pseudobinary eutectic is almost entirely elastic, i.e. ~0.1 percent plastic strain, when the δ phase is present in 44 percent by volume. The γ-δ eutectic on the other hand, which contains approximately 32 volume percent δ, exhibited extensive ductility, i.e. ~10 percent plastic strain, as shown in Fig. 33. Examination of room temperature γ'-δ fractures has shown that deformation is inhomogeneous and only observable in the region local to the fracture while γ-δ specimens deformed uniformly over the entire gage length. Copious twinning and cleavage of δ lamellae on {211} planes was observed for γ-δ (Ref. 45); the same active twinning and fracture plane was observed in the inhomogeneous deformation of γ'-δ (Ref. 2). Since the amount of plastic strain at fracture decreases with increasing volume percent reinforcement, fracture of the δ, Ni_3Cb lamellae may be critical because of the higher stress at which cracks form and because there is a smaller volume of ductile material to deform for crack accommodation.

The bivariant quaternary alloys, Ni - 20.0 w/o Cb - 6.0 w/o Cr - 2.5 w/o Al, and Ni - 19.7 w/o Cb - 9.0 w/o Cr - 1.0 w/o Al, exhibited a decrease in room temperature ductility compared with that observed in the Ni,Al-Ni_3Cb monovariant eutectic alloys as seen in Table IX and Figs. 32,33. As the room temperature ductility goal of this program was five percent, the columbium content of the quaternary alloy containing 6.0 w/o Cr was reduced to 19.7 w/o to insure that this property would be met as shown in Fig. 34. Examination of these two bivariant quaternary alloys on sections parallel to the gage length indicated that fracture was associated once again with copious twinning of Ni_3Cb eventually leading to fracture in a manner similar to that reported

Table IX

Tensile Properties of Directionally Solidified Ni, Cr-Ni_3Cb; (Ni)/(Ni_3Al)-Ni_3Cb and (Ni,Cr)/(Ni_3Al)-Ni_3Cb Alloys Tested in Air

Specimen No.	Composition wt/o	Alloy #	Freezing Rate cm/hr	Temp. (°C)	UTS $10^7 N/m^2$	UTS (psi)	Elong. (%)	$\dot{\epsilon}$ min^{-1}	Comments
A72-320-02	Ni-21Cb-6Cr	1	3	25	91.4	132,500	1.4	0.01	lamellar
A71-321T	Ni-21Cb-6Cr	1	10	1093	49.6	72,000	8.7	0.05	colony
A71-322	Ni-21Cb-6Cr	1	20	1093	45.6	66,200	1.7	0.05	colony
A71-364-02	Ni-21Cb-6Cr	1	2	1149	27.9	40,500	5.8	0.05	lamellar
A72-364-01	Ni-21Cb-6Cr	1	2	1204	23.9	34,700	14.7	0.05	lamellar
A71-109C	Ni-21Cb-9Cr	-	2	1093	41.5	60,200	6.0	0.05	lamellar
A71-171	Ni-20Cb-9Cr	-	10	1093	51.3	74,400	8.5	0.05	colony
A71-173	Ni-20Cb-9Cr	-	20	1093	54.1	78,400	3.6	0.05	colony
A70-611-01H	Ni-20Cb-10Cr	2	10	25	117.9	171,000	0.5	0.01	lamellar
A71-344-03	Ni-20Cb-10Cr	2	10	1149	31.2	45,150	4.9	0.05	lamellar
A71-344-01	Ni-20Cb-10Cr	2	10	1204	>12.6	>18,300	---	0.05	pulled thru grip
A70-611-01H	Ni-19Cb-12Cr	-	2	25	117.9	171,000	0.5	0.01	colony
A70-109B	Ni-19Cb-12Cr	-	2	1093	39.3	57,000	6.0	0.05	lamellar
A70-611-02T	Ni-19Cb-12Cr	-	2	1093	40.9	59,250	2.2	0.05	colony
A71-314	Ni-19Cb-12Cr	-	2	1093	50.4	73,100	12.3	0.05	lamellar
A71-546-01	Ni-21.0Cb-2.5Al	3	2	25	109.6	159,000	29.0	0.01	lamellar
A72-288-02	Ni-21.0Cb-2.5Al	3	2	815	81.2	117,700	12.6	0.05	lamellar
A71-546-02	Ni-21.0Cb-2.5Al	3	2	1093	45.7	66,300	17.3	0.02	lamellar
A72-288-03	Ni-21.0Cb-2.5Al	3	2	1149	33.8	49,000	24.0	0.05	lamellar
A72-288-04	Ni-21.0Cb-2.5Al	3	2	1204	23.4	34,000	25.6	0.05	lamellar
A71-651-02	Ni-20.8Cb-2.8Al	4	2	25	102.4	148,200	8.7	0.01	lamellar
A71-651-01	Ni-20.8Cb-2.8Al	4	2	815	83.4	122,000	9.1	0.01	lamellar
A71-085-03	Ni-20.8Cb-2.8Al	4	2	1149	34.6	50,100	15.2	0.05	lamellar
A71-651-03	Ni-20.8Cb-2.8Al	4	2	1204	>21.4	>31,000	---	0.05	pulled thru threads

Table IX (Cont'd)

Specimen No.	Composition wt/o	Alloy #	Freezing Rate cm/hr	Temp. (°C)	UTS $10^7 N/m^2$	UTS (psi)	Elong. (%)	$\dot{\varepsilon}$ min^{-1}	Comments
A72-140-01	Ni-19.5Cb-9.0Cr-1.0Al	6	2	25	124.4	180,500	1.1	0.01	lamellar, failed in fillet
A71-258	Ni-20.2Cb-9.1Cr-1.0Al	6	10	1093	36.2	52,500	17.9	0.01	prior to erosion test
A71-258	Ni-20.2Cb-9.1Cr-1.0Al	6	10	1093	36.8	53,400	14.2	0.02	post erosion test
A72-080-02	Ni-19.7Cb-9.0Cr-1.0Al	6	10	1149	>30.3	>43,900	--	0.05	pulled thru grip
A72-080-04	Ni-19.7Cb-9.0Cr-1.0Al	6	10	1204	--	36,600	14.0	0.05	lamellar
A72-097-04	Ni-19.7Cb-9.0Cr-1.0Al	6	2	1149	18.1	26,200	6.7	0.05	lamellar
A71-277T	Ni-20.4Cb-9.2Cr-0.5Al	-	2	1093	39.6	57,500	3.75	0.05	colony
A72-202-01	Ni-20.0Cb-6.0Cr-2.5Al	5	2	25	25.2	177,000	1.6	0.01	lamellar, failed in fillet
A71-589C-01	Ni-20.0Cb-6.0Cr-2.5Al	5	2	25	108.3	157,000	6.0	0.01	slight colony
A71-589C-02	Ni-20.0Cb-6.0Cr-2.5Al	5	2	1093	47.0	68,200	17.0	0.02	slight colony
A72-197-01	Ni-20.0Cb-6.0Cr-2.5Al	5	2	1149	40.7	59,100	9.2	0.05	lamellar
A72-197-02	Ni-20.0Cb-6.0Cr-2.5Al	5	2	1204	27.5	39,900	9.0	0.05	lamellar

TENSILE CURVES FOR $\gamma - \delta$, Ni–21.0 WT % Cb–6.0 WT % Cr

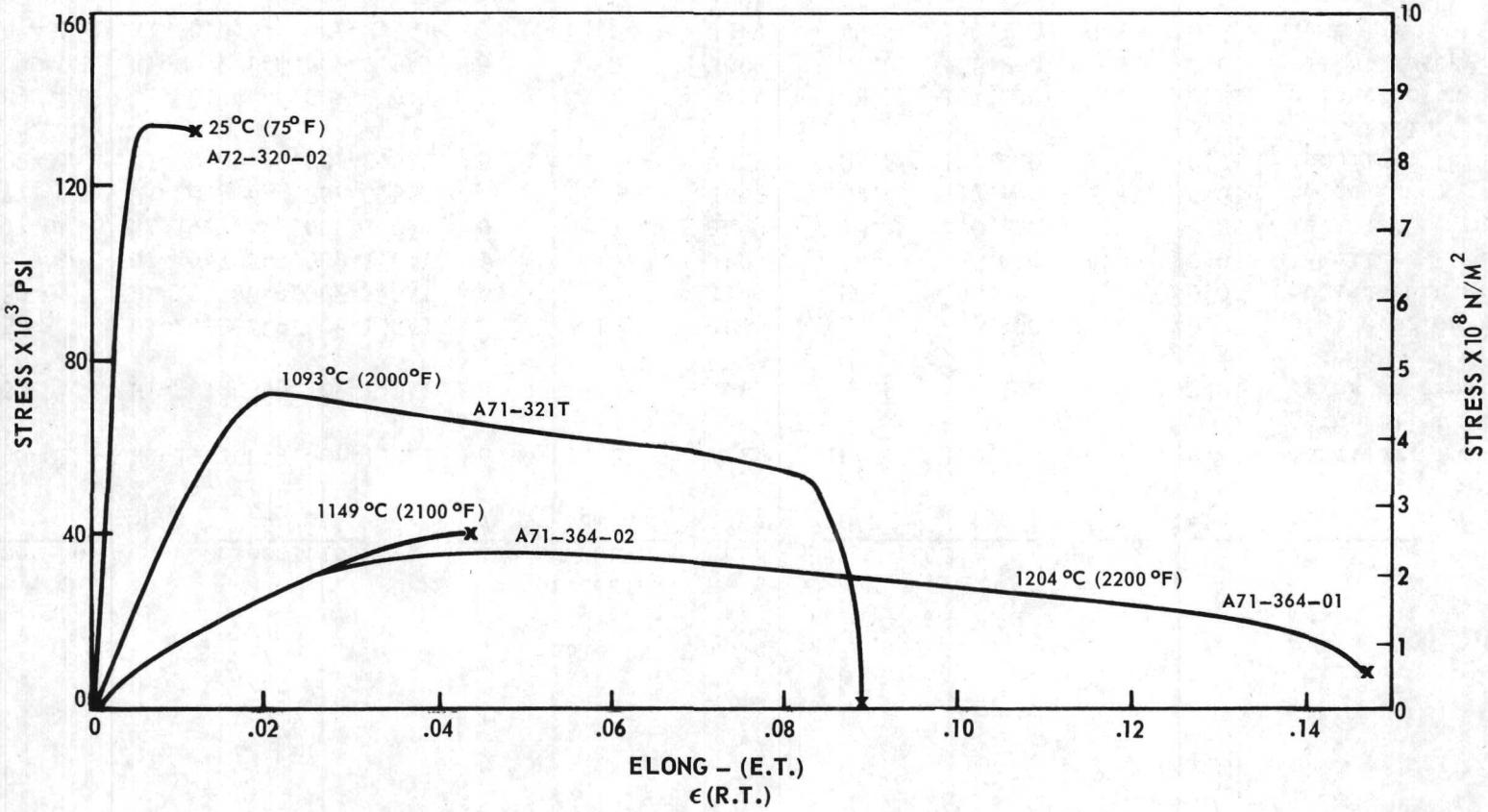

FIGURE 27

TENSILE CURVES FOR $\gamma - \delta$, Ni–20.0 WT % Cb–10 WT% Cr

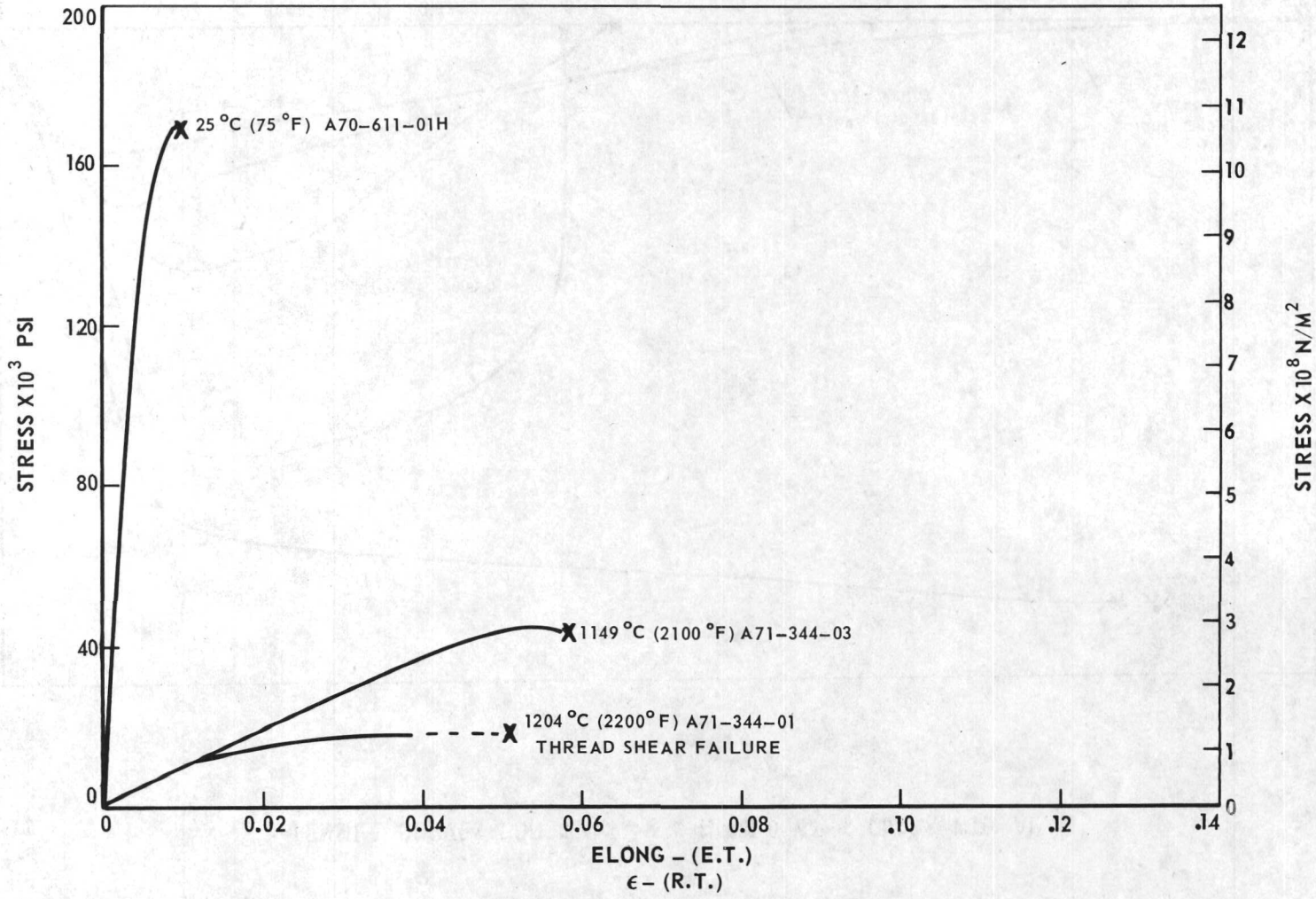

FIGURE 28

TENSILE CURVES FOR $\gamma/\gamma' - \delta$, Ni–21.0 WT % Cb–2.5 WT% Al

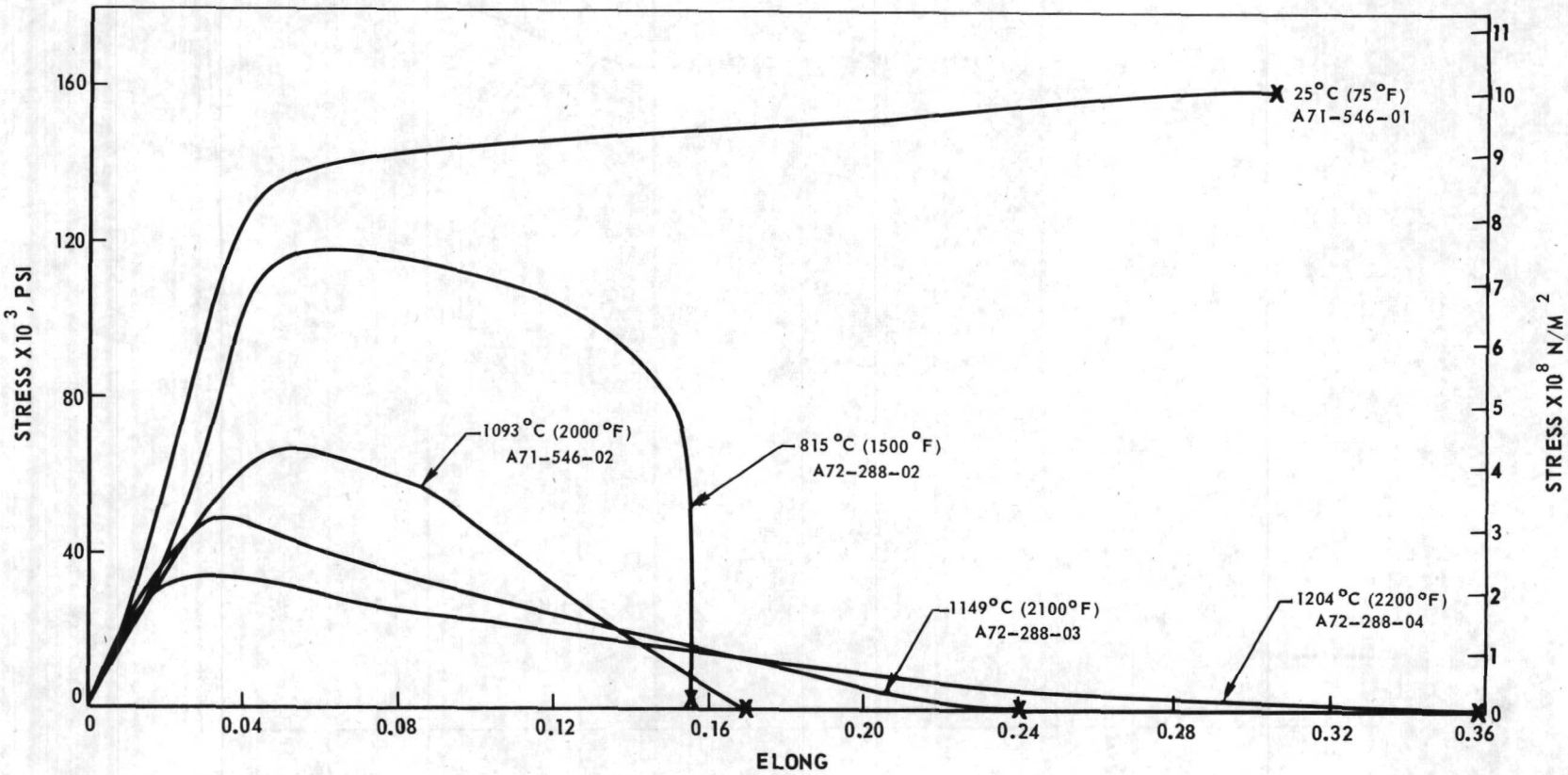

FIGURE 29

TENSILE CURVES FOR $\gamma / \gamma' - \delta$ Ni–20.8 WT % Cb–2.8 WT % Al AT VARIOUS TEMPERATURES

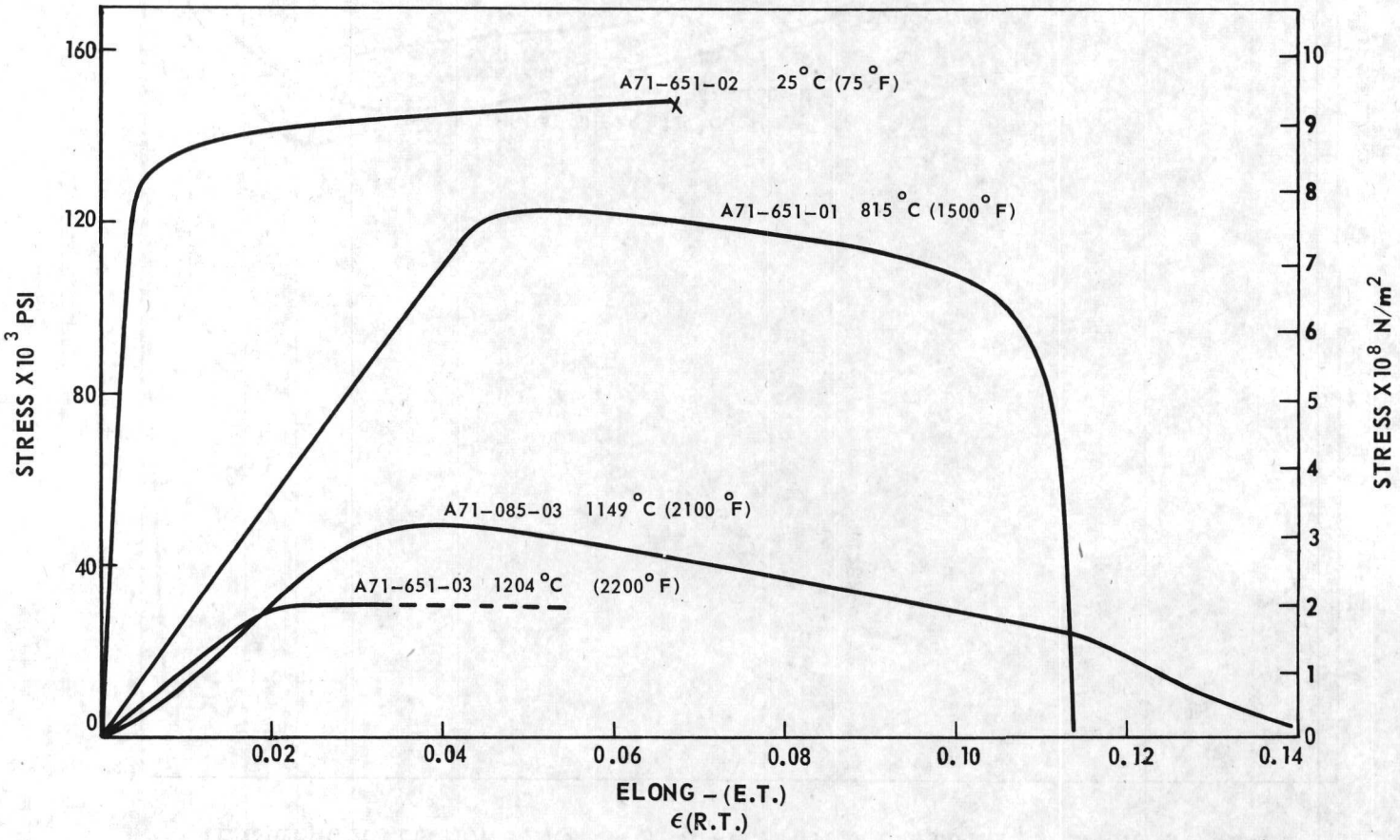

FIGURE 30

TENSILE CURVES FOR $\gamma/\gamma' - \delta$ Ni–19.7 WT % Cb–9.0 WT % Cr–1.0 WT % Al

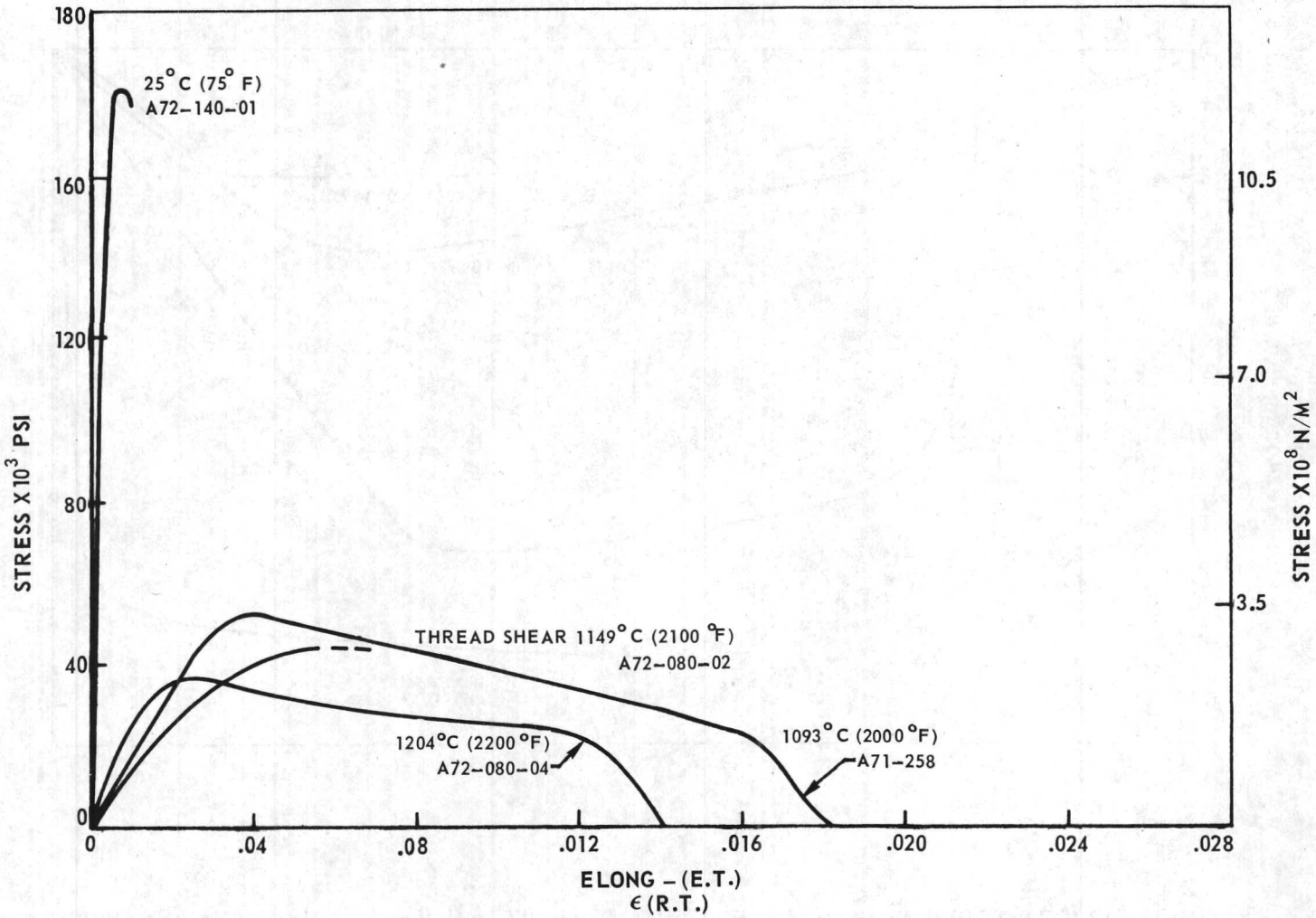

FIGURE 31

TENSILE CURVES FOR $\gamma/\gamma'-\delta$; Ni–20.0 WT % Cb–6.0 WT % Cr–2.5 WT % Al

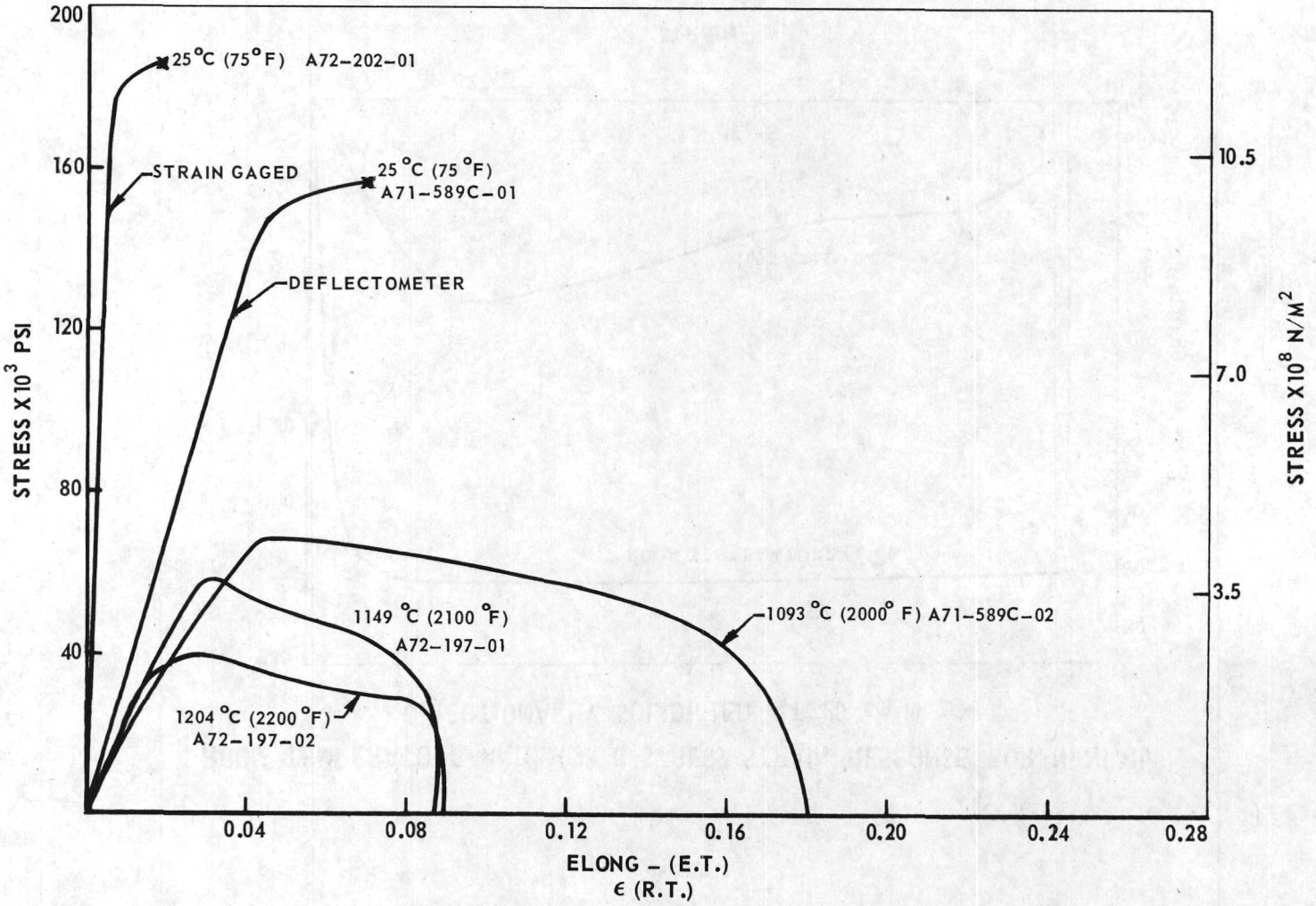

FIGURE 32

ROOM TEMPERATURE AND 1093°C STRESS STRAIN RESPONSE FOR Ni-Ni_3Cb
DIRECTIONALLY SOLIDIFIED AT 20 cm/hr

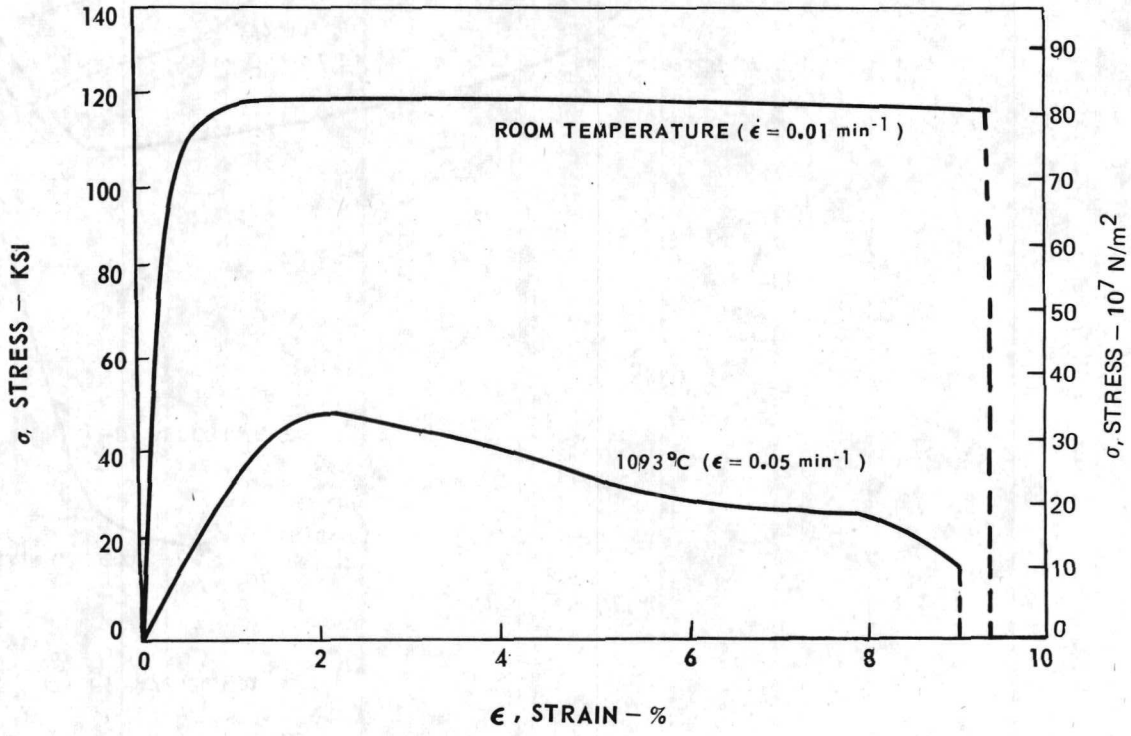

FIGURE 33

ROOM TEMPERATURE LONGITUDINAL STRESS–STRAIN CURVE FOR $\gamma/\gamma'-\delta$

(Ni–19.7 w/o Cb–6.0 w/o Cr–2.5 w/o Al) PRODUCED AT 3 cm/hr

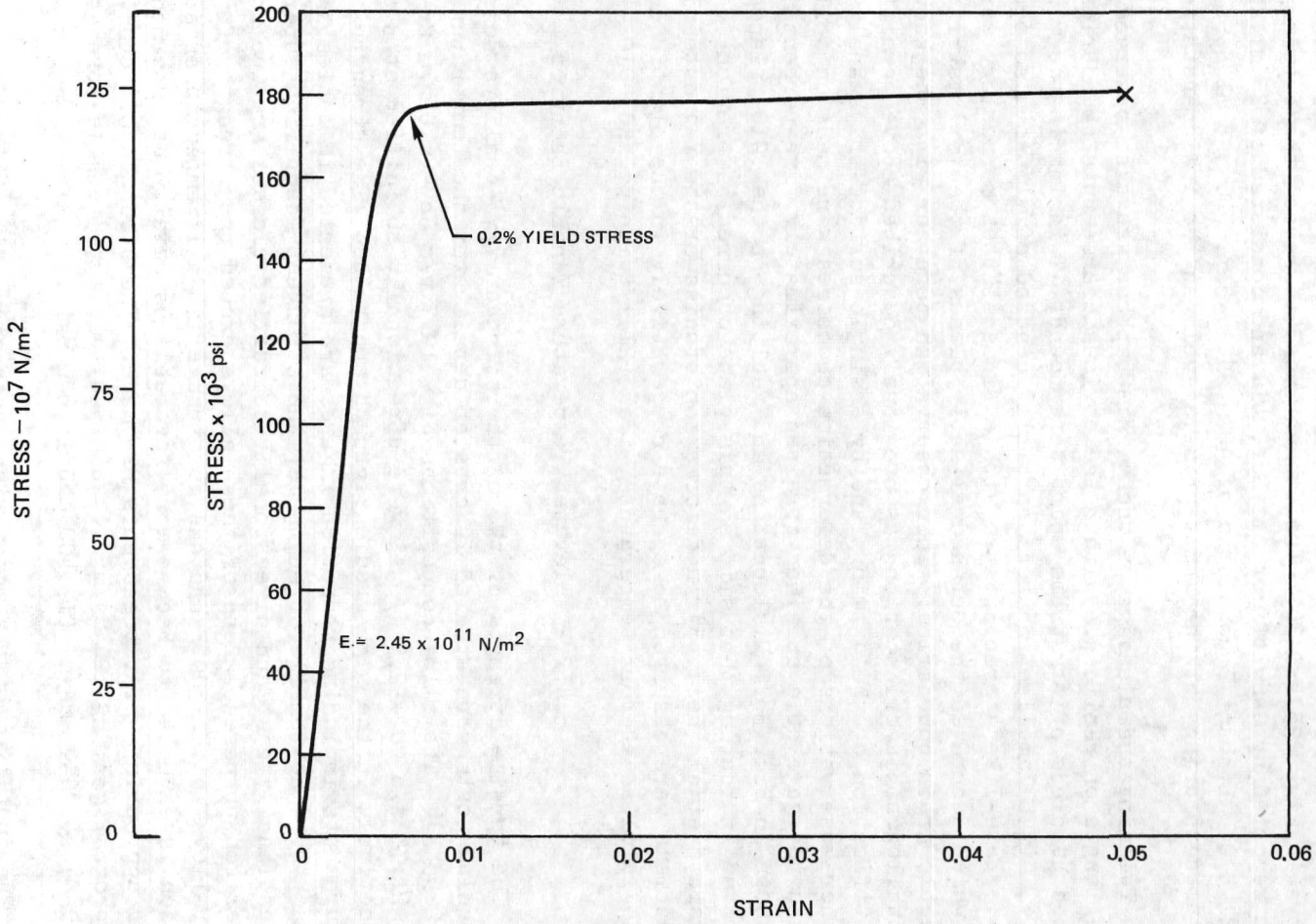

FIGURE 34

for γ-δ (Ref. 21). Photomicrographs representative of deformation near the fracture surface and within the gage of specimens tested at room temperature are shown for both alloys in Figs. 35 and 36. The etchant used to reveal the δ twinning (etchant A) was that reported by Gangloff et al (Ref. 41) and consisted of 35 ml HNO_3, 2 ml HF and 63 ml H_2O. Etchant B consisted of 40 ml HCl, 3 ml HNO_3, 5 ml H_2SO_4 and 52 ml H_2O and was used to bring out the gamma prime as well as the δ Widmanstätten precipitates.

Twinning and cleavage of the δ, Ni_3Cb phase was also observed throughout the gage length on replicas. Within the obvious coarse twin boundaries, fine twins spaced hundreds of Ångströms apart were found. Twinning in the γ phase adjacent to the δ, Ni_3Cb lamellae in areas partially denuded of γ' was also occasionally noted. Thin, plate-like δ precipitates with a Widmanstätten morphology were observed, Fig. 37, which decorated the octahedral habit planes of the γ/γ' matrix particularly near eutectic grain boundaries. This observation together with the knowledge of the crystallographic orientations as previously described above permitted the indirect identification of the δ twin plane by a single surface trace analysis (Ref. 46). Further observations of the deformation processes were made on foils prepared from within the gage of a specimen strained approximately five percent at room temperature as shown in Fig. 38. Dislocations and faulting on the (010) planes of Ni_3Cb were observed indicating that slip on this plane occurred as previously noted by Grossiard et al (Ref. 45) in deformation studies of the γ-δ eutectic. Thus two mechanisms were observed to operate cooperatively in the plastic deformation of Ni_3Cb lamellae at room temperature, i.e. {211} twinning and 010 slip.

3.4.2.2 Elevated Temperature Tensile Behavior

The tensile strength of two of the stronger γ/γ'-δ alloys determined from initial screening tests were studied in greater detail over the temperature range 25-1235°C (70-2255°F). The alloy compositions Ni - 19.7 w/o Cb - 6.0 w/o Cr - 2.5 w/o Al and Ni - 21.75 w/o Cb - 2.5 w/o Al were directionally solidified at 3 and 38 cm/hr respectively in the high gradient growth apparatus. The strength and ductility measurements including reduction in area are presented in Tables X and XI and Figs. 39 and 40. The tensile strengths of the strongest identified superalloys of the conventionally cast and directionally solidified classes are included in Fig. 39 for comparison purposes. Both of these alloys exceed the strength of all nickel-base superalloys above 1500°F and one is stronger at all temperatures studied. This comparison is expected to become more favorable especially at intermediate temperatures after appropriate heat treatments are made. The strength of both γ/γ'-δ alloys exceeds the program goal of 120 MN/m^2 (17,000 psi) ultimate tensile strength at 1235°C (2255°F) by 90-99 MN/m^2 (13,400 and 14,800 psi).

The ductility of the monovariant eutectics, Ni - 21.0 w/o Cb - 2.5 w/o Al (Fig. 29), Ni - 21.75 w/o Cb - 2.55 w/o Al (Fig. 40) and the bivariant Ni - 19.7 w/o Cb - 6.0 w/o Cr - 2.5 Al (Fig. 39) did not exhibit as marked an inversion with temperature as indicated in the previous studies on the binary eutectic γ-δ (Refs. 22,41). The first monovariant eutectic, Ni - 21.0 w/o Cb - 2.5 w/o Al, exhibited

DEFORMATION TWINNING AND TWIN BOUNDARY CRACKING IN Ni_3Cb OF THE $\gamma/\gamma' - \delta$ EUTECTIC AFTER TENSILE LOADING AT ROOM TEMPERATURE
(Ni–20 Cb–6.0 Cr–2.5 Al)

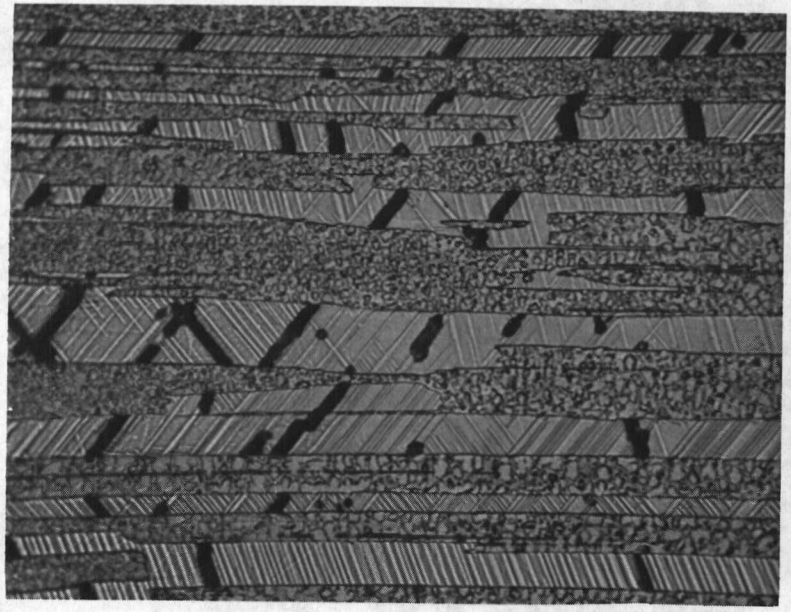

NEAR FRACTURE SURFACE

10μm

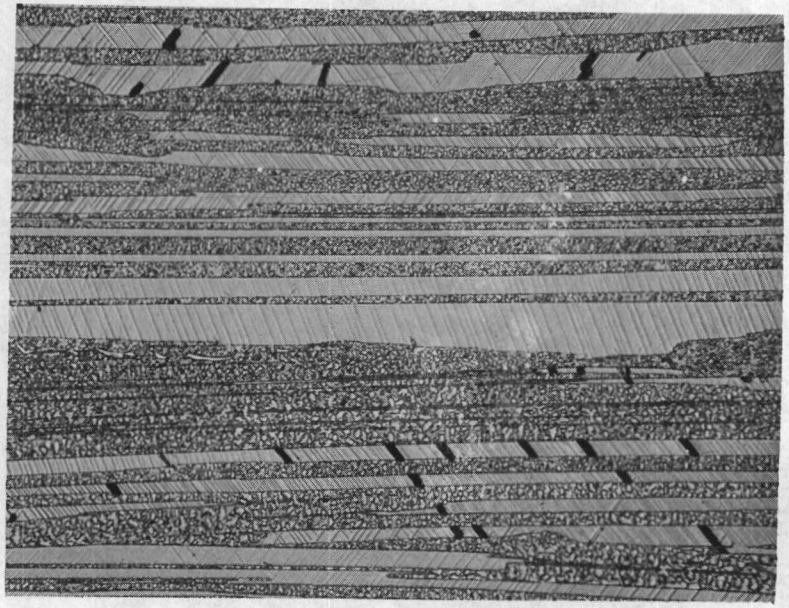

IN GAGE AWAY FROM FRACTURE

10μm

FIGURE 35

LONGITUDINAL SECTION NEAR FRACTURE OF ROOM TEMPERATURE TENSILE DEFORMATION OF $\gamma/\gamma' - \delta$ (Ni – 19.7 Cb – 6.0 Cr – 2.5 Al)

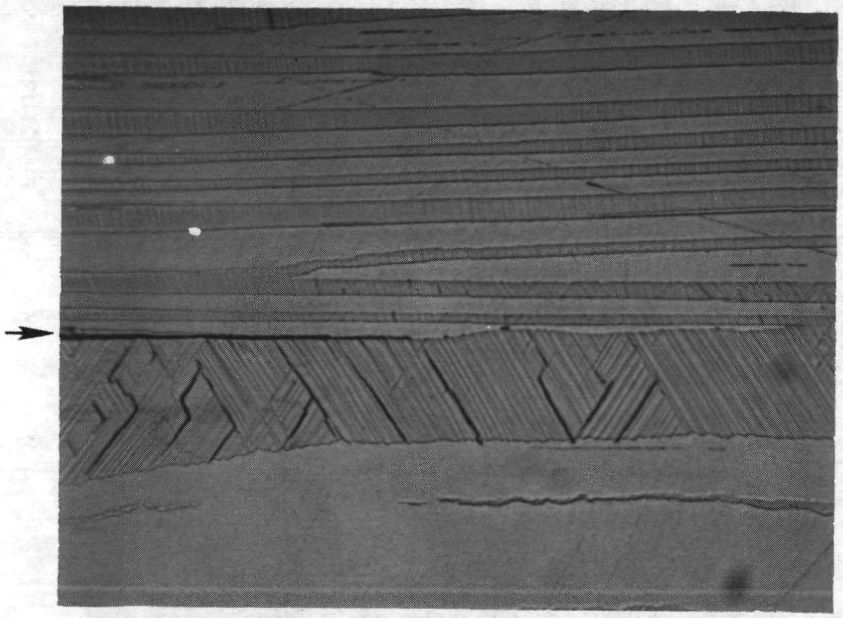

10 μm

(a) TWINNING MORPHOLOGY, δ–Ni_3 Cb CLEAVAGE AND INTERFACIAL DECOHESION (ARROW), ETCHANT A

10 μm

(b) γ, γ' PRECIPITATE MORPHOLOGY, ETCHANTS A & B

FIGURE 36

LONGITUDINAL ELECTRON MICROGRAPH OF ROOM TEMPERATURE TENSILE SPECIMEN ILLUSTRATING δ PHASE TWIN MORPHOLOGIES, TWIN BOUNDARY CRACKING AND WIDMANSTATTEN δ AND GOBULAR γ' PRECIPITATION

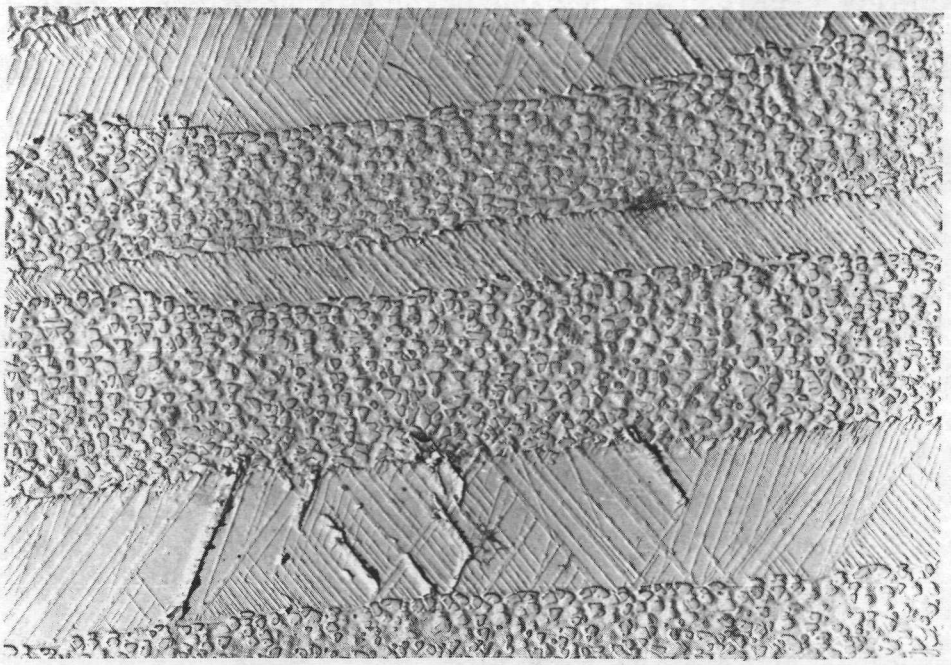

a) WITHIN TYPICAL EUTECTIC GRAIN OF Ni - 19.7 w/o Cb - 6.0 w/o Cr - 2.5 w/o Al

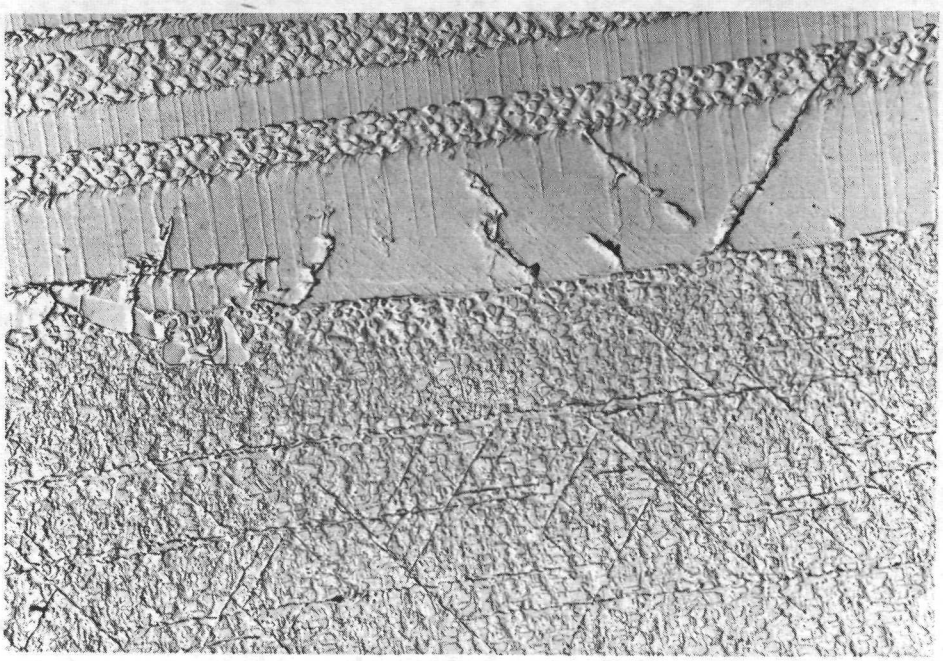

b) NEAR EUTECTIC GRAIN BOUNDARY 10 μm

FIGURE 37

TRANSMISSION ELECTRON MICROGRAPH OF ROOM TEMPERATURE TENSILE SPECIMEN TRANSVERSE TO STRESS AXIS (5% TOTAL STRAIN)

BOTH 211 TWINNING AND 010 SLIP DEFORMATION MODES EXHIBITED IN Ni_3Cb

FIGURE 38

Table X

Tensile Properties of Ni- 19.7 w/o Cb - 6.0 w/o Cr - 2.5 w/o Al Specimens
Directionally Solidified at 3 cm/hr and Tested in Air

Specimen No.	Temperature		0.2% Y.S.		E	E	UTS		Elong.	R.A.	$\dot{\varepsilon}$
	°F	°C	$10^7 N/m^2$	ksi	msi	$10^{10} N/m^2$	$10^7 N/m^2$	ksi	%	%	min^{-1}
A72-634-01	78	25	119.715	173.5	36.4	251	125.58	182	2.9	1.4	.01
A72-634-03	78	25	116.61	169	36.4	251	120.75	175	2.9	3.8	.01
A72-249-01	78	25	122.13	177	38.0	262	124.89	181	5.0	7.8	.01
A72-634-02	1380	749	96.6	140	23.7	163	100.05	145	15.2	21.3	.01
A72-621-02	1380	749	97.98	142	24.9	172	100.05	145	12.2	18.8	.01
A72-617-01	1500	815.5	96.6	140	21.2	146	96.6	140	7.9	13.4	.01
A72-636-02	1500	815.5	93.84	136	22.4	155	93.84	136	5.1	10.5	.05
A72-244-01	1500	815.5	96.6	140	--	--	100.05	145	10.0	18.1	.01
A72-617-03	1600	871.1	--	--	--	--	91.77	133	5.1	6.7	.05
A72-613-02	1600	871.1	92.46	134	20.0	138	92.46	134	6.5	9.5	.05
A72-613-03	1700	926.7	86.25	125	20.0	138	86.25	125	5.1	4.1	.05
A72-597-03	1700	926.7	86.94	126	14.8	102	86.94	126	4.0	2.9	.05
A72-621-01	1830	999	72.45	105	11.4	78.6	74.52	108	15.6	24.2	.05
A72-621-03	1830	999	74.52	108	10.3	71.0	76.59	111	5.5	5.0	.05
A72-631-01	1920	1049	62.79	91	9.7	66.9	63.894	92.6	20.2	36.2	.05
A72-631-03	1920	1049	64.86	94	10.0	68.9	65.067	94.3	18.3	26.9	.05
A72-631-02	2000	1093	55.2	80	9.7	66.9	55.752	80.8	17.5	30.7	.05
A72-617-02	2000	1093	51.75	75	10.3	71.0	52.992	76.8	18.4	30.6	.05
A72-255-01	2000	1093	55.476	80.4	--	--	55.476	80.4	14.5	30.3	-
A72-281-02	2000	1093	55.545	80.5	--	--	55.545	80.5	7.5	24	-
A72-636-01	2100	1148.9	40.572	58.8	9.3	64.1	40.572	58.8	14.8	24.2	.05
A72-636-03	2100	1148.9	40.572	58.8	10.4	71.7	40.572	58.8	13.8	30.2	.05
A72-597-01	2190	1199	26.427	38.3	6.2	42.7	26.427	38.3	17.5	28.9	.05
A72-597-02	2190	1199	27.531	39.9	4.8	33.1	27.531	39.9	17.3	24.2	.05
A72-604-03	2255	1235	21.942	31.8	4.9	33.7	21.942	31.8	6.3	7.0	.05
A72-613-01	2255	1235	20.976	30.4	6.5	44.8	20.976	30.4	26.4	12.5	.05

Table XI

Tensile Properties of Ni - 21.75 w/o Cb - 2.55 w/o Al Specimens
Directionally Solidified at 38 cm/hr and Tested in Air

Specimen No.	Temperature °F	Temperature °C	0.2% Y.S. $10^7 N/m^2$	0.2% Y.S. ksi	E msi	E $10^{10} N/m^2$	UTS $10^7 N/m^2$	UTS ksi	Elong. %	R.A. %	$\dot{\varepsilon}$ min^{-1}
A72-819-01	70	25	133.9	194	34.6	238	133.9	194	2.0	11	.01
A72-836-04	70	25	133.9	194	34.8	240	133.9	194	2.2	7.5	.01
A72-808-01	1380	749	---	---	--	-	118.5	171.8	10.0	20.2	.05
A72-808-02	1380	749	110.4	160	25.3	174	115.8	167.8	11.4	21.7	
A72-809-01	1500	815	120.1	174	21.3	147	120.1	174.0	6.6	11.2	
A72-809-02	1500	815	103.8	150.5	22.6	156	120.1	174.0	7.3	12.5	
A72-810-01	1600	871	98.3	142.5	22.4	154	111.9	162.2	9.4	12.5	
A72-808-03	1600	871	92.5	134	22.0*	152	107.8	156.3	8.6	11.2	
A72-809-03	1700	927	80.7	117	21.0*	145	94.3	136.6	19.1	24.2	
A72-810-02	1700	927	83.5	121	21.0*	145	96.9	140.5	19.0	26.7	
A72-810-03	1830	999	57.3	83	20.9	144	77.0	111.6	17.6	29.1	
A72-814-01	1830	999	55.1	79.8	15.9	110	75.3	109.2	17.8	29.5	
A72-814-02	1920	1049	53.8	78	15.0	103	66.6	96.5	16.4	22.9	
A72-814-04	1920	1049	48.8	70.7	14.1	97	65.3	94.6	14.8	26.8	
A72-832-01	2000	1093	45.9	66.5	10.1	70	54.5	79.0	12.5	18.9	
A72-832-02	2000	1093	48.4	70.2	9.5	66	54.9	79.6	18.0	20.0	
A72-832-03	2100	1149	33.3	48.3	8.9	61	41.5	60.1	15.4	18.9	
A72-836-01	2100	1149	32.2	41.7	9.4	65	40.0	57.9	18.0	16.5	
A72-836-02	2190	1199	21.8	31.6	7.1	50	25.9	37.6	17.8	17.8	
A72-837-01	2190	1199	25.9	37.6	6.5	45	28.1	40.7	24.4	13.8	
A72-837-02	2255	1235	18.6	26.9	6.9	48	21.0	30.5	18.5	16.6	
A72-837-03	2255	1235	17.5	25.3	8.8	61	21.0	30.4	19.7	16.5	

* E fitted

TEMPERATURE DEPENDENCE OF ULTIMATE STRENGTH, ELONGATION AND REDUCTION OF AREA FOR 3 CM/HR D.S. EUTECTIC SUPERALLOY, Ni–19.7w/o Cb–6.0 w/o Cr–2.5 w/o Al

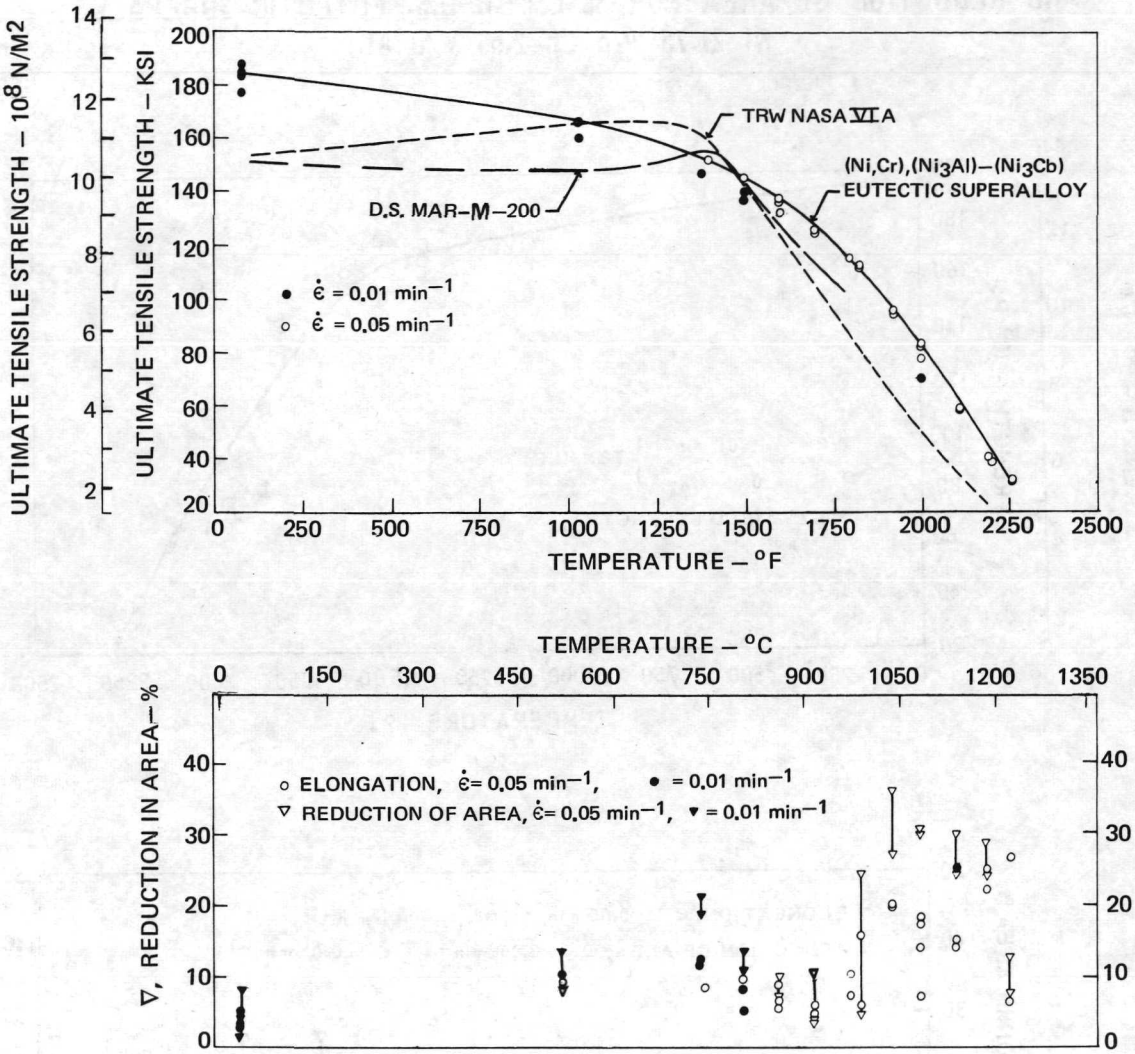

FIGURE 39

TEMPERATURE DEPENDENCE OF ULTIMATE STRENGTH, 0.2% YIELD STRENGTH, AND REDUCTION OF AREA FOR 38 CM/HR D.S. EUTECTIC SUPERALLOY, Ni-21.75 w/o Cb-2.55 w/o Al

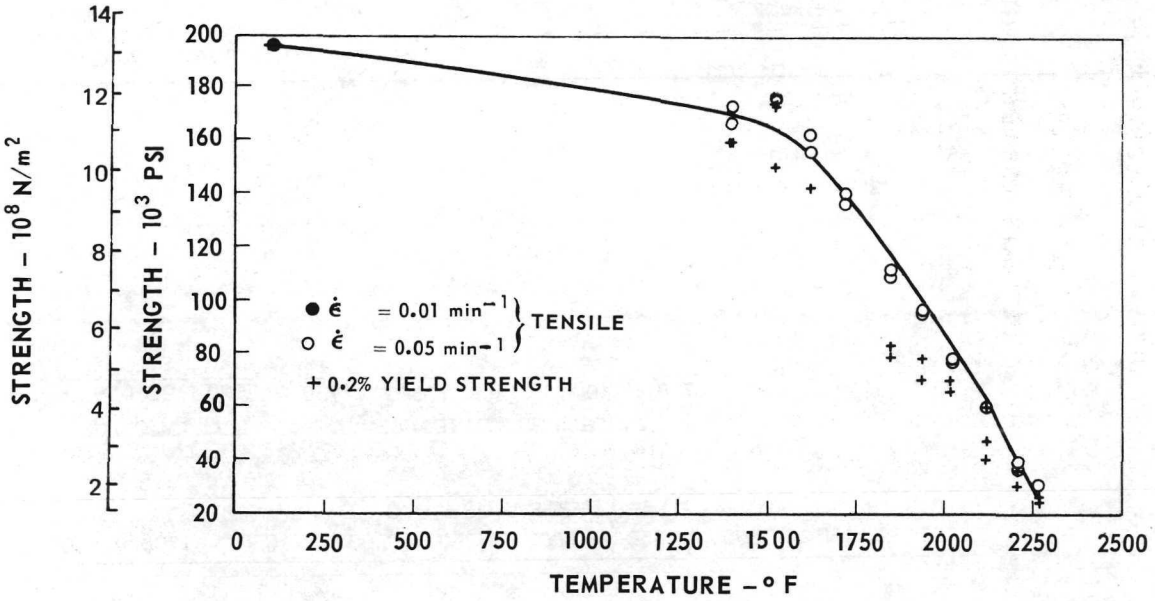

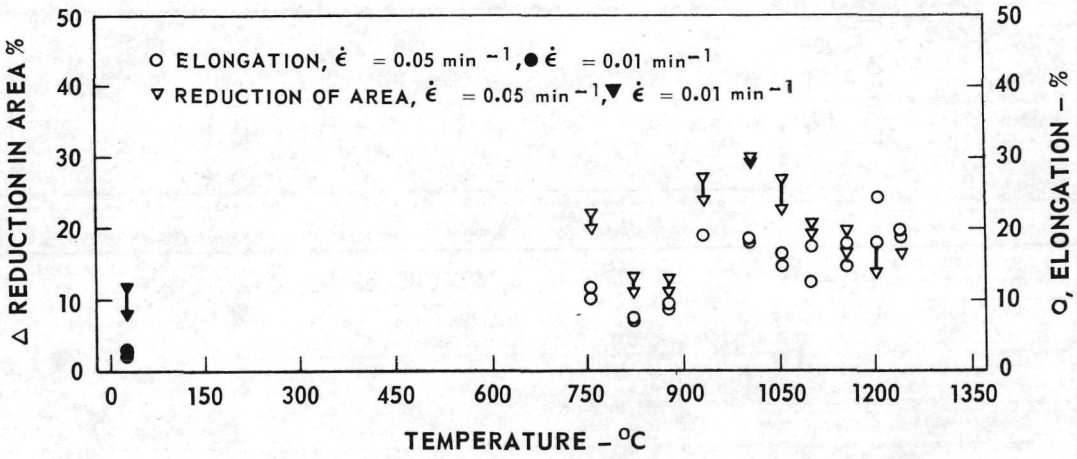

FIGURE 40

a ductility minimum of 11 to 15 percent near 815°C (1500°F) and the second eutectic Ni - 21.75 w/o Cb - 2.55 w/o directionally solidified much faster at 38 cm/hr showed a minimum in ductility of approximately 7 percent at 815°C (1500°F) also. The bivariant eutectic Ni - 19.7 w/o Cb - 6.0 w/o Cr - 2.5 w/o Al alloy's minimum in tensile ductility of approximately 5 percent was near 927°C (1700°F) and was observed to be strain rate dependent (Ref. 42). These reductions in elongation and concomitant reduction in area were considered to be associated in part with the intrinsic γ' ductility minimum characteristic of most γ' precipitation hardened nickel base superalloys, rather than a basic fracture mechanism change in the cooperative deformation of the lamellar phases.

At 815°C (1500°F) deformation was characterized by intense translamellar shear bands concentrated in the necked region of the gage length. Twins parallel to the $\{211\}_{\delta}$, whose width increased with increasing temperature as noted in a Ni - 19.7 w/o Cb - 6.0 w/o Cr - 2.5 w/o Al specimen tested at 815°C (1500°F), are shown in the longitudinal sections, Figs. 41,43a. At 2000°F other twin and possibly slip systems were operable, and broader and more irregular twin traces were observed. Extensive local δ, Ni_3Cb lamellae damage occurred within very broad deformation bands as shown in Figs. 42 and 43b. Voids were observed only near the fracture surfaces.

Because a definite improvement in the creep strength of the γ/γ'-δ alloys was derived from directional solidification at faster velocities, as will be discussed below, experiments were designed to optimize the freezing velocity of the Ni,Al-Ni_3Cb alloy (Ni - 21.0-22.2 w/o Cb - 2.5 w/o Al) prior to creep testing. The tensile strengths of specimens, directionally solidified at rates between 2 and 100 cm/hr were measured at 1093°C (2000°F) at a very slow strain rate ($\dot{\varepsilon}$) of 0.005 min^{-1} and are presented in Table XII. This slower strain rate was used to evaluate the 1093°C tensile strength in order to more closely approximate creep conditions. Thus the absolute strength values are below those values reported for tests at $\dot{\varepsilon}$ = .02-.05 min^{-1}, Tables IX and XI. The results of these experiments are also graphically presented in Fig. 44 and do not include the 100 cm/hr data point as is discussed below. A slight monotonic increase in strength was noted with the decrease in interlamellar spacing which corresponds to an increase in freezing velocity as was previously observed (Ref. 2). A slight but measurable decrease in tensile elongation was noted which accompanied the increasing trend in strength with decreasing interlamellar spacing.

After close examination of the microstructures of the specimens directionally solidified at various rates from 2-100 cm/hr it was noted within the specimen produced at 100 cm/hr (Fig. 17) that primary γ existed near grain boundaries of coupled composite γ/γ'-δ. The other specimens contained less or no primary γ or δ. Thus considering the values of strength and ductility for the 100 cm/hr specimen as conservative, then the inference of a slight trend upwards in strength and downwards in ductility with increasing solidification velocity appears justified.

LONGITUDINAL SECTION NEAR FRACTURE OF 815°C (1500°F) TENSILE SPECIMEN (A72–244)

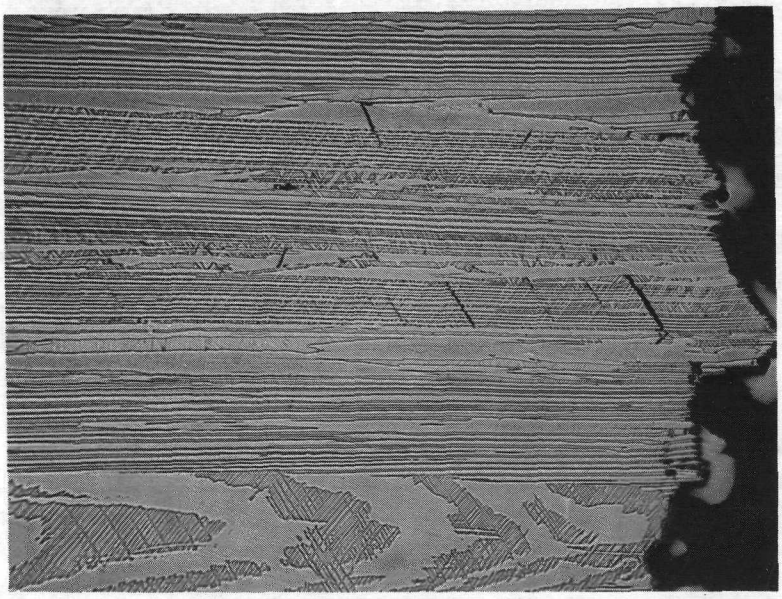

50 μm

(a) TRANSGRANULAR DEFORMATION BANDS AND CRACKING, ETCHANT A

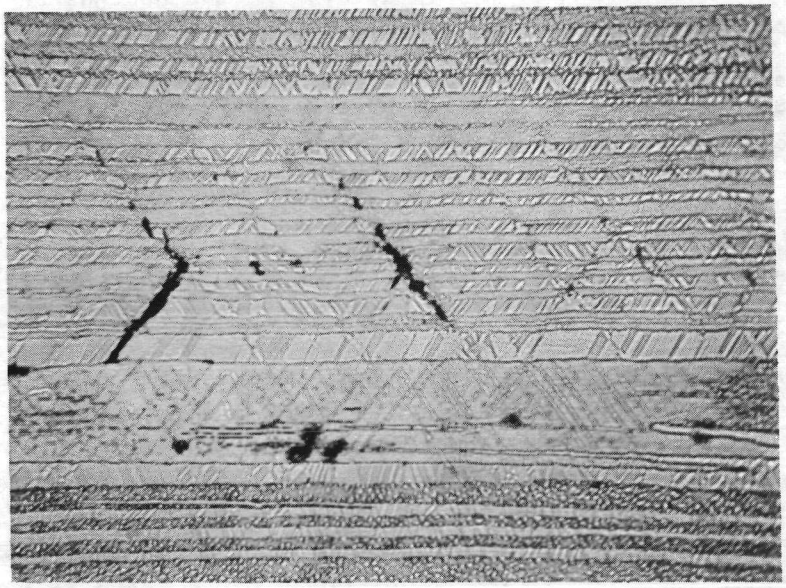

10 μm

(b) BEHIND FRACTURE SURFACE, ETCHANT A & B

FIGURE 41

1093° C (2000° F) TENSILE DEFORMATION OF $\gamma/\gamma' - \delta$ (Ni – 20 Cb – 6.0 Cr – 2.5 Al)

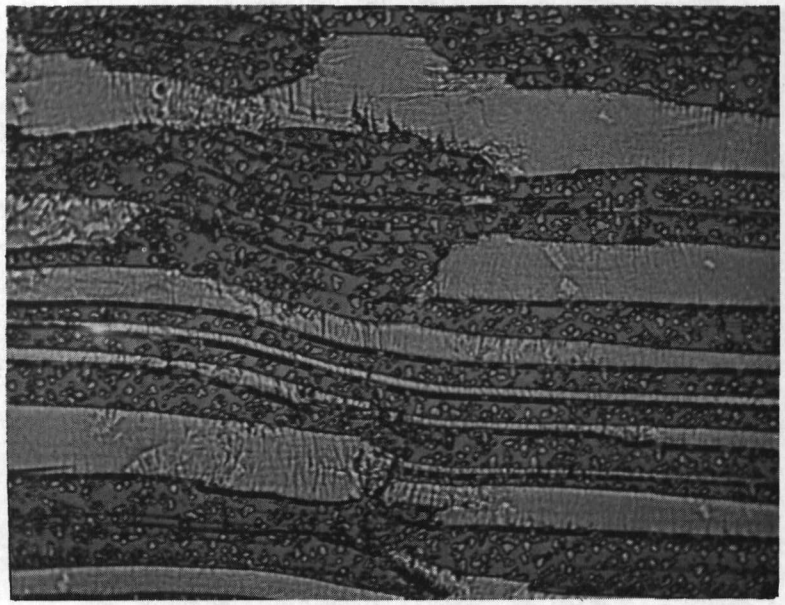

10 μm

NEAR FRACTURE SURFACE

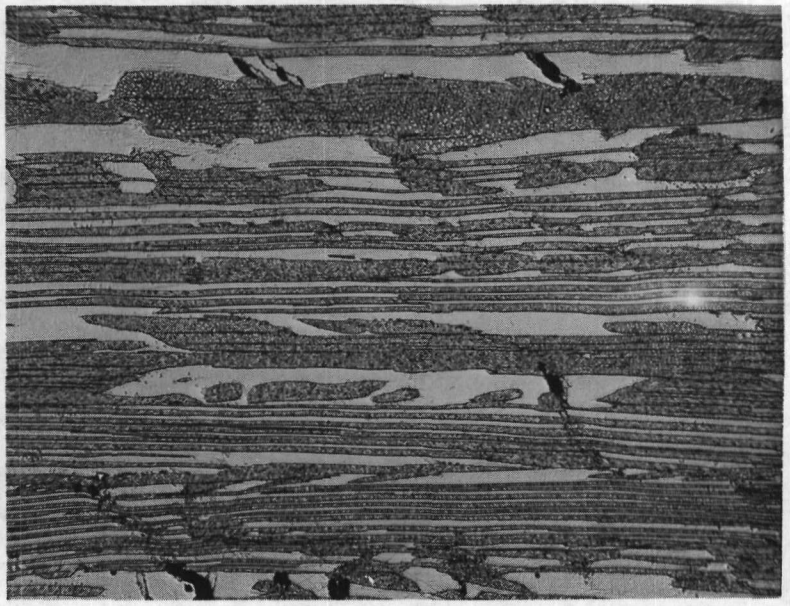

50 μm

IN GAGE AWAY FROM FRACTURE

FIGURE 42

LONGITUDINAL ELECTRON MICROGRAPHS OF ELEVATED TEMPERATURE TENSILE SPECIMENS NEAR FRACTURE

(Ni–19.7 w/o Cb – 6.0 w/o Cr – 2.5 w/o Al) PRODUCED AT 3 cm/hr

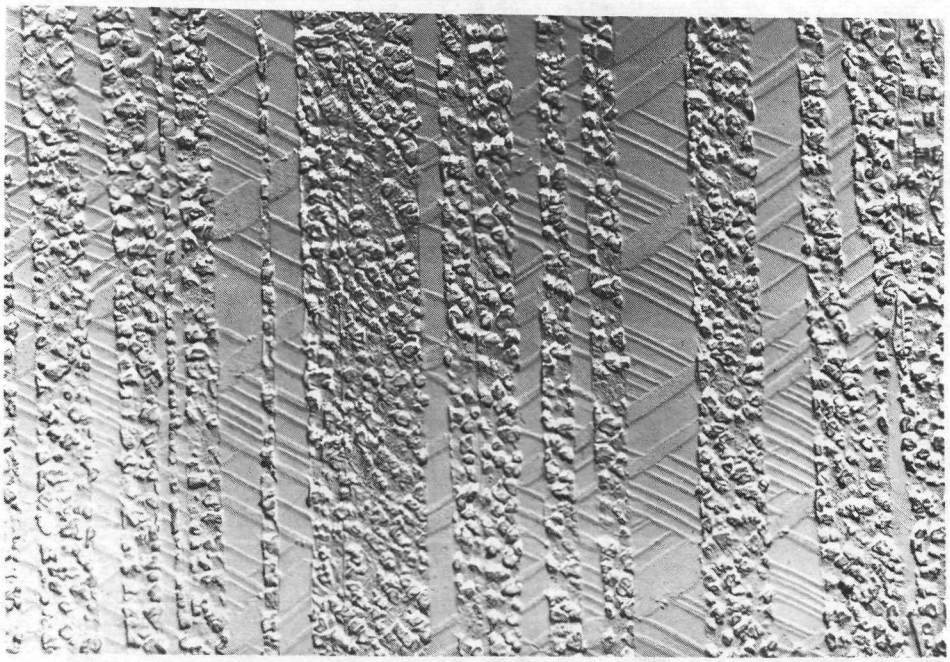

a) 815°C (1500°F) STRESS AXIS VERTICAL 10μm

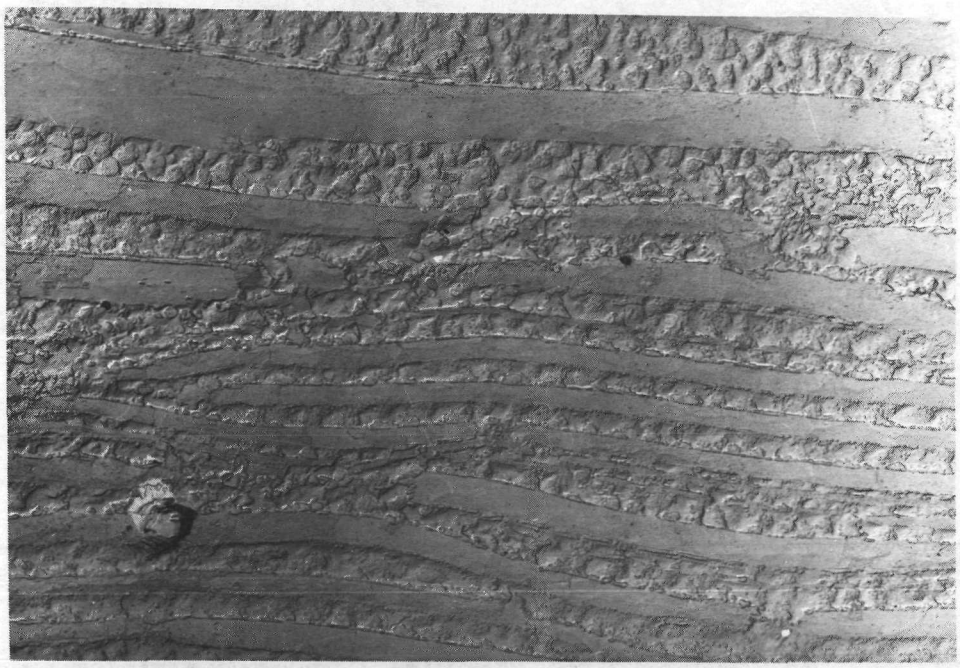

b) 1093°C (2000°F) STRESS AXIS HORIZONTAL 10μm

FIGURE 43

Table XII

1093°C (2000°F) Tensile Strengths of γ/γ'-δ (No Cr) Alloys Produced at Solidification Rates Between 2-100 cm/hr ($\dot{\varepsilon}$ = 0.005 min^{-1})

Specimen Identification	Composition w/o	Rate cm/hr	UTS ksi	UTS $10^7 MN/m^2$	Elongation % $\Delta\ell/\ell$	Elongation % Deflectometer
A72-506-12	Ni-21.0Cb-2.5Al	2	44.8	30.9	14.9	14.9
A72-625-01	Ni-20.8Cb-2.8Al	7.5	56.9	39.2	10.2	11.4
A72-623	Ni-21.5Cb-2.5Al	10	51.5	35.5	20.2	17.9
A72-663-01	Ni-21.5Cb-2.5Al	25	50.8	35.0	15.0	14.4
A72-657-01	Ni-21.75Cb-2.5Al	28.8	52.3	36.0	15.4	14.0
A72-669-01	Ni-21.67Cb-2.5Al	38.4	60.0	41.4	13.3	13.3
A72-692-01	Ni-21.8Cb-2.5Al	50.0	55.0	37.9	13.6	13.5
A72-679-02	Ni-22.0Cb-2.5Al	50.5	49.8	34.3	11.7	12.0
A72-690-01	Ni-22.0Cb-2.5Al	75.0	55.3	38.1	12.0	12.0
A72-694-01	Ni-22.2Cb-2.5Al	100.0	46.9	32.3	13.0	12.9

1093° C (2000° F) ULTIMATE TENSILE STRENGTH OF γ γ'- δ ALLOYS (2.5 w/o Al, 0 Cr) AS A FUNCTION OF FREEZING RATE

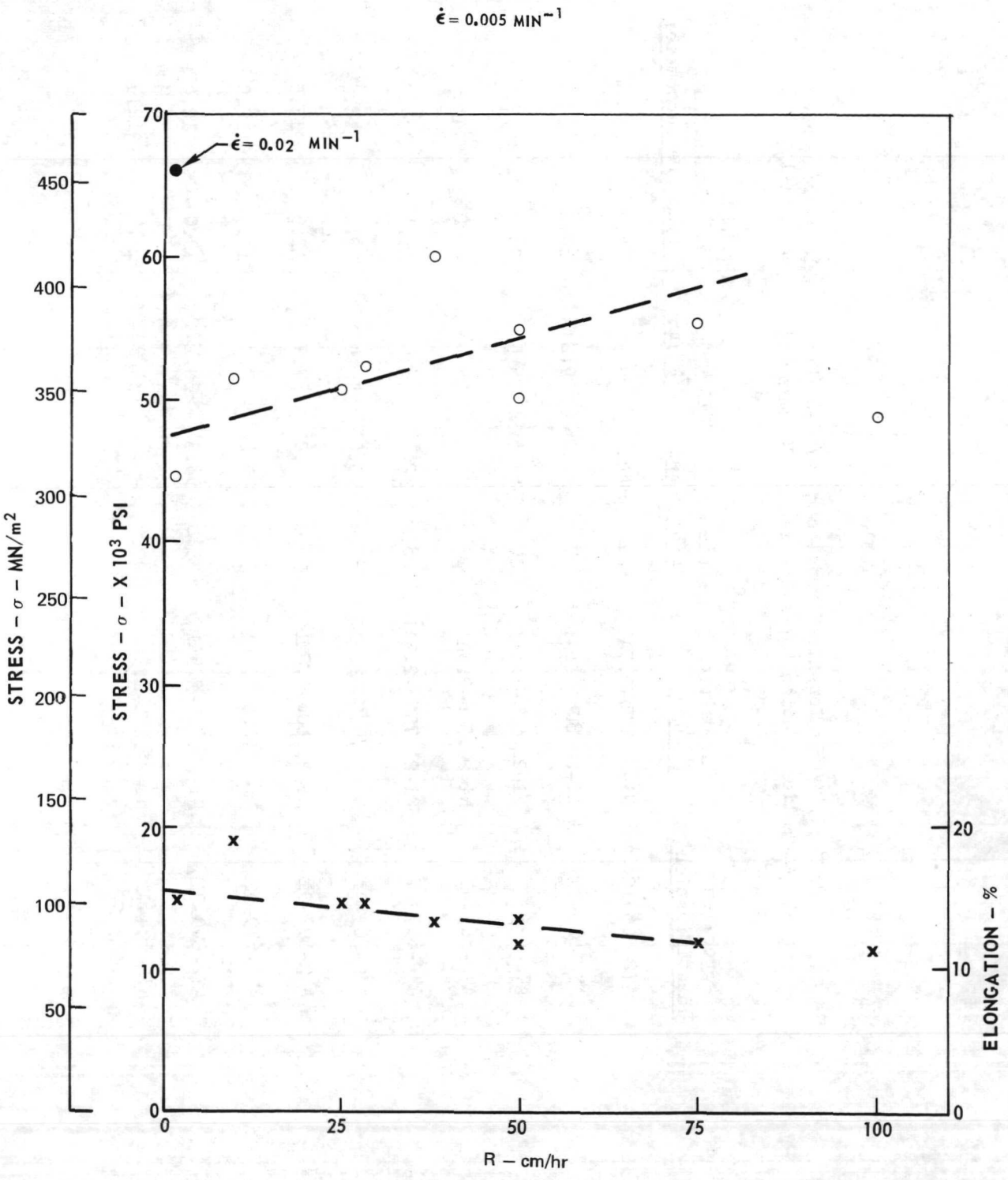

FIGURE 44

To assess any change in volume fraction which may have occurred during rapid solidification as a result of the dissolution kinetics of columbium, the volume percentage δ Ni_3Cb present in representative alloys of Table XII was measured by quantitative metallography. The δ Ni_3Cb lamellae were cut from high resolution electron photomicrographs of replicated transverse sections and weighed. The volume fractions presented in Table XIII were computed from the weight fraction of the δ Ni_3Cb present in the photomicrograph. Within the spread in values obtained and the accuracy of this technique applied to such a small volume of sample, no significant change in the volume fraction of δ Ni_3Cb with freezing velocity changes are believed to exist. The freezing rate of 38 cm/hr (15 in./hr) was chosen as an alloy condition since the maximum value of hot tensile strength was found for this specimen.

3.4.3 Stress Rupture

The results of the constant load stress rupture tests conducted on the alloys screened in Task I are presented in Table XIV. Larson-Miller parameters (constant = 20) for the representative alloy conditions were computed and summarized with the comparison alloys D.S. Mar M200, TRW-NASA VIA, D.S. Co,Cr,Ni-TaC, and D.S. γ'-δ in Fig. 45. The aligned lamellar alloys which contained both chromium in solid solution and aluminum in the form of γ' precipitates within the matrix lamellae possessed the greatest rupture lives at 1149°C (2100°F). One γ/γ'-δ alloy, Ni - 21.0 w/o Cb - 2.5 w/o Al, indicated improvement in rupture life resulting from the decrease in lamellar spacing achieved by directional solidification at 5 cm/hr compared with that found for a similar alloy grown at 2 cm/hr. This result together with the previously described improvements in hot tensile properties and observed low critical value of the G/R processing ratio led to the choice of this alloy for further creep rupture characterization. The γ/γ'-δ alloy, Ni - 19.7 w/o Cb - 6.0 w/o Cr - 2.5 w/o Al, was also chosen for further characterization due to its greater strength.

Longitudinal sections were prepared through the stress rupture fractures of representative γ/γ'-δ alloys and are shown in Figs. 46-49. At 1149°C the $\{211\}_\delta$ twin traces were absent throughout the gage. More diffuse twinning of δ was observed and is shown in Fig. 49, photographed in polarized light. Extensive bands of severe plastic deformation were manifested by recrystallized matrix areas observed within them, Fig. 47. For alloys which contained as much as 2.5 w/o Al, the gamma prime precipitates were observed to coarsen especially near the fracture surface, Fig. 48. This observation of stress-assisted coarsening of gamma prime was made by comparing the size and distribution of the precipitates within the gage with those within the threaded ends of the specimen, both of which were at the same temperature for the same length of time.

Table XIII

Apparent Volume Fraction δ-Ni_3Cb in γ/γ'-δ Alloys Directionally Solidified at Rates Between 2-100 cm/hr

Specimen No.	Composition w/o	Freezing Rate cm/hr	Vol. % δ
A72-506	Ni-21.0Cb-2.5Al	2.0	35.3
A72-623	Ni-21.5Cb-2.5Al	10.0	39.6
A72-663	Ni-21.5Cb-2.5Al	25.0	34.8
A72-669	Ni-21.67Cb-2.5Al	38.4	33.7
A72-679	Ni-22.0Cb-2.5Al	50.5	34.0
A72-690	Ni-22.0Cb-2.5Al	75.0	34.5
A72-694	Ni-22.2Cb-2.5Al	100.0	37.4

Table XIV

Task I

Stress Rupture Properties of Directionally Solidified Ni,Cr-Ni_3Cb; (Ni)/(Ni_3Al)-Ni_3Cb and (Ni,Cr)/(Ni_3Al)-Ni_3Cb Alloys in Vacuum

Specimen No.	Composition w/o	Freezing Rate cm/hr	Temp. °C	Stress ($10^7 N/m^2$)	Stress (ksi)	Time to Rupture hrs	Room Temp. Elong. %	R.A. %	Comments
A72-320-04	Ni-21.0Cb-6.0Cr	3	1149	10.41	15.0	0.8	none	meas.	
A71-341-0M	Ni-20.0Cb-10.0Cr	2	1149	8.64	12.5	1.2	3.1	0	
A71-695-02	Ni-21.0Cb-2.5Al	5	1149	8.64	12.5	>15.0	none meas.	-	*
A71-695-03	Ni-21.0Cb-2.5Al	5	1149	8.64	12.5	>12.0	none meas.	-	*
A72-325-03	Ni-21.0Cb-2.5Al	5	1149	10.41	15.0	16.9	7.8	21.0	
A72-325-04	Ni-21.0Cb-2.5Al	5	1149	8.64	12.5	51.3	7.6	9.6	
A72-288-05	Ni-21.0Cb-2.5Al	2	1149	8.64	12.5	9.9	15.3	12.9	
A72-085-01	Ni-20.8Cb-2.8Al	2	1149	8.64	12.5	11.3	12.4	15.1	
A72-085-02	Ni-20.8Cb-2.8Al	2	1149	6.91	10.0	25.6	18.1	15.3	
A71-639-01	Ni-20.0Cb-5.5Cr-2.5Al	5	1093	13.8	20.0	40.0	9.0	-	**
A71-639-02	Ni-20.0Cb-5.5Cr-2.5Al	5	1093	10.3	15.0	193.0	4.0	-	**
A71-711C-01	Ni-20.0Cb-6.0Cr-2.5Al	2	1149	8.64	12.5	14.1	11.6	12.2	***
A71-711C-02	Ni-20.0Cb-6.0Cr-2.5Al	2	1149	6.91	10.0	34.9	17.0	17.0	***
A72-202-02	Ni-20.0Cb-6.0Cr-2.5Al	2	1149	10.41	15.0	46.3	5.5	4.3	
A72-202-03	Ni-20.0Cb-6.0Cr-2.5Al	2	1149	12.15	17.5	18.7	3.8	7.6	
A71-730-04	Ni-20.2Cb-9.2Cr-2.2Al	2	1149	8.64	12.5	5.4	18.3	19.6	***
A72-097-02	Ni-19.7Cb-9.0Cr-1.0Al	2	1149	8.64	12.5	> 98.7	> 4.2	-	*
A72-097-03	Ni-19.7Cb-9.0Cr-1.0Al	2	1149	10.3	15.0	4.9	8.5	9.1	
A72-187-02	Ni-19.5Cb-9.0Cr-1.0Al	2	1149	10.41	15.0	38.1	11.7	7.5	
A72-187-03	Ni-19.5Cb-9.0Cr-1.0Al	2	1149	8.64	12.5	15.8	1.5	4.3	***

*sheared threaded end
**air
***cellular microstructure

LARSON MILLER PARAMETER DATA FOR RUPTURE OF VARIOUS δ Ni_3Cb REINFORCED ALLOYS

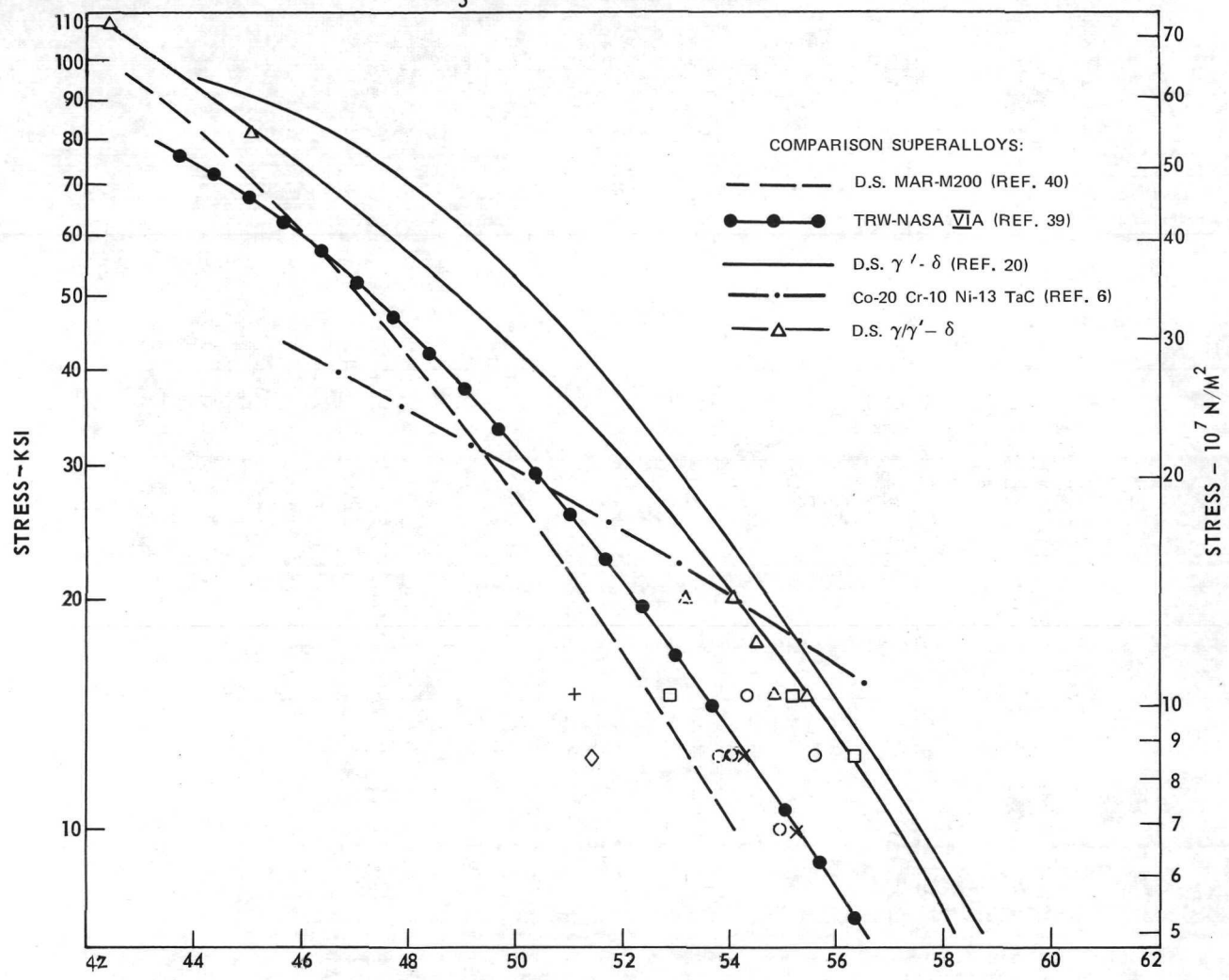

◇ Ni–20.0 Cb–10.0 Cr (2CM/HR) HIGH GRADIENT

\+ Ni–21.0 Cb–6.0 Cr (3 CM/HR) HIGH GRADIENT

○ Ni–21.0 Cb–2.5 Al (5 CM/ HR) HIGH GRADIENT

○ Ni–21.0 Cb–2.5 Al (2 CM/HR) LOW GRADIENT

○ Ni–20.8 Cb–2.8 Al (2 CM/HR) LOW GRADIENT

△ Ni–20.0 Cb–6.0 Cr–2.5 Al (2 CM/HR) HIGH GRADIENT

△ Ni–20.0 Cb–5.5 Cr–2.5 Al (5CM/HR) HIGH GRADIENT

× Ni–20.0 Cb–6.0Cr–2.5 Al (2 CM/HR) CELLULAR, LOW GRADIENT

□ Ni–19.5 Cb–9.0 Cr–1.0 Al (2 CM/HR) HIGH GRADIENT

FIGURE 45

LONGITUDINAL SECTION THROUGH FRACTURE OF STRESS RUPTURE SPECIMEN (A72–325–04) Ni – 21.0 Cb – 2.5 Al; STRESS = 86 MN/m^2 (12.5 KSI); 1149°C, TIME TO RUPTURE 51.3 HOURS

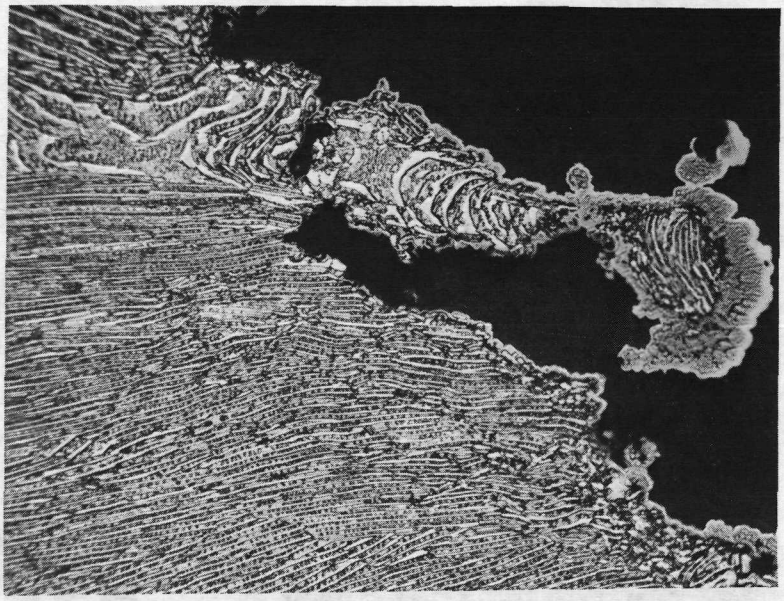

a)

|50μm|

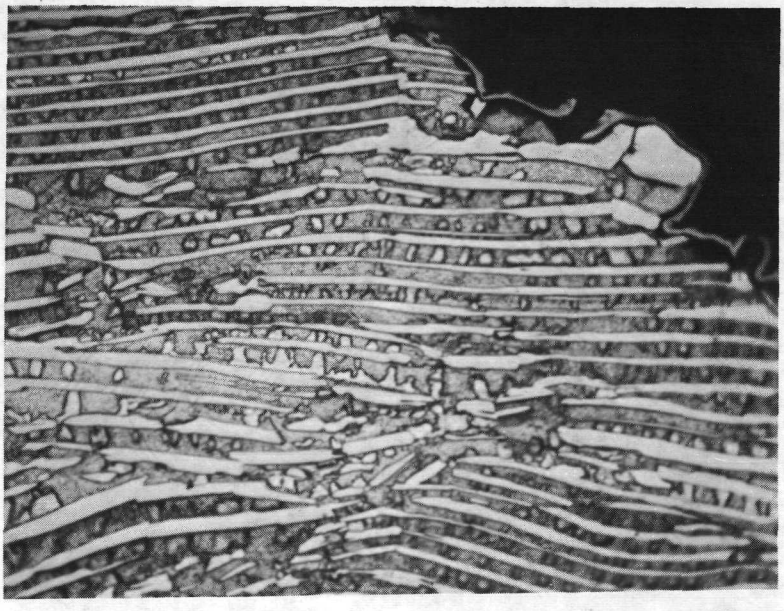

b)

|10μm|

FIGURE 46

LONGITUDINAL SECTION THROUGH FRACTURE OF STRESS RUPTURE SPECIMEN (A72–187–02) Ni – 19.5 Cb – 9.0 Cr – 1.0 Al; STRESS = 104 MN/m^2 (15 KSI); 1149°C, TIME TO RUPTURE 38.1 HRS

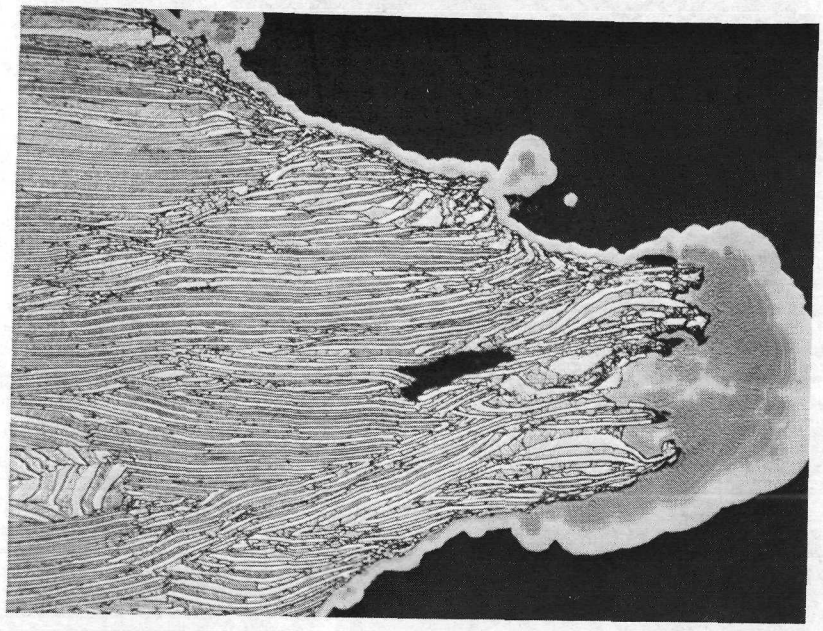

a)

50 μm

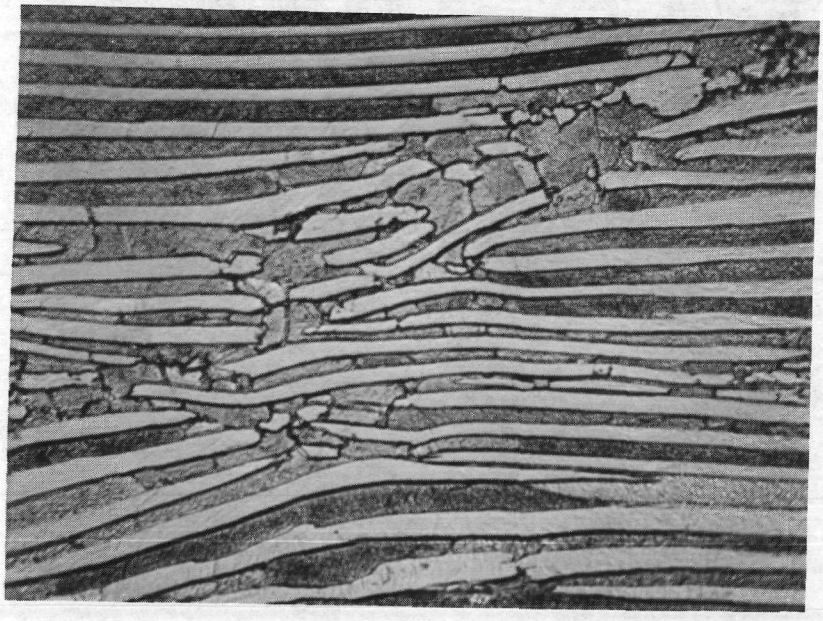

b)

10 μm

FIGURE 47

LONGITUDINAL SECTION THROUGH FRACTURE OF STRESS RUPTURE SPECIMEN (A72–202–02) Ni–20.0 Cb–6.0 Cr–2.5 Al; STRESS = 104 MN/m^2 (15 KSI), 1149° C TIME TO RUPTURE 46.3 HRS

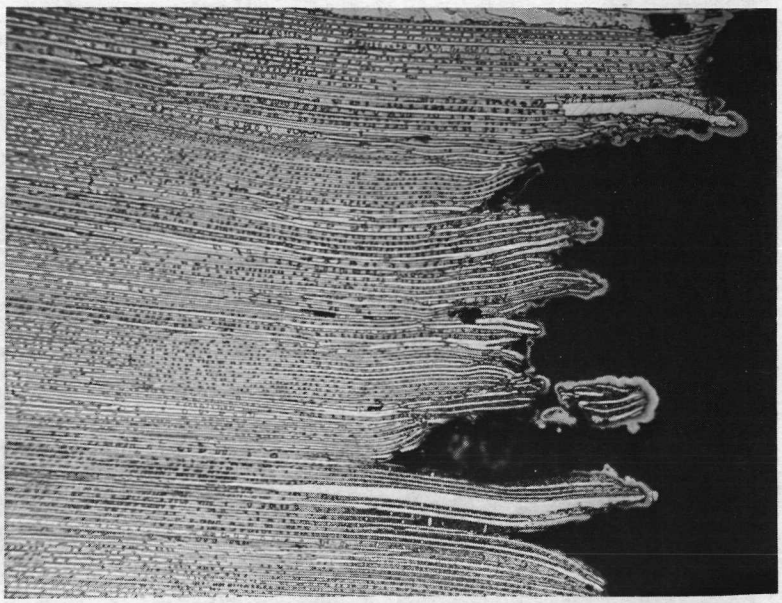

a) 50 μm

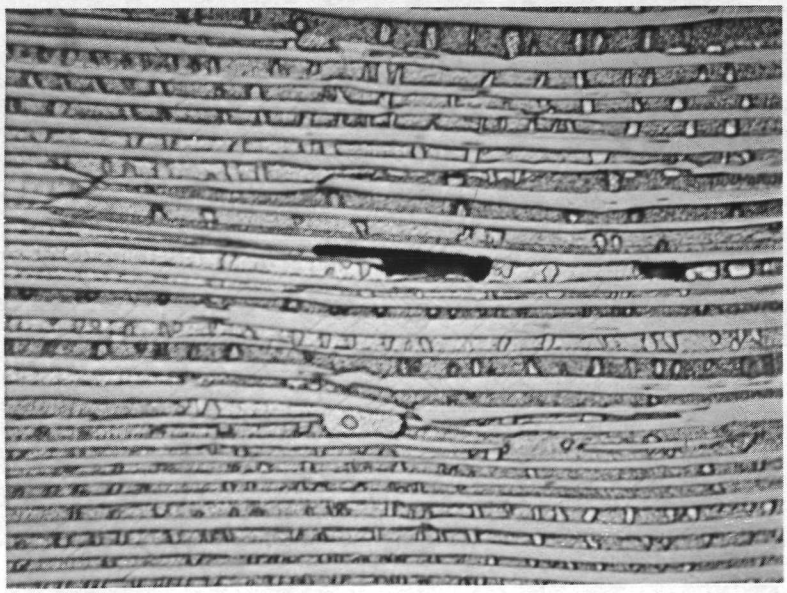

b) 10 μm

FIGURE 48

LONGITUDINAL AREAS REVEALING Ni_3Cb TWINNING IN STRESS–RUPTURE SPECIMEN (A72–202–02) Ni – 20.0 Cb – 6.0 Cr – 2.5 Al IN POLARIZED LIGHT; STRESS = 104 MN/m^2 (15 KSI), 1149°C

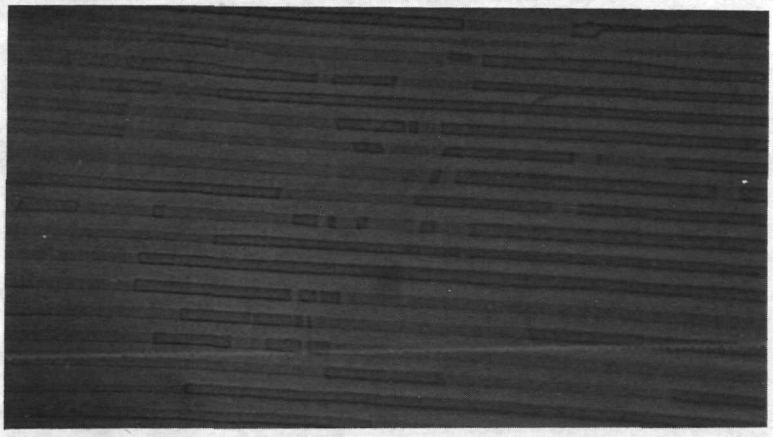

(a) AWAY FROM FRACTURE, ETCHANT A ONLY

10μm

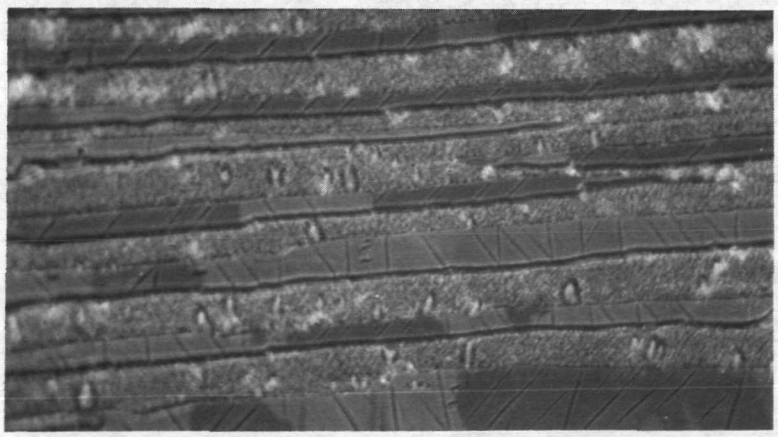

(b) ADJACENT FRACTURE, ETCHANT A AND B

10μm

FIGURE 49

3.4.4 Creep Rupture

The results of vacuum creep tests conducted at various temperatures between 815-1200°C for the two γ/γ'-δ alloys, Ni - 19.7 w/o Cb - 6.0 w/o Cr - 2.5 w/o Al and Ni - 21.75 w/o Cb - 2.55 w/o Al, are presented in Table XV. The stresses for these tests were selected to cause failure in between 50 and 200 hrs. The time to 0.1, 0.2 and 0.5 percent strain, failure elongation, and reduction of area are also reported therein. A typical creep curve for the Ni - 19.7 w/o Cb - 6.0 w/o Cr - 2.5 w/o Al tested at 1093°C (2000°F) and 138 MN/m^2 (20,000 psi) is shown in Fig. 50. The Larson-Miller parameter data of Table XV are plotted in Figs. 51 and 52 for the γ/γ'-δalloys, Ni - 19.7 w/o Cb - 6.0 w/o Cr - 2.5 w/o Al, directionally solidified at 3 cm/hr and the Ni - 21.75 w/o Cb - 2.55 w/o Al directionally solidified at 38 cm/hr, respectively. For comparison purposes an averaged rupture curve for each 'eutectic superalloy' was determined and plotted in Fig. 53 with the current representative superalloys D.S. Mar M200 (Ref. 40) and NASA TRW VIA (Ref. 39) together with other strong 'eutectic superalloys' D.S. γ'-δ (Refs. 1,2) and D.S. Co,Cr,Ni-TaC (Ref. 6). It can be seen that the γ/γ'-δ alloys exceed all known superalloys in rupture strength, a fact which further suggests that these <u>in situ</u> composites have potential for use in turbine blades/vanes operating at temperatures higher than those currently used. This success has been largely the result of the persistent application of essentially Edisonian techniques to an increasingly complex alloy problem. All the strength goals of this program have been successfully met with this alloy system.

3.4.5 Thermal Fatigue and Expansion

To assess phase stability of γ/γ'-δ alloys and their resistance to thermal fatigue cracking and delamination under conditions of thermal cycling, a specimen of Ni - 19.7 w/o Cb - 6.0 w/o Cr - 2.5 w/o Al (A72-323-02) was cycled 3000 times between 400-1120-400°C (750-2050-750°F) in 2.1 minutes in a specially constructed thermal cycling test rig where the specimen is heated resistively and cooled with an argon jet (Ref. 47). No externally induced stresses are present in this test as it was designed to examine damage resulting from internally generated stresses. After 3000 cycles no microstructural damage to the reinforcing Ni_3Cb lamellae was observed. The strength and ductility measured on this specimen after cycling was 516 MN/m^2 (74,800 psi) and 24 percent respectively at 1093°C (2000°F) which compares favorably with hot tensile tests of this material in the as-directionally solidified condition, Table X. Additional specimens of both γ/γ'-δ alloys, Ni - 19.7 w/o Cb - 6.0 w/o Cr - 2.5 w/o Al and Ni - 21.75 w/o Cb - 2.55 w/o Al, were cycled 3000 times between 400°C/min/1120°C max (750°F min/2050°F max), in 2.1 minute cycles and tested in vacuum creep rupture at 1093°C (2000°F). The rupture lives measured after cycling were within the low range of the scatter of the virgin as-directionally solidified materials. No microstructural damage of the δ reinforcing phase was noted but coarsening of the gamma prime precipitates was observed after cyclic plastic deformation of the matrix had taken place. It should be noted that this thermal fatigue

Table XV

Task II

Stress Rupture Properties of Directionally Solidified (Ni)/(Ni_3Al)-(Ni_3Cb) and (Ni,Cr)/(Ni_3Al)-(Ni_3Cb) Alloys in Vacuum

Specimen No.	Composition w/o	Freezing Rate cm/hr	Temp °C	Stress ($10^7 N/m^2$)	Stress (ksi)	Time to Rupture hrs	Time to 0.1% (hrs)	Time to 0.2% (hrs)	Time to 0.5% (hrs)	Room Temp. Elong. %	R.A. %	LMP C=20 x 10^{-3}
A72-682-01	Ni-19.7Cb-6.0Cr-2.5Al	3	1000	27.6	40	18.1	5	7	10	8.5	28.5	48.72
A72-682-02	"	3	1000	27.6	40	24.5	3	5	12	10.4	35.4	49.02
A72-675-03	"	3	1000	27.6	40	46.2	10	15	23	10.8	20.8	49.66
A72-628-03	"	3	1093	13.8	20	77.3	7	12	50	6.8	14.8	53.83
A72-682-03	"	3	1093	13.8	20	71.4	10	20	38	9.2	20.5	53.76
A72-675-01	"	3	1200	5.5	8.5	2.8	-	-	-	-	-	**
A72-684-03	"	3	1200	5.5	8.5	115.2	99	106	110	6.4	11.9	58.46
A72-675-02	"	3	1200	5.5	8.5	61.8	10	28	48	4.3	2.0	57.75
A72-911-03	"	3	900	48.3	70.0	87.6	0.7	3.5	19.5	6.5	9.0	46.29
A72-735-01	"	3	900	44.9	65.0	114.4	32	43	63	11.6	19.7	46.55
A72-735-02	"	3	815	69.0	100.0	>200.0	5	39	152	1.0	-	>43.71*
A72-735-02 reloaded	"	3	815	75.9	110.0	119.9	10	18	37	10.1	19.7	43.27
A72-734-01	"	3	815	75.9	110.0	22.9	1	2	8	10.1	22.6	41.76
A72-769-01	Ni-21.75Cb-2.55Al	38	1000	20.7	30	65.0	4	8	25	10.4	8.9	49.99
A72-769-03	"	38	1000	20.7	30	97.0	2	5	43	8.3	8.9	50.39
A72-768-01	"	38	1093	12.4	18	122.5	3	14	68	7.4	9.6	54.33
A72-768-02	"	38	1093	12.4	18	153.6	90	106	134	3.7	7.6	54.58
A72-800-01	"	38	1200	5.5	8.5	64.3	25	38	49	9.3	16.1	57.79
A72-800-02	"	38	1200	5.5	8.5	143.1	95	108	126	8.2	10.9	58.71
A72-771-01	"	38	900	39.7	57.5	58.8	2	5	25	9.6	22.2	45.93
A72-819-01	"	38	900	39.7	57.5	62.3	6	15	21	9.4	17.5	45.99
A72-669-02	"	38	900	48.3	70.0	15.8	11	13	15	23.0	9.0	44.82
A72-817-01	"	38	815	58.7	85	130.5	9	40	79	8.2	16.6	43.37
A72-817-02	"	38	815	58.7	85	162.1	0	1	55	9.6	13.3	43.53

*discontinued

**did not fail in gage as threads alloyed with TZM grip and failed by thread shear

CREEP CURVE OF $\gamma/\gamma'-\delta$ (Ni–19.7 w/o Cb–6.0 w/o Cr–2.5 w/o Al)

A72–628–03 AT 1093°C (2000°F) AND 13.8 x 10^7 N/m^2 (20,000 psi) IN VACUUM

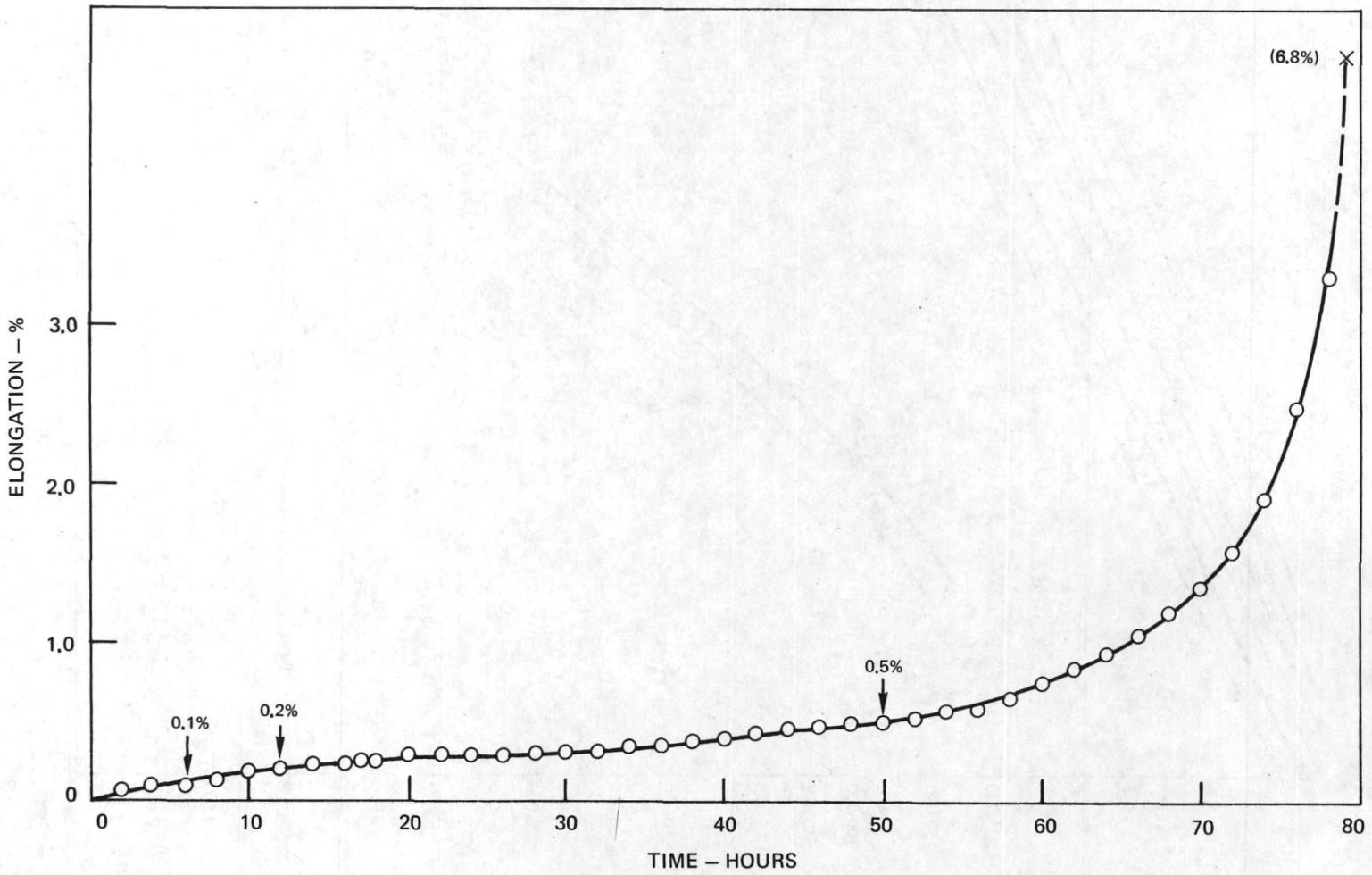

FIGURE 50

LARSON MILLER RUPTURE CURVE FOR γ/γ'-δ

Ni - 19.7 w/o Cb - 6.0 w/o Cr - 2.5 w/o Al

(R = 3 cm/hr, $G_L \sim 300^{o}$ C/cm)

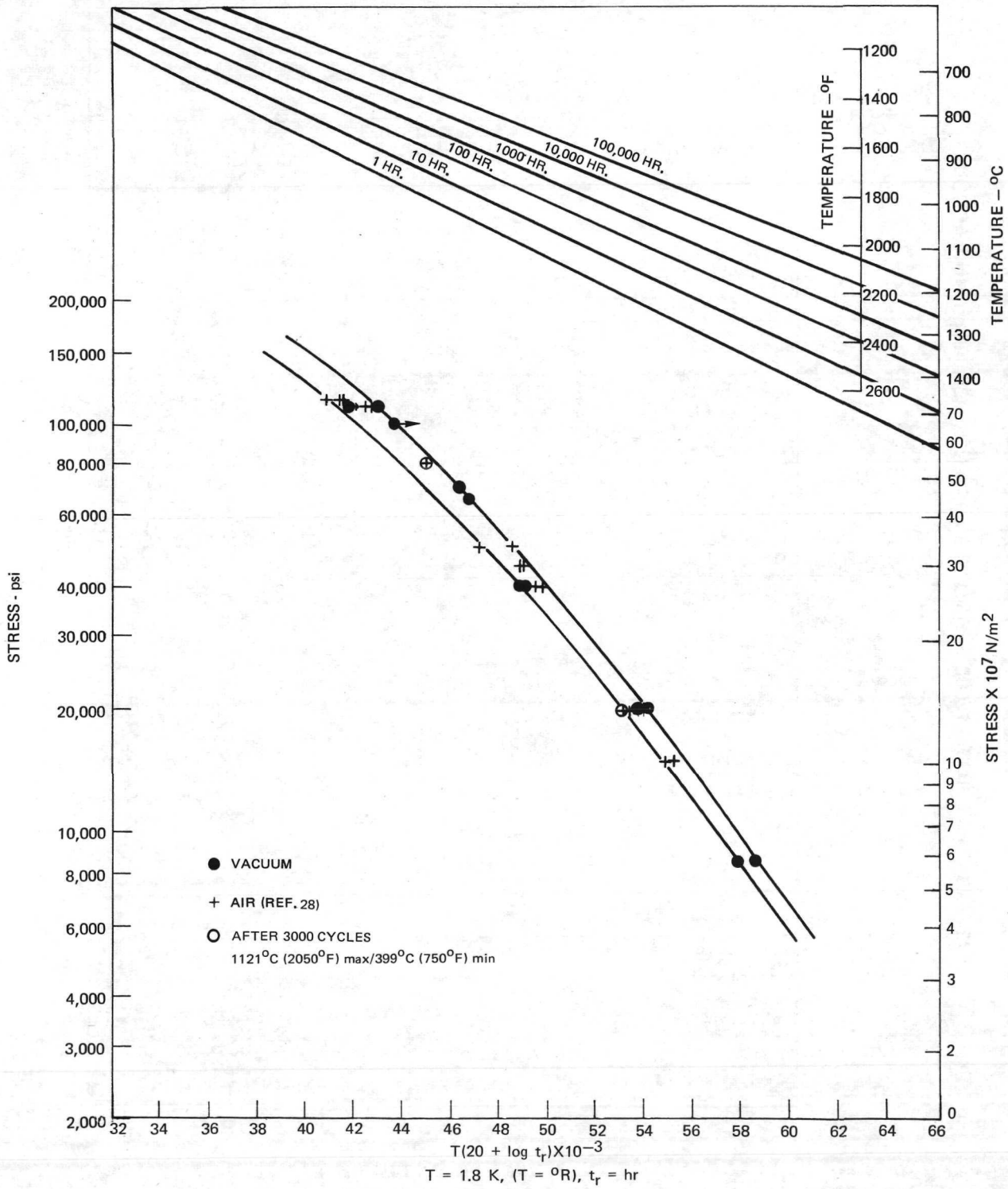

FIGURE 51

LARSON MILLER RUPTURE CURVE FOR γ/γ'-δ

Ni - 21.75 w/o Cb - 2.55 w/o Al

(R = 38 cm/hr, G_L ~ 300°C/cm)

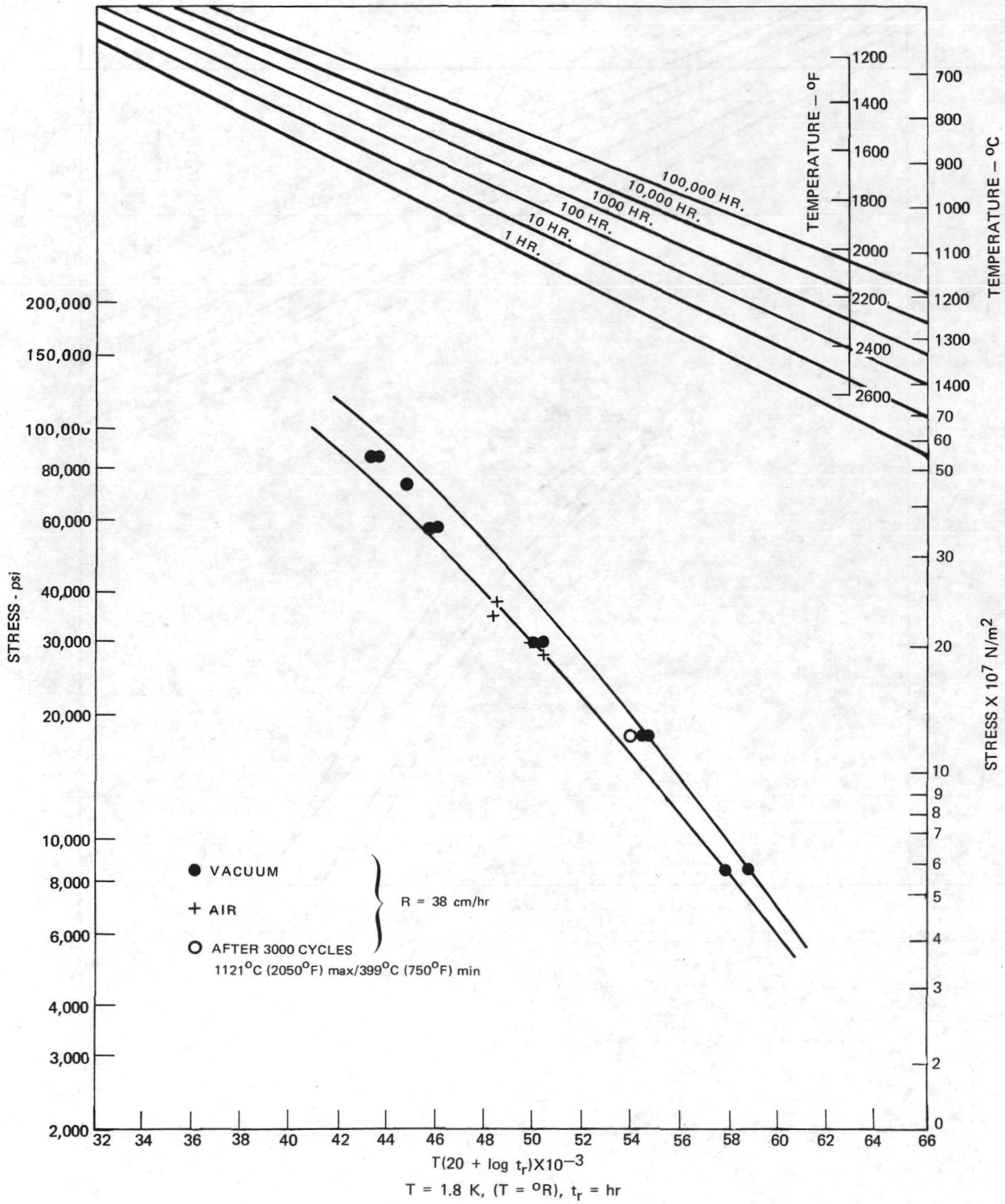

FIGURE 52

LARSON MILLER PARAMETER – RUPTURE CURVES OF VARIOUS δ – Ni_3Cb REINFORCED ALLOYS AND COMPARISON SUPERALLOYS

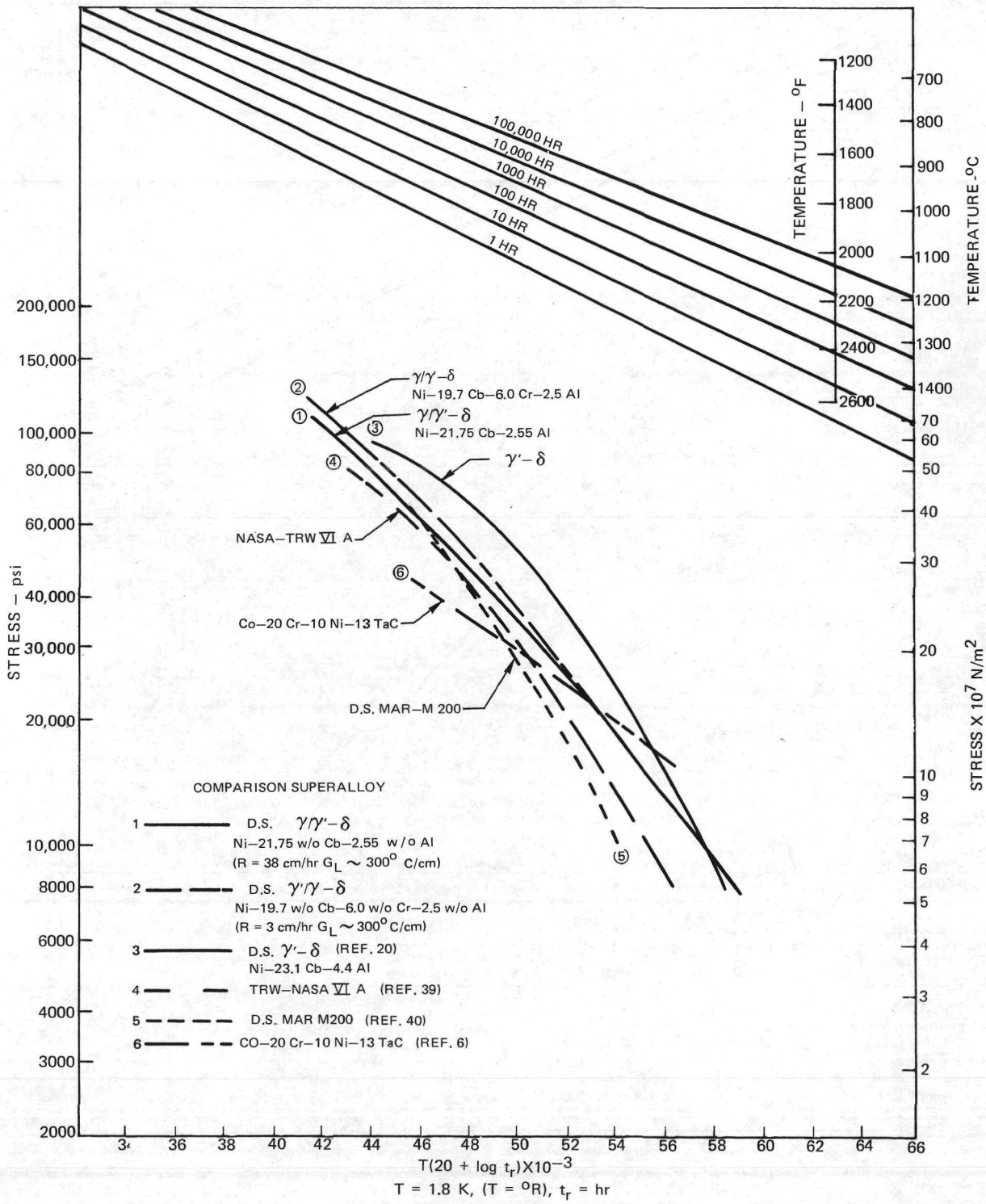

FIGURE 53

test produces no bulk thermal stresses (as occur in parts of varying cross section) nor are external mechanical stresses imposed - both of which are present in actual turbine engine environments.

The thermal expansion of γ/γ'-δ, Ni - 19.7 w/o Cb - 6.0 w/o Cr - 2.5 w/o Al, was measured over the temperature interval 25-1000°C in the direction of growth as shown in Fig. 54. The mean coefficient of thermal expansion of the γ/γ'-δ alloy is $14.4 \times 10^{-6}/°C$ which is less than that of nickel superalloys which have coefficients of the order of $16 \times 10^{-6}/°C$ but greater than that for γ'-δ (Ref. 2). The as-directionally solidified material is thus not free of internal stresses since $\alpha_{Ni,Ni3Al} > \alpha_{Ni_3Cb}$ and the matrix will be under some residual tensile stress after growth. On heating the δ should be placed in tension and the γ/γ' matrix into compression. As the crystallographic interface planes between the eutectic phases are also the favored precipitation habit planes in this system, the local shape of the lamellar interfaces does not change as primarily columbium atoms are cyclically diffused into the matrix lamellae from the δ, Ni_3Cb lamellae and back again due to differences in the mutual solid solubility of these phases at elevated temperatures. No account at this time can be taken for the stress assistance to diffusion in the interfacial region where locally high deformation gradients exist due to differences in coefficients of thermal expansion. In comparison, the phases of the refractory metal monocarbide-nickel and cobalt 'eutectic' systems do not possess this coincident relationship between the preferred eutectic growth interfacial planes and the preferred precipitation habit planes. This incompatibility leads to the development of serrations after thermal cycling to a temperature where an appreciable mutual solid solubility of the carbide in the matrix phases exist. These serrations grow in size with increasing number of cycles at a constant maximum temperature or at a constant number of cycles with ever increasing exposure temperatures (Ref. 48). This type of damage to <u>in situ</u> composites is a recognized source of great concern and must be taken into consideration in the design of future alloys (Refs. 47,49).

3.4.6 Impact Strength

Subsize Charpy V-notched impact tests were performed at room temperature on as-directionally solidified (3 cm/hr) and heat treated Ni - 19.7 w/o Cb - 6.0 w/o Cr - 2.5 w/o Al in the direction normal to phase alignment as indicated in Figs. 55-58. The specimens 5 mm by 10 mm possessed one-half the cross sectional area of the standard ASTM Type A Charpy (single beam) impact test bar and conformed to the recommended subsize design (Ref. 19). The heat treatment consisted of an exposure to 850°C (1560°F) for 1500 hrs in vacuum. The notched impact values before and after heat treatment were 2.3-1.6 J (1.69 and 1.19 ft-lbs) respectively. Examination by both optical and scanning electron microscopy indicated no changes in microstructure, i.e. new phases or coarsening. The fracture mode in both instances was characterized by cleavage of the δ, Ni_3Cb lamellae and ductile fracture of the γ/γ' matrix as shown in the montages of Figs. 55 and 56. More extensive twinning within the δ, Ni_3Cb lamellae was observed within the unheat-treated specimen especially in the vicinity of the notch. Widmanstätten δ precipitation was observed along octahedral planes within the γ/γ' lamellae. These fine plate-like precipitates could be resolved only by replication and subsequent electron microscopic examination.

THERMAL EXPANSION OF $Ni_3(Al,Cb)$, Ni_3Cb, $\gamma'-\delta$ AND $\gamma/\gamma'-\delta$ (Ni– 19.8 w/o Cb – 6.0 w/o Cr – 2.5 w/o Al)

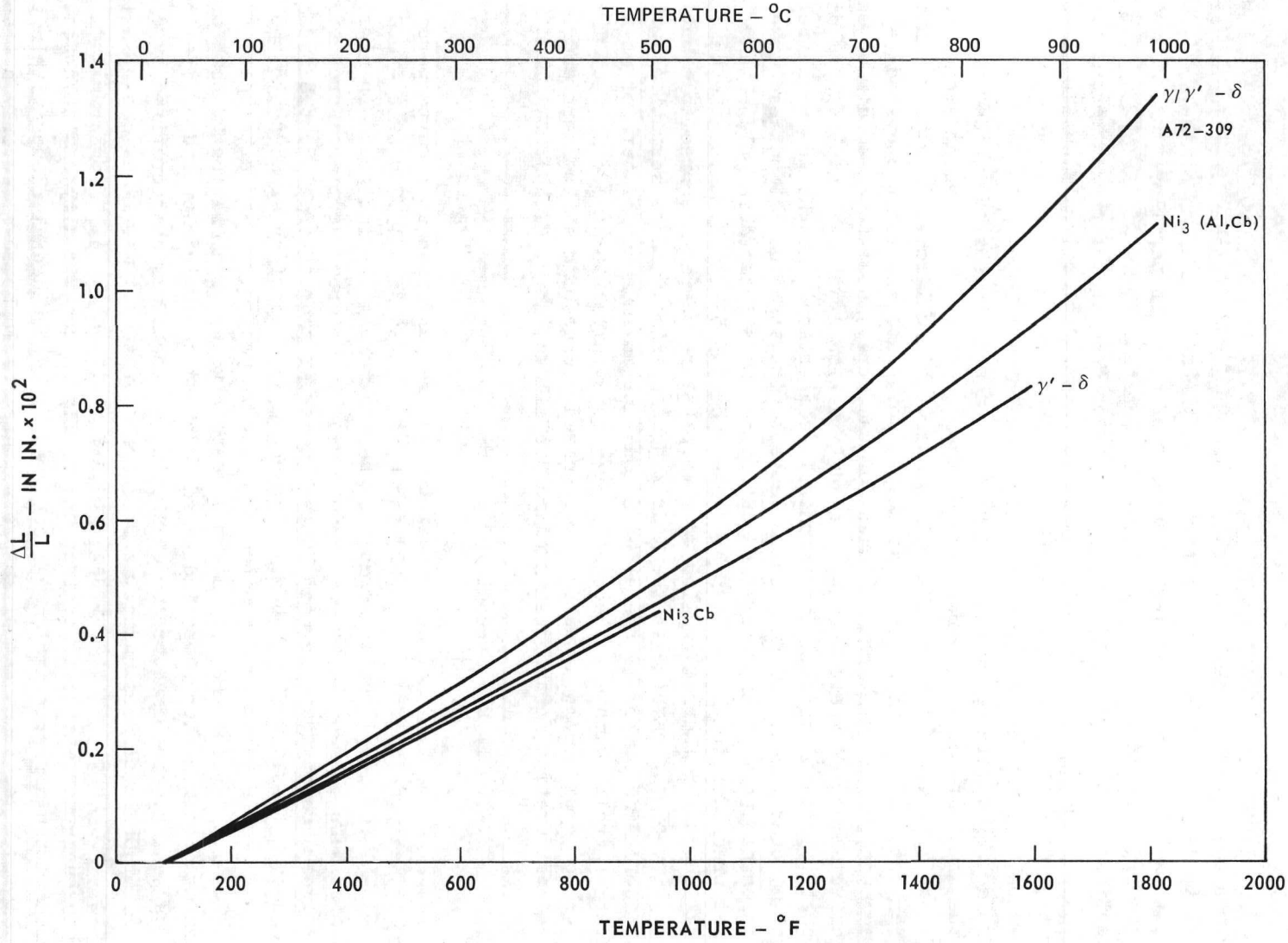

FIGURE 54

FRACTURE SURFACE MONTAGE OF $\gamma/\gamma' - \delta$ (Ni – 19.7 w/o Cb – 6.0 w/o Cr – 2.5 w/o Al)
SUBSIZE CHARPY IMPACT SPECIMEN TESTED AT ROOM TEMPERATURE
2.28 JOULES (1.69 ft–lbs)

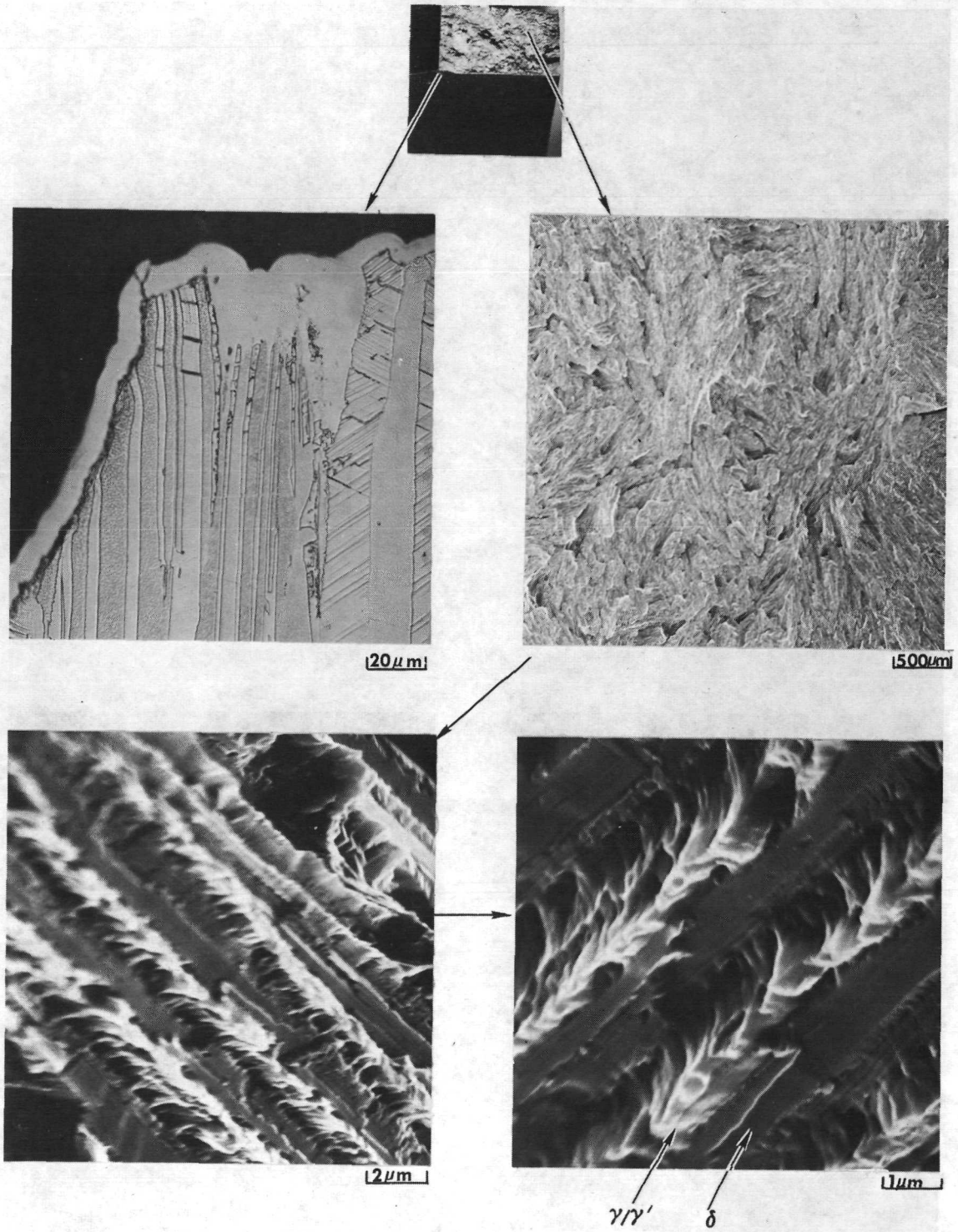

FIGURE 55

FRACTURE SURFACE MONTAGE OF $\gamma/\gamma' - \delta$ (Ni – 19.7 w/o Cb – 6.0 w/o Cr – 2.5 w/o Al) SUBSIZE CHARPY IMPACT SPECIMEN TESTED AT ROOM TEMPERATURE AFTER 1500 HOURS EXPOSURE AT 850°C, 1.5 JOULES (1.11 ft–lbs)

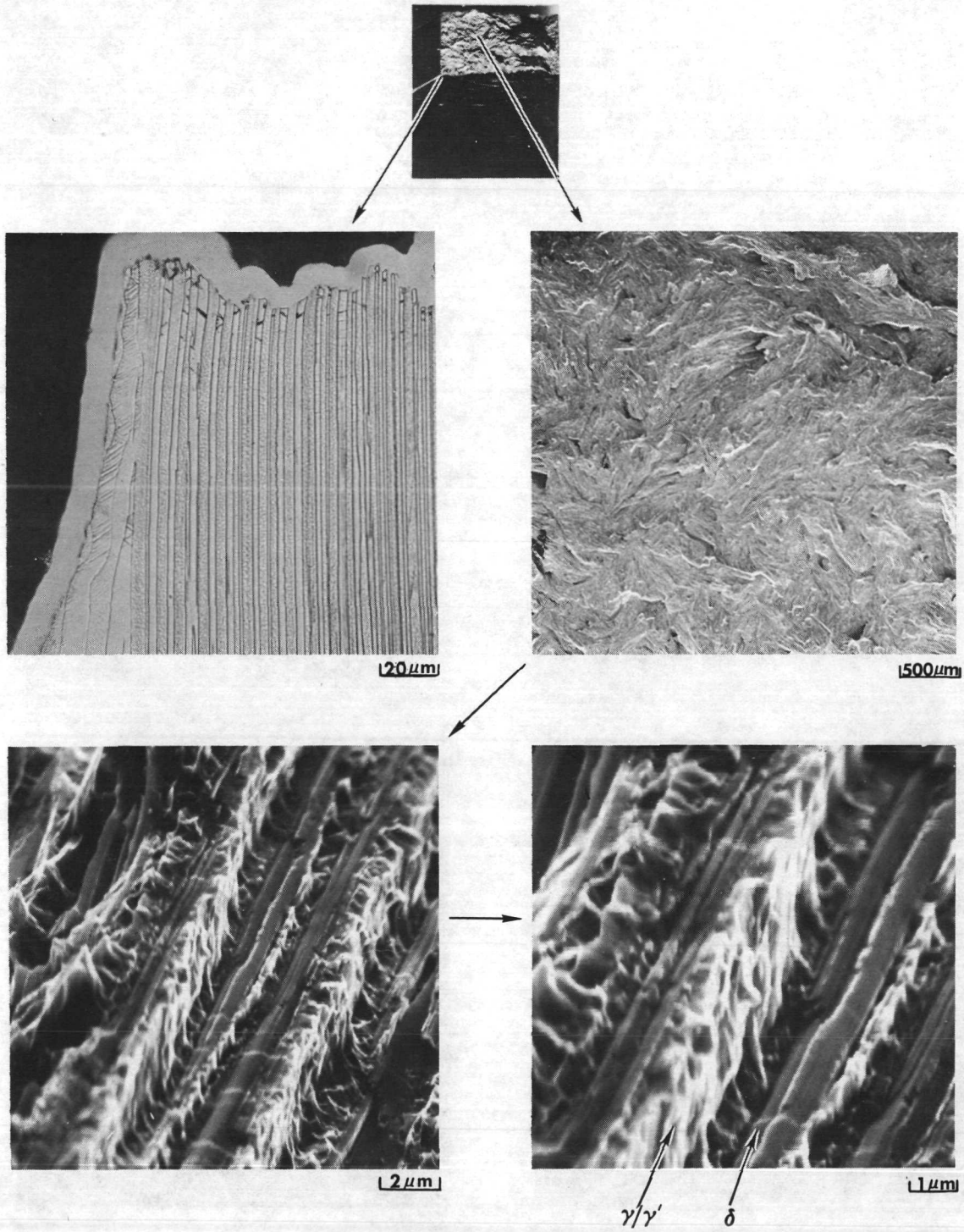

FIGURE 56

Preliminary results on full sized V-notched Charpy impact specimens of Ni - 19.7 w/o Cb - 6.0 w/o Cr - 2.5 w/o Al have indicated at least a 2.7 J (2 ft-lb) impact strength at room temperature and 8.1-10.8 J (6 to 8 ft-lbs) at root attachment and airfoil temperatures respectively (Ref. 28).

Subsize Charpy V-notched specimens of as-grown (38 cm/hr) and heat treated Ni - 21.75 w/o Cb - 2.55 w/o Al were again tested in the direction normal to the phase alignment. The notch impact energies measured before and after heat treatment (1500 hrs exposure at 850°C) were 13.3-7.7 J (9.85 and 5.75 ft-lbs) respectively. Examination by both optical and scanning electron microscopy indicated no coarsening or new phases in the microstructure. Each fracture surface displayed both ductile fracture of the γ/γ' matrix and cleavage of the δ, Ni_3Cb lamellae and exhibited marked off-plane cracking at eutectic grain boundaries as shown in Figs. 57 and 58. Less extensive grain boundary decohesion normal to the fracture surface was observed after heat treatment, Fig. 58. This alloy thus displays improved impact toughness compared with conventional and directionally solidified nickel-base superalloys (Ref. 40), and Co,Ni,Cr-TaC alloys (Refs. 7,49) despite the presence of over thirty percent of thin aligned, more brittle lamellar reinforcement. It is also considerably tougher than the Ni - 19.7 w/o Cb - 6.0 w/o Cr - 2.5 w/o Al, γ/γ'-δ alloy and indicates the large range of impact toughness achievable in the γ/γ'-δ system at room temperature.

3.5 Oxidation

3.5.1 Isothermal

Oxidation tests in still air were performed on γ/γ'-δ specimens of Ni - 21.75 w/o Cb - 2.55 w/o Al, Ni - 19.5 w/o Cb - 9.0 w/o Cr - 1.0 w/o Al, and Ni - 19.7 w/o Cb - 6.0 w/o Cr - 2.5 w/o Al at 1000, 1100 and 1200°C for periods of 5, 50, 200 and 500 hrs. Hastelloy X (Ni - 22 w/o Cr - 18.5 w/o Fe - 9 w/o Mo - 1.5 w/o Co - 0.6 w/o W - 0.5 w/o Si - 0.5 w/o Mn - 0.1 w/o C) was examined as a reference alloy. All specimens were lapped with 600 grit paper. The results of these tests are presented in Table XVI and graphically in Fig. 59. There was one feature of the oxidation reaction in common for all γ/γ'-δ alloys at these three temperatures. This was the cracking and spallation of the external scale on cooling to room temperature. The spall weights, measured after each exposure, are presented in Table XVII. In general an increase in spall weight was observed with increasing exposure temperature and time at temperature for each γ/γ'-δ alloy. The addition of chromium was very beneficial to the static oxidation rate of each γ/γ'-δ alloy containing aluminum. Macroscopic observations of the spalling and the total thickness changes (both sides) were made on polished cross sections of each sample tested and are recorded in Tables XVIII and XIX. The alloy depletion measured as mm/side during static oxidation for three alloys, Ni - 19.7 w/o Cb - 6.0 w/o Cr - 2.5 w/o Al, Ni - 21.75 w/o Cb - 2.55 w/o Al, and Hastelloy X were plotted as a function of time and temperature of exposure in Figs. 60-62. The alloy depletion zone thickness measurements represent the depth per side

FRACTURE SURFACE MONTAGE OF $\gamma/\gamma' - \delta$ (Ni – 21.75 w/o Cb – 2.55 w/o Al) SUBSIZE CHARPY IMPACT SPECIMEN TESTED AT ROOM TEMPERATURE, 13.31 JOULES (9.85 ft–lbs)

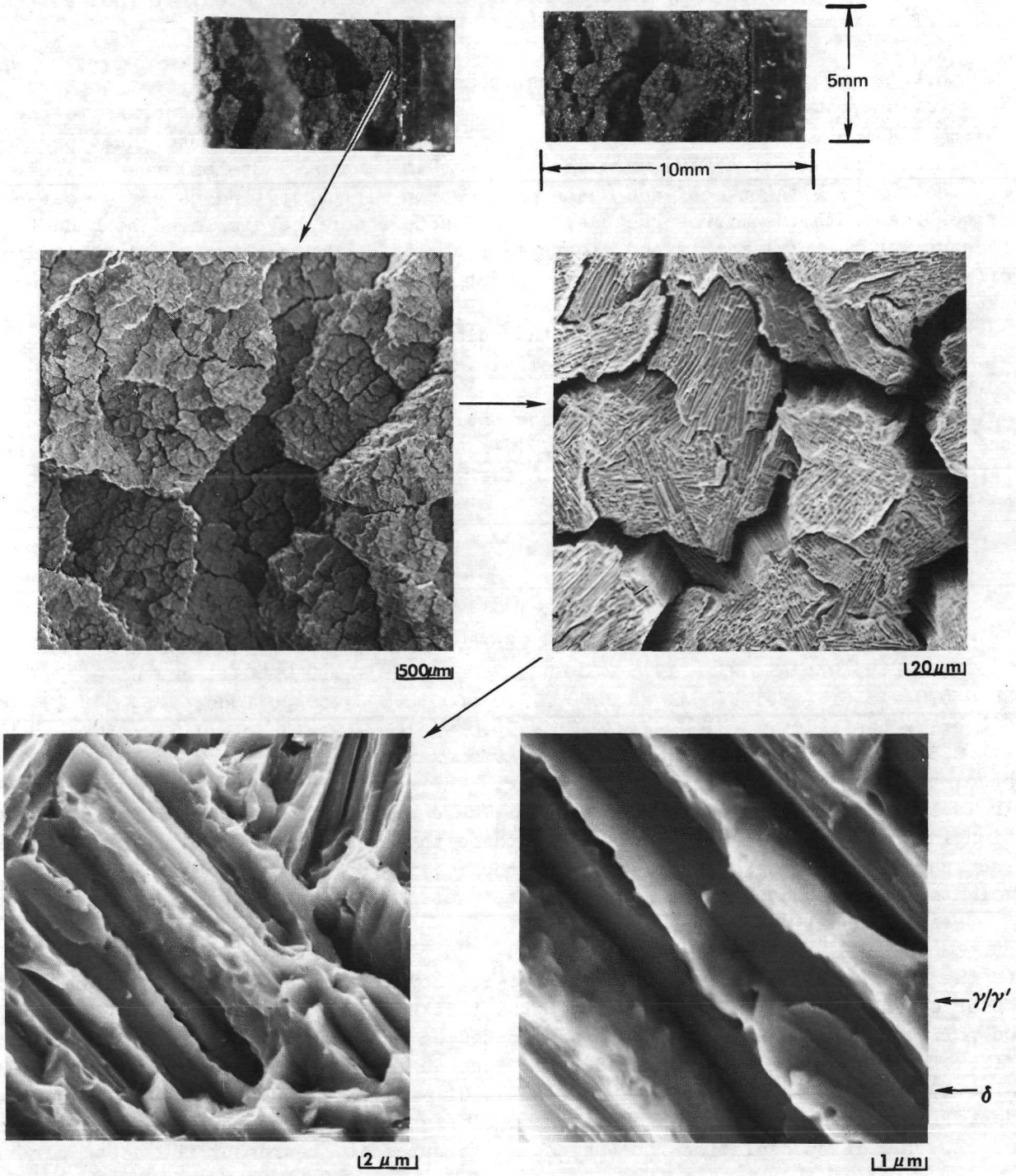

FIGURE 57

FRACTURE SURFACE MONTAGE OF $\gamma/\gamma' - \delta$ (Ni – 21.75 w/o Cb – 2.55 w/o Al) SUBSIZE CHARPY IMPACT SPECIMEN TESTED AT ROOM TEMPERATURE AFTER 1500 HRS EXPOSURE AT 850°C, 7.7 JOULES (5.7 ft–lbs)

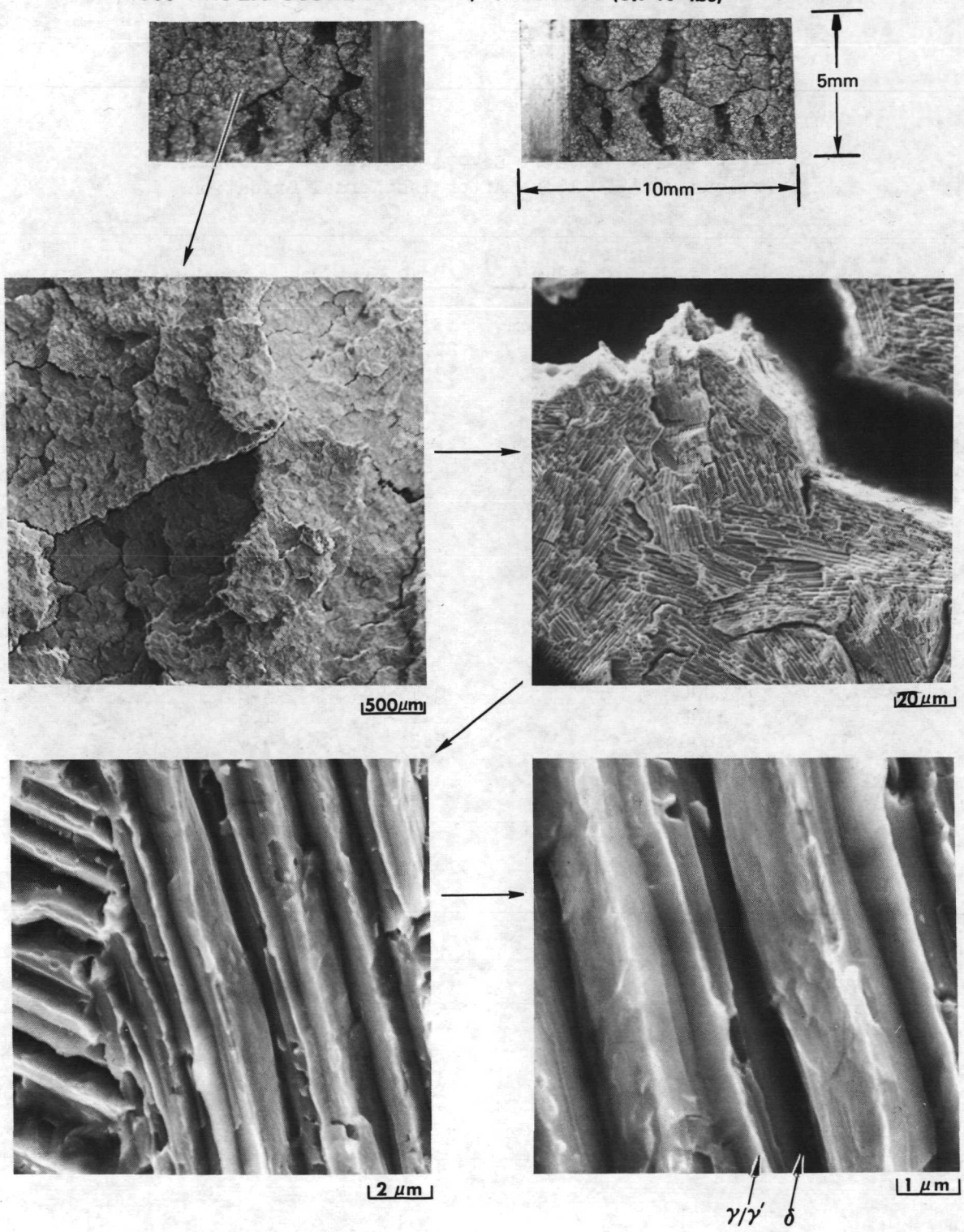

FIGURE 58

Table XVI

Specific Weight Change (mg/cm^2) (Exclusive of Spall) of Various γ/γ'-δ Alloys After Isothermal Oxidation

		5 hr	50 hr	200 hr	500 hr
Ni-21.75w/oCb-2.55w/oAl (A72-807)	1000°C	5.2 mg/cm^2	13.6 mg/cm^2	30.6 mg/cm^2	42.2 mg/cm^2
	1100	7.8	21.4	43.9	67.2
	1200	16.7	53.8	106.5	(-132.4)
Ni-19.5w/oCb-9.0w/oCb-1.0w/oAl (A72-559)	1000	-	-	-	6.1
	1100	-	-	-	8.7
	1200	-	-	-	33.5
Ni-19.7w/oCb-6.0 w/oCr-2.5w/oAl (A72-628)	1000	.9	1.8	3.4	7.1
	1100	1.2	3.2	4.8	10.2
	1200	2.4	7.2	16.8	29.6
Hastelloy X	1000	-	0.75	1.2	1.8
	1100	-	1.1	1.6	3.5
	1200	-	2.3	4.0	2.3

SPECIFIC WEIGHT GAIN VS TIME

(ISOTHERMAL OXIDATION)

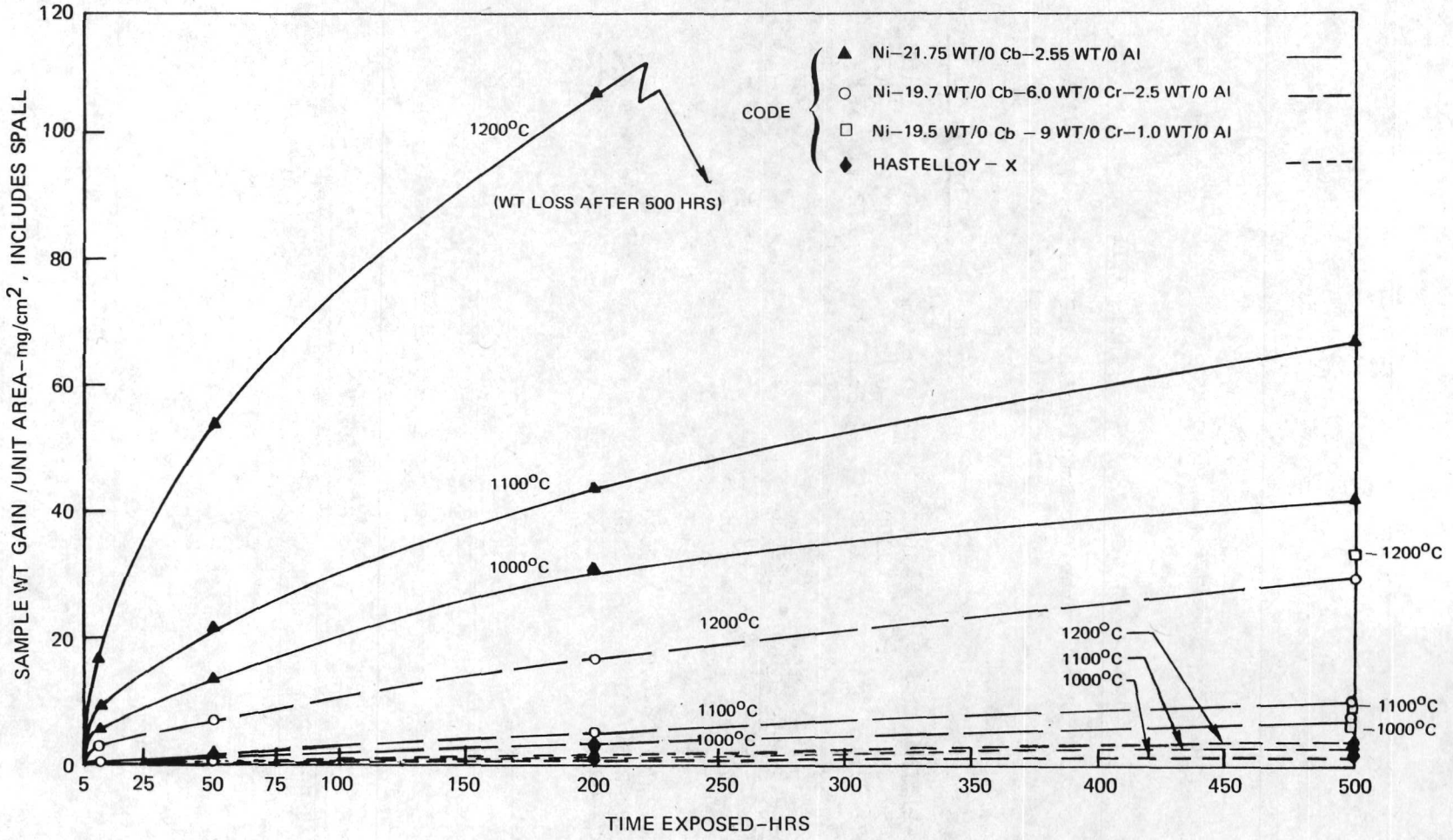

FIGURE 59

Table XVII

Specific Spall Weight of Various γ/γ'-δ Alloys
After Isothermal Oxidation

		5 hr	50 hr	200 hr	500 hr
Ni-21.75w/oCb-2.55w/oAl (A72-807)	1000°C	~0 mg/cm^2	~0	38.2	67.3
	1100	~0	49.2	74.1	170.2
	1200	36.8	172.1	*	88.3
Ni-19.5w/oCb-9.0 w/oCr-1.0w/oAl (A72-559)	1000	-	-	-	15.7
	1100	-	-	-	18.7
	1200	-	-	-	53.8
Ni-19.7w/oCb-6.0 w/oCr-2.5w/oAl (A72-628)	1000	~0	~0	2.7	17.7
	1100	~0	1.9	6.1	26.2
	1200	1.5	17.3	50.2	83.8
Hastelloy X	1000	~0	~0	~0	~0
	1100	~0	~0	~0	~0
	1200	~0	.5	.4	~0

*did not spall

Table XVIII

Total Thickness Changes and Scale/Oxide Penetration from Microscopic Observations after Isothermal Oxidation

Alloy wt/o	Temp °C	5 hr Thickness Change (mm)	5 hr Scale Obs.	50 hr ΔT (mm)	50 hr Scale Obs.	200 hr ΔT (mm)	200 hr Scale Obs.	500 hr ΔT (mm)	500 hr Scale Obs.
Ni-21.75Cb-2.55Al	1000	+.02	a	+.025	a	+.03	pa	+.07	s
	1100	nil	a	+.03	pa	+.06	pa	+.07	s
	1200	-.10	s	-.17	s	ind.	ind.	ind.	ind.
Ni-19.5Cb-9.0Cr-1.0 Al	1000	-	-	-	-	-	-	-.08	s
	1100	-	-	-	-	-	-	-.09	s
	1200	-	-	-	-	-	-	-.22	s
Ni-19.7Cb-6.0Cr-2.5Al	1000	-.03	a	-.01	a	-.04	pa	-.03	s/pa
	1100	-.02	a	-.01	pa	-.04	pa	-.05	s
	1200	-.04	a	-.04	a	-.18	s	-.15	s
Hastelloy X	1000	nil	a	nil	a	+.002	a	+.008	a
	1100	-	a	+.010	a	+.015	a	+.024	a
	1200	-	a	-.010	a	-.05	a	-.04	ind.

nil = no change
ind = indeterminate (total consumption)
s = spalled oxidation product(s)
pa = partially adherent oxide(s)
a = adherent oxidation product(s)

Table XIX

Depletion Zone Thickness Measurements from Microscopic Observations after Isothermal Oxidation

Alloy wt/o	Temp °C	Original Thicknesses (mm)	Depletion Zone Thickness (mm)/side 5 hr	50 hr	200 hr	500 hr
Ni-21.75Cb-2.55 Al	1000	1.00-1.37	0.05	0.16	0.27	0.29-.32
	1100	1.10-1.37	0.05	0.18	0.30	0.41
	1200	1.00-1.37	0.19	0.34	ind.	ind.
Ni-19.5Cb-9.0 Cr-1.0Al	1000	1.32	-	-	-	0.11
	1100	1.34	-	-	-	0.16
	1200	1.34	-	-	-	ind.
Ni-19.7Cb-6.0 Cr-2.5Al	1000	1.27-1.30	0.02	0.03	0.06	0.095
	1100	1.30-1.32	0.03	0.05	0.08	0.13
	1200	1.30-1.40	0.05	0.07	0.25	0.345
Hastelloy X	1000	0.66-0.76	-	0.005	0.008	0.01
	1100	0.74-0.78	-	0.015	0.025	0.045
	1200	0.78-0.83	-	0.095	0.11	0.36

ind. = indeterminate due to total consumption

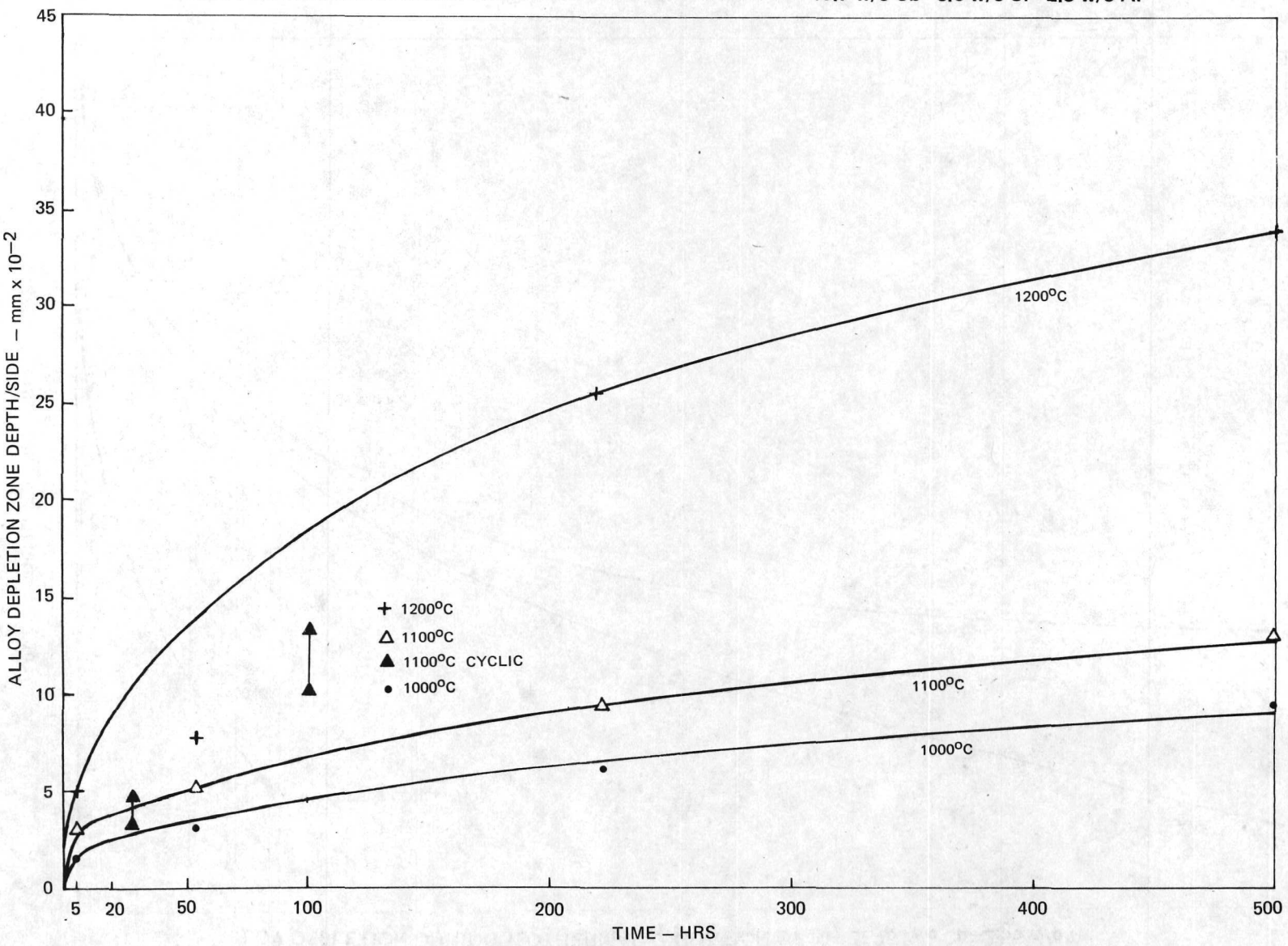
ALLOY DEPLETION DURING ISOTHERMAL OXIDATION OF Ni–19.7 w/o Cb–6.0 w/o Cr–2.5 w/o Al
ALLOY DEPLETION ZONE DEPTH/SIDE – mm x 10⁻²
TIME – HRS
0
5
10
15
20
25
30
35
40
45
5
20
50
100
200
300
400
500
+ 1200°C
△ 1100°C
▲ 1100°C CYCLIC
• 1000°C
1200°C
1100°C
1000°C

FIGURE 60

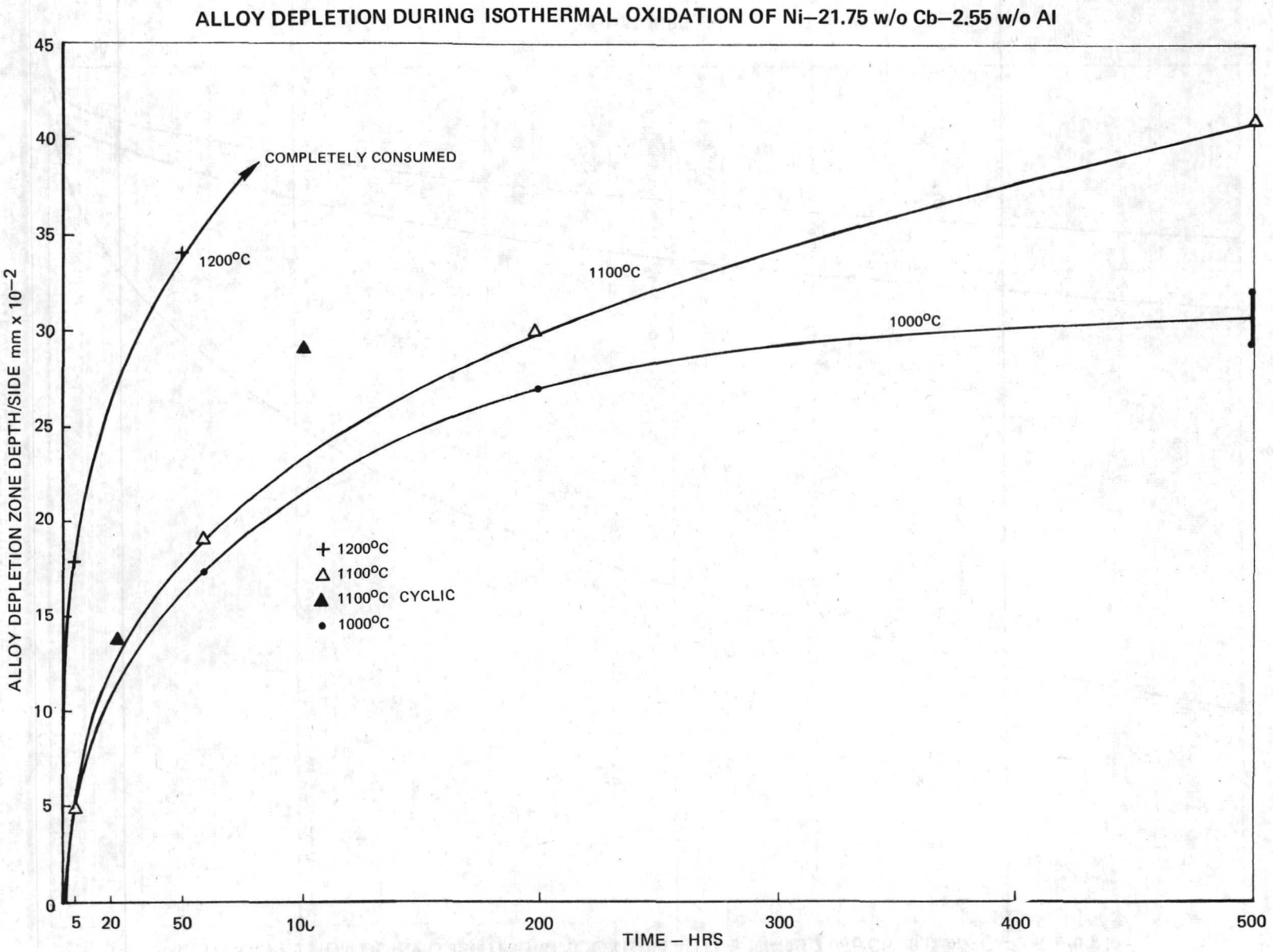
ALLOY DEPLETION DURING ISOTHERMAL OXIDATION OF Ni–21.75 w/o Cb–2.55 w/o Al
ALLOY DEPLETION ZONE DEPTH/SIDE mm x 10⁻²
45
40
35
30
25
20
15
10
5
0
COMPLETELY CONSUMED
1200°C
1100°C
1000°C
+ 1200°C
△ 1100°C
▲ 1100°C CYCLIC
• 1000°C
5
20
50
100
200
300
400
500
TIME – HRS

FIGURE 61

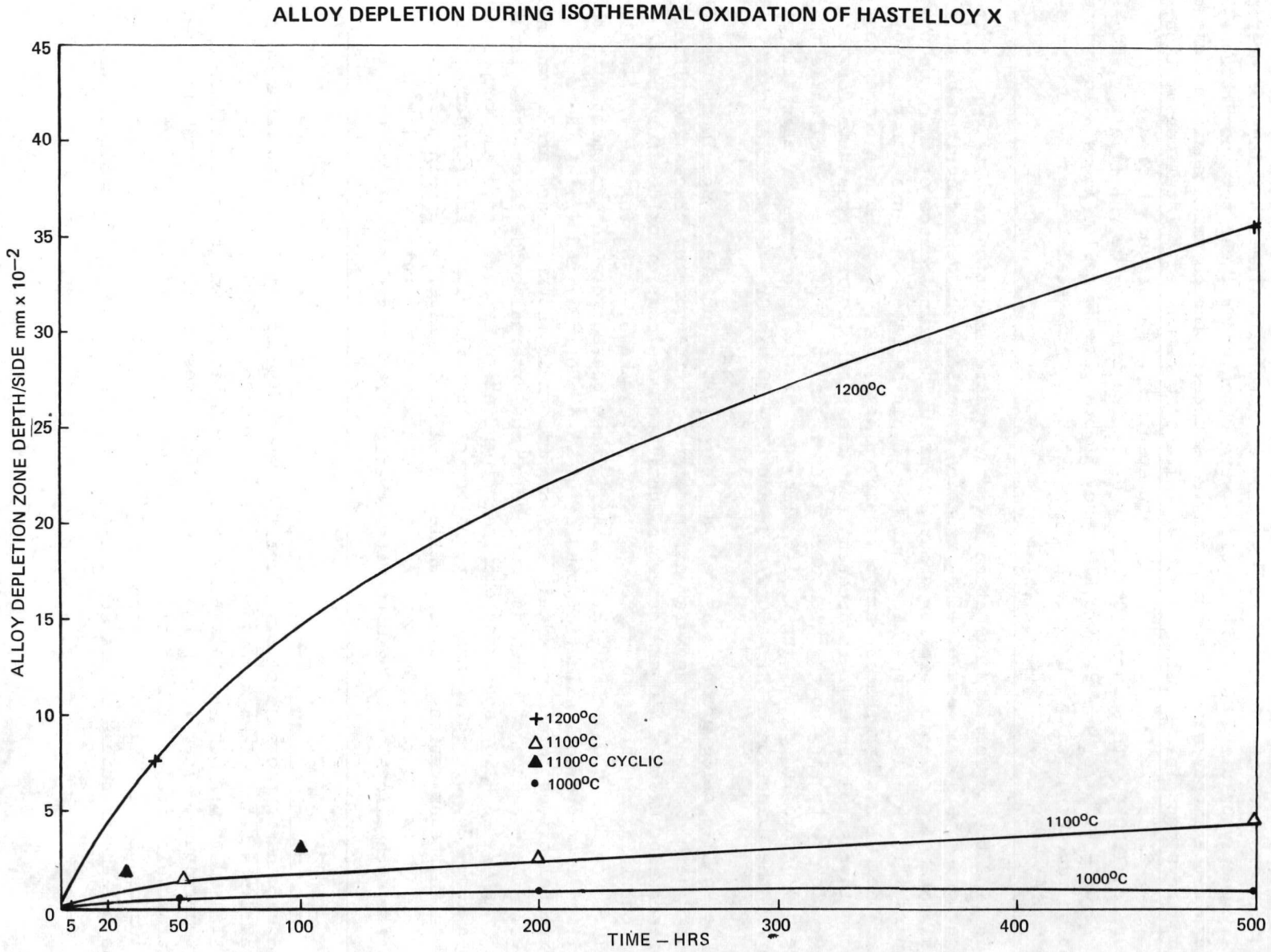
ALLOY DEPLETION DURING ISOTHERMAL OXIDATION OF HASTELLOY X
ALLOY DEPLETION ZONE DEPTH/SIDE mm x 10⁻²
45
40
35
30
25
20
15
10
5
0
5
20
50
100
200
300
400
500
TIME – HRS
+ 1200°C
△ 1100°C
▲ 1100°C CYCLIC
• 1000°C
1200°C
1100°C
1000°C

FIGURE 62

to which oxidation attack denuded the δ, Ni_3Cb lamellae from the homogeneous lamellar eutectic microstructure as shown in Fig. 63. No internal oxidation spikes or preferentially deeply oxidized δ, Ni_3Cb lamellae were noted under these test conditions. Once again the improvement in penetration resistance by the chromium addition to the γ/γ'-δ alloys containing nominally 2.5 w/o Al was quite marked. Total consumption of the Ni - 21.75 w/o Cb - 2.55 w/o Al test specimen was observed after a 200 hr exposure at 1200°C. In contrast the alloy depletion zone of the γ/γ'-δ alloy, Ni - 19.7 w/o Cb - 6.0 w/o Cr - 2.5 w/o Al, behaved more like Hastelloy X, an alloy whose oxidation is controlled by the growth of an external Cr_2O_3 scale which is more volatile than Al_2O_3 at 1200°C (Ref. 50).

To find the appropriate oxidation law, the static oxidation results were plotted on a cubic and parabolic scale. The oxidation kinetics were best described by an initial parabolic relationship for about 200 hrs. The significance of this conformance to a parabolic rate law is not clear but the resulting rate constants can be used to compare them with other phases common to superalloys (Ref. 50). Such a comparison is shown in Fig. 64 where it is apparent that the parabolic rate constants for the γ/γ'-δ alloy containing no chromium were greater than that of pure nickel while that of the 6 w/o chromium containing γ/γ'-δ alloy was of the same order of magnitude as those for the oxidation of Ni - 30 w/o Cr and Ni - 30 w/o Cr - 2 w/o Al alloys.

The spalled oxide products as well as the oxidized surface of specimens tested at 1100°C were examined using X-ray diffraction. Diffractometer traces identified the presence of $NiCbO_4$, NiO and other unidentified more complex oxides for the γ/γ'-δ alloy containing no chromium and $CbCrO_4$, NiO, Cr_2O_3 and α, Al_2O_3 for the γ/γ'-δ alloy, Ni - 19.7 w/o Cb - 6.0 w/o Cr - 2.5 w/o Al. These phases were in agreement with those identified from previous oxidation studies of γ'-δ (Ref. 51) and γ/γ'-δ (Ref. 52). The external oxides formed were generally nonuniform in thickness and are shown in Fig. 63. The presence of a denuded zone below the external oxide layer was typical of all the γ/γ'-δ alloy specimens examined depending on exposure time and temperature between 1000-1200°C. Sometimes the retention of the alloy lamellar microstructure was seen in the oxidation product. While the oxidation kinetics obtained for these γ/γ'-δ alloys are considered promising, the metal recession rates are still too great for such alloys to be used uncoated (Ref. 52).

3.5.2 Cyclic

Specimens of the same alloys identified above lapped with 600 grit paper were exposed for a total of 24 hrs in still air at 1100°C (2010°F). After every hour they were allowed to air cool to room temperature for typically one hour and returned to test temperature. They were weighed every four cycles and the change in weight per unit area which includes the spall weight is reported in Table XX and plotted as a function of time in Fig. 65. Discontinuities in the weight change curves are evident due to the uneven nature of the cracking and spalling of the oxide products which

REPRESENTATIVE SECTIONS OF $\gamma/\gamma'-\delta$ ALLOYS AFTER STATIC AND CYCLIC AIR EXPOSURES OF 1100°C

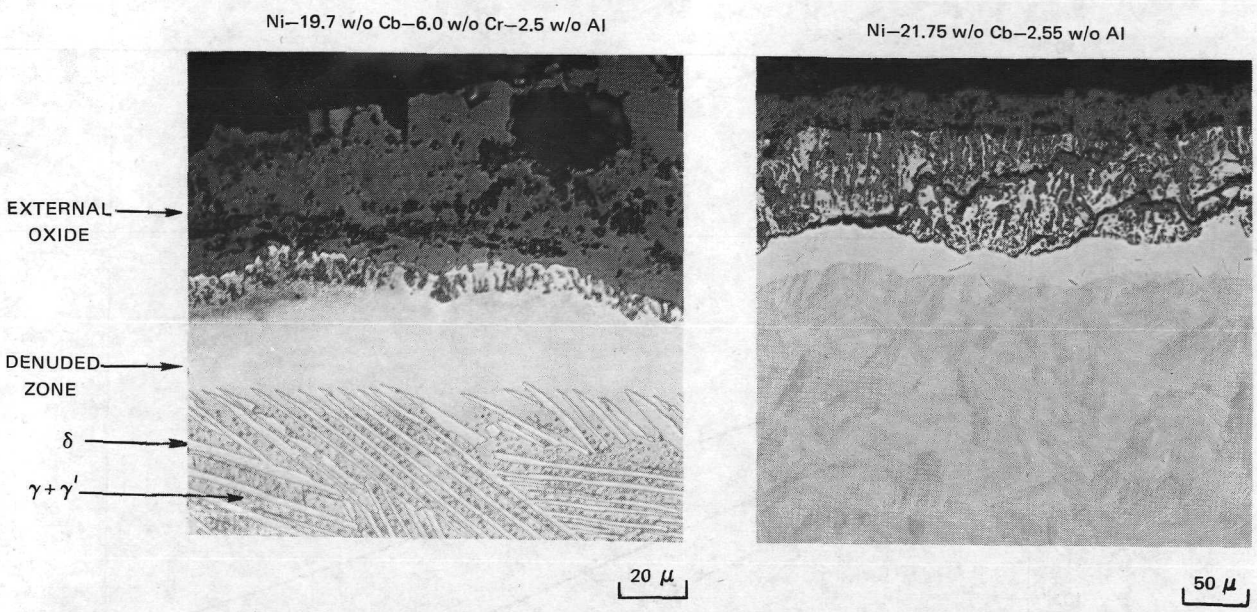

a) POST 100 CYCLIC EXPOSURES OF 1 HR

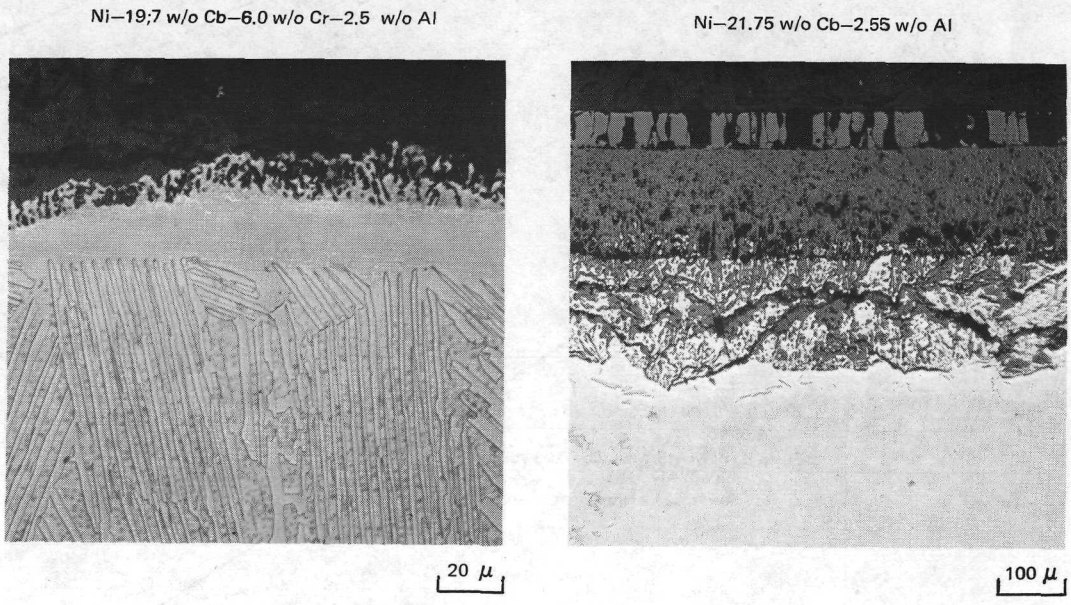

b) POST 200 HOURS ISOTHERMAL EXPOSURE

FIGURE 63

TEMPERATURE DEPENDENCE OF THE PARABOLIC RATE CONSTANTS FOR $\gamma/\gamma' - \delta$ ALLOYS, HASTELLOY X, AND VARIOUS Ni ALLOYS (0 - 200 hrs)

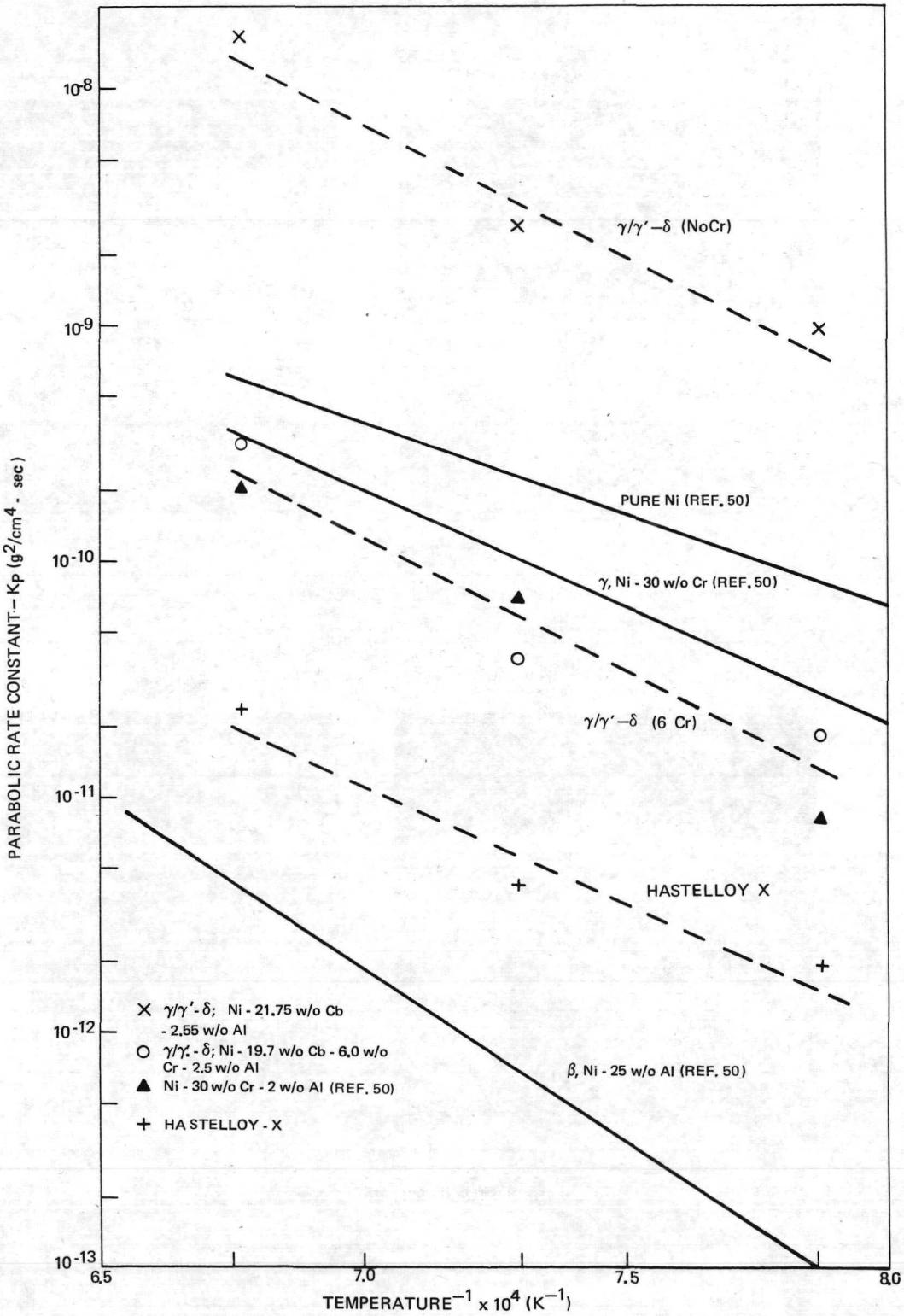

FIGURE 64

Table XX

Weight Gain (Including Spall) After Twenty-four One Hour Exposures at 1100°C (2010°F)

Time	Ni-21.75w/oCb-2.55w/oAl (A72-807)	Ni-19.5w/oCb-9.0w/oCr-1.0 w/oAl (A72-559)	Ni-19.7w/oCb-6.0w/oCr-2.5 w/oAl (A72-599)	Hasteloy X
4 hr	6.88 mg/cm^2	3.19 mg/cm^2	1.56 mg/cm^2	0.69 mg/cm^2
8	10.15	3.58	1.99	0.73
12	12.37	3.92	2.27	0.71
16	14.58	4.39	2.64	0.66
20	17.84	6.26	3.77	1.06
24	19.57	6.47	3.97	0.68

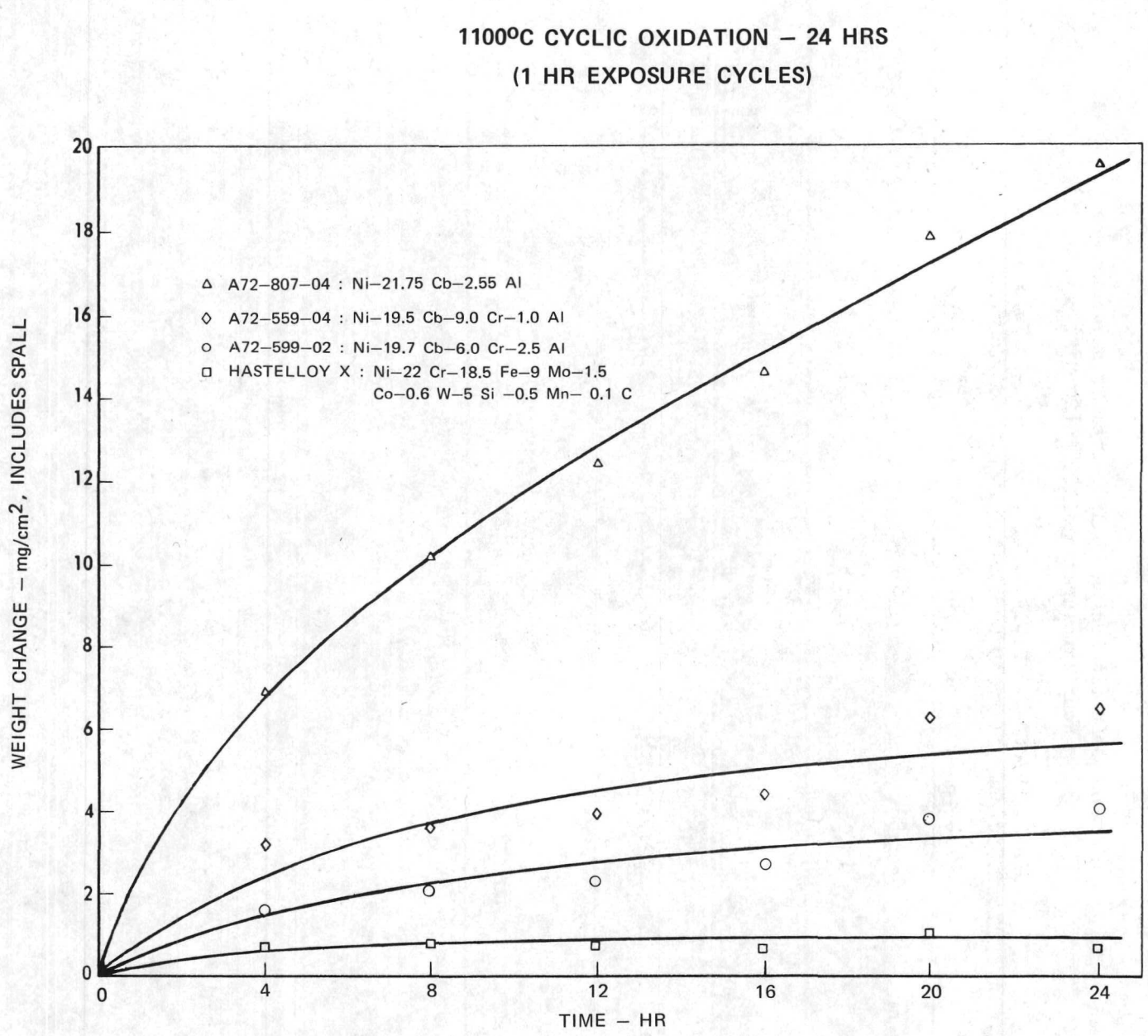
1100°C CYCLIC OXIDATION – 24 HRS
(1 HR EXPOSURE CYCLES)
WEIGHT CHANGE – mg/cm², INCLUDES SPALL
TIME – HR
△ A72–807–04 : Ni–21.75 Cb–2.55 Al
◇ A72–559–04 : Ni–19.5 Cb–9.0 Cr–1.0 Al
○ A72–599–02 : Ni–19.7 Cb–6.0 Cr–2.5 Al
□ HASTELLOY X : Ni–22 Cr–18.5 Fe–9 Mo–1.5
Co–0.6 W–5 Si –0.5 Mn– 0.1 C
0
2
4
6
8
10
12
14
16
18
20
0
4
8
12
16
20
24

FIGURE 65

occurred on cooling. A similar series of experiments were repeated on additional specimens of the same alloys with an increase in total exposure time to 100 hrs. After every hour these specimens were allowed to air cool to room temperature in approximately one hour and returned to test temperature. In this case they were weighed every 10 cycles and the change in weight per unit area was computed which included the spall weight (Table XXI) and is plotted as a function of time in Fig. 66. The trend in the accelerated oxidation attack with cyclic spalling for the γ/γ'-δ alloys indicates the desirability of further compositional modification and quinary additions to achieve a more adherent oxide scale and the development of a coating system. Microscopic observations of the total thickness changes (both sides) and the alloy depletion zone thickness (depth per side) were made on polished and etched cross sections of each sample tested. These measurements are recorded in Table XXII. Measurements of alloy depletion during cyclic oxidation are further shown in Figs. 60-62 and are compared with measurements during isothermal oxidation, indicating the degree of accelerated oxidation associated with scale removal on cycling.

As the weight of each alloy specimen plus the oxide product was continuously weighed in covered Al_2O_3 crucibles, no cyclic data was obtained from separate measurements of the specimen weight change alone. As it was deemed desirable to compare Hastelloy X with Ni - 19.7 w/o Cb - 6.0 w/o Cr - 2.5 w/o Al in such a manner, these tests were independently performed (Refs. 52,53). The results of 100 hrs of cyclic exposures at 1000°C are presented in Fig. 67. The γ/γ'-δ specimens were weighed after every four hours of exposure and the solid and unfilled circular symbols in Fig. 67 represent separate measurements. The deleterious effect of the spalling oxide scale is not as prevalent at 1000°C for the γ/γ'-δ alloy as was observed at more elevated temperatures.

3.5.3 Sulfidation

Finally, the results of a burner rig vane cyclic sulfidation test on an uncoated γ/γ'-δ alloy (Ni - 20.2 w/o Cb - 9.1 w/o Cr - 1.0 w/o Al) together with various other uncoated nickel-base superalloys are shown in Fig. 68. The specimens in this test were held in cycles of 954°C (1750°F) for three minutes followed by heating to 1121°C (2050°F) for two minutes and cooling to 315°C (600°F) while rotating in a Mach 0.3 jet burner using JP-5R fuel containing 3.5 ppm synthetic sea salt. The subsequent microstructural examination for alloy depletion indicated that this γ/γ'-δ alloy ranked with the best nickel-base superalloys in resistance to hot corrosion.

Of additional interest was the fact that a tensile specimen, ground from this erosion bar such that the area of greatest erosion was within the gage, indicated no decrease in strength measured at 1093°C after 219.5 hrs of cyclic thermal exposure.

Table XXI

Specific Weight Gain (Including Spall) of Various γ/γ'-δ Alloys After 1 Hr Cyclic Exposures at 1100°C (2010°F) Measured Every 10 Hrs

Time (hr)	Ni-21.75w/oCb-2.55w/oAl (A72-807)	Ni-19.5w/oCb-9.0w/oCr-1.0w/oAl (A72-559)	Ni-19.7w/oCb-6.0w/oCr-2.5w/oAl (A72-599)	Hastelloy X
10	11.02 mg/cm^2	3.63 mg/cm^2	1.80 mg/cm^2	0.58 mg/cm^2
20	17.57	5.78	3.30	0.98
30	23.18	10.06	4.99	1.19
40	28.27	16.28	7.56	1.27
50	33.54	22.24	10.99	1.52
60	39.04	29.15	15.19	1.62
70	44.37	34.67	19.51	1.61
80	49.46	40.52	23.90	1.81
90	54.32	46.05	28.41	1.99
100	59.16	52.08	34.17	2.14

1100°C CYCLIC OXIDATION – 100 HRS

(1 HR EXPOSURE CYCLES)

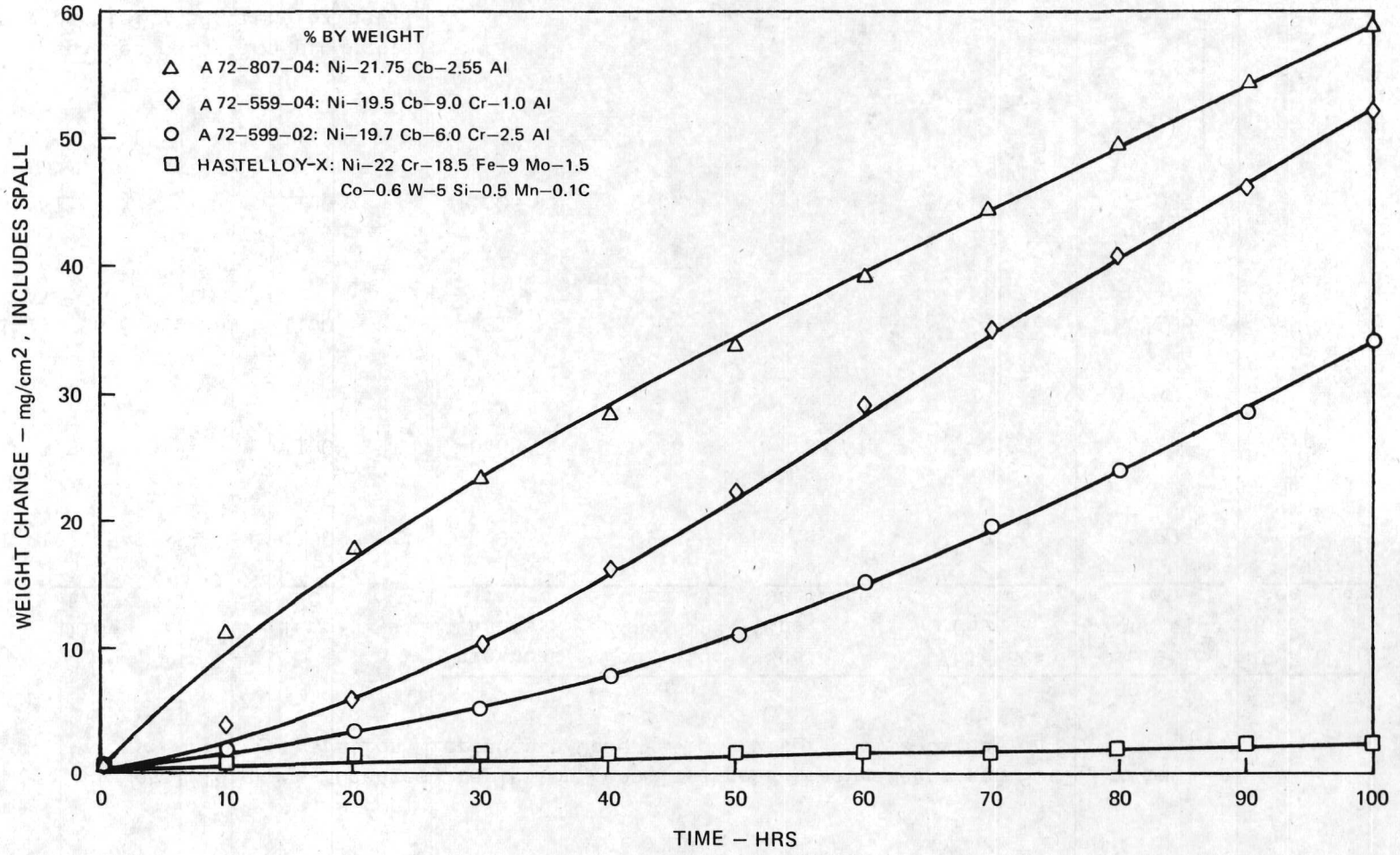

FIGURE 66

Table XXII

Total Thickness Changes, Depletion Zone Thickness Measurements and Scale/Oxide Penetration Microscopic Observations after Cyclic Oxidation

Alloy wt/o	Temp °C	24 hrs			100 hrs		
		Thickness Change mm	Depletion Zone/side mm	Scale Obs. see code	Thickness Change mm	Depletion Zone/side mm	Scale Obs. see code
Ni-21.75Cb-2.55Al	1100	-0.06	0.135	s	-0.36	0.295	s
Ni-19.5Cb-9.0Cr-1.0Al	1100	-0.05	0.06	a	-0.33	0.19	s/pa
Ni-19.7Cb-6.0Cr-2.5Al	1100	-.01	0.035	a	-.03 to -.11	0.105	s/pa
Hastelloy X	1100	+.005	0.02	a	+.015	0.025	a

s = spalled oxidation product(s)
pa = partially adherent oxide(s)
a = adherent oxidation products

CYCLICAL OXIDATION BEHAVIOR OF Ni–19.7 wt/o Cb–6.0 wt/o Cr–2.5 wt/o Al ($\gamma/\gamma'-\delta$) AND HASTELLOY X AT 1000°C

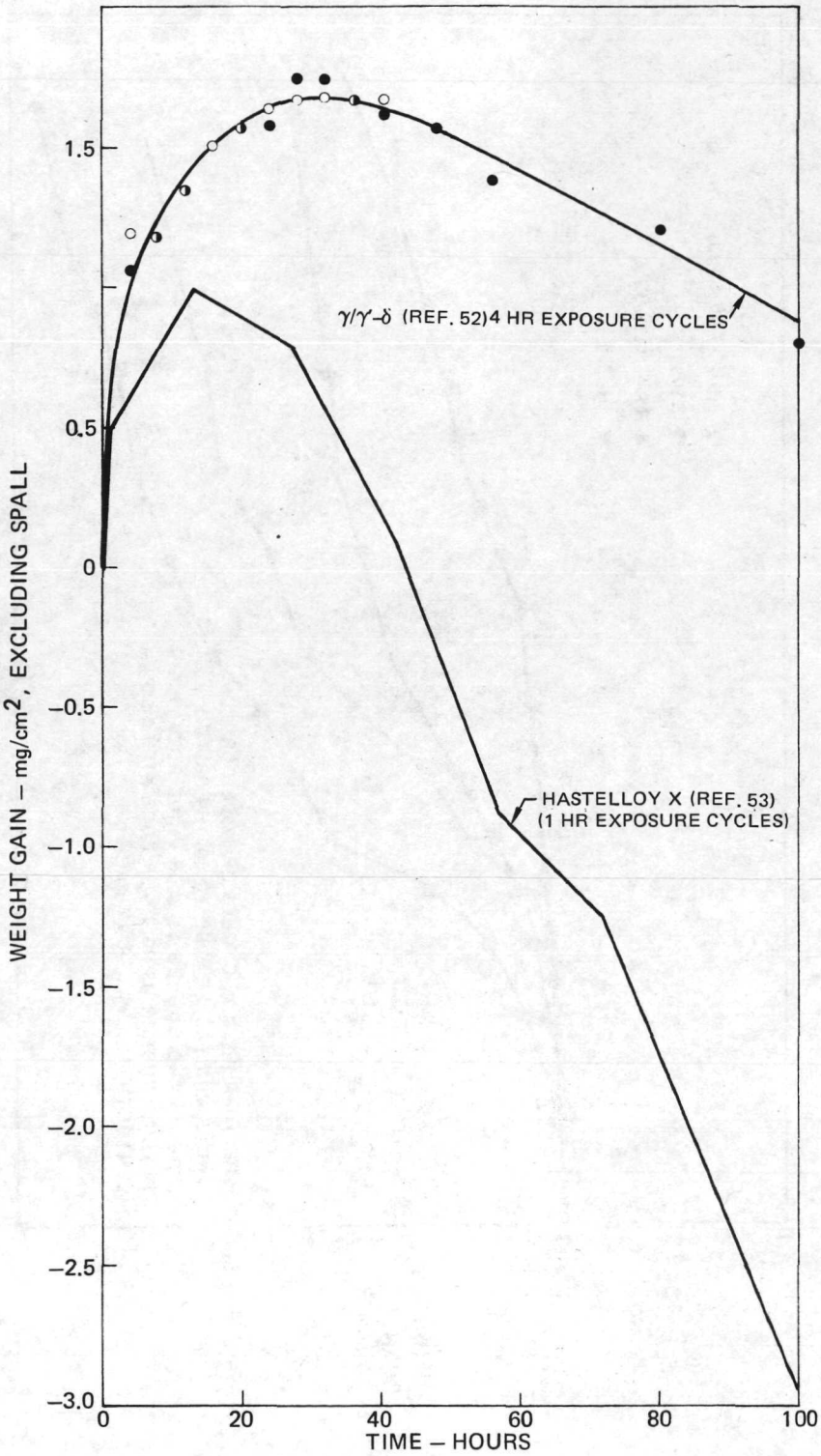

FIGURE 67

CYCLIC SULFIDATION–EROSION TEST*

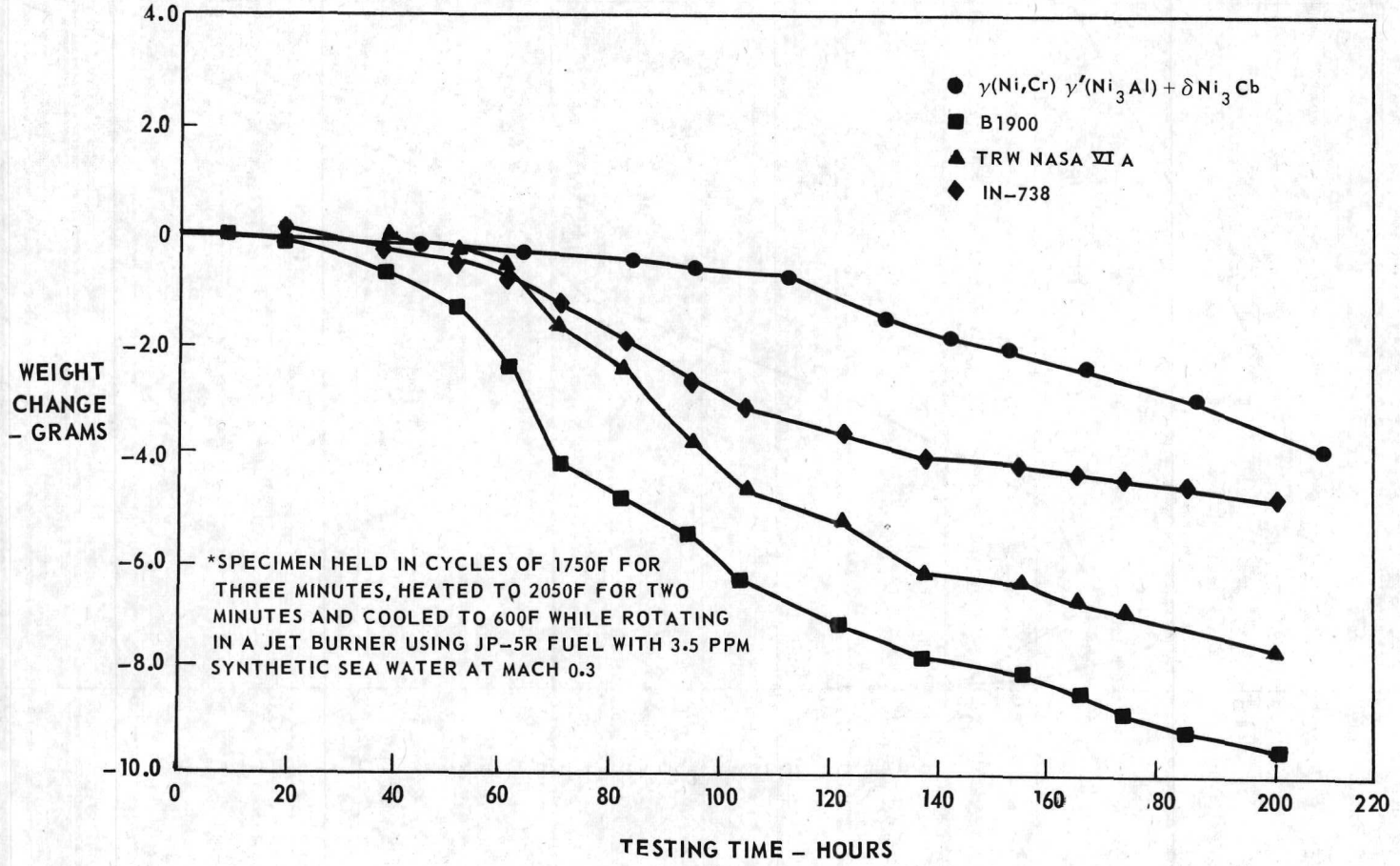

FIGURE 68

IV. CONCLUSIONS

1. Bivariant eutectic alloys located on the γ-δ liquidus surface within the Ni-Cb-Cr-Al quaternary were identified which permitted the production of lamellar microstructures aligned in the direction of growth. This liquidus surface was found to be bounded in the pertinent ternary systems by two monovariant eutectic troughs. In the Ni-Cr-Cb system, this trough extended between the binary eutectic Ni-Ni_3Cb and the ternary eutectic Ni-$NbCr_2$-Ni_3Cb, and in the Ni-Al-Cb system extended between the binary eutectic Ni-Ni_3Cb and the ternary eutectic Ni-Ni_3Al-Ni_3Cb.

2. Tensile strengths in excess of 210 MN/m^2 (30,000 psi) were measured for two γ/γ'-δ alloys (Ni - 19.7 w/o Cb - 6.0 w/o Cr - 2.5 w/o Al) and (Ni - 21.75 w/o Cb - 2.55 w/o Al) at 1235°C (2255°F) which exceeds the contract goal of 120 MN/m^2.

3. The densities of all the γ/γ'-δ alloys investigated, i.e. 8.5-8.7 g/cm^3 were within the contract goal of less than 9.0 g/cm^3.

4. The rupture strength of two γ/γ'-δ alloys defined above, substantially exceeded those of advanced nickel superalloys, e.g. NASA-TRW VIA and D.S. Mar M200, at all temperatures tested above 700°C.

5. The ductility of one γ/γ'-δ alloy, Ni - 19.7 w/o Cb - 6.0 w/o Cr - 2.5 w/o Al, as measured by elongation and reduction in area in tensile tests, met or exceeded 5 percent over the entire temperature interval from room to 1235°C. The second γ/γ'-δ alloy although displaying lower room temperature tensile ductility exhibited 9.85 ft-lbs impact energy, measured on a subsize Charpy V-notched specimen. This degree of toughness greatly exceeds that of all cast nickel superalloys.

6. Phase stability and resistance to thermal fatigue cracking and delamination after 3000 thermal exposures between 400°C min/1120°C max in 2.1 minute cycles was observed for the two γ/γ'-δ alloys. Phase stability after prolonged (1500 hr) exposure at 850°C and exposures in excess of 100 hrs under stress at 1200°C was exhibited.

7. An inherent resistance to oxidation and high temperature hot corrosion was exhibited for the γ/γ'-δ alloy, Ni - 19.7 w/o Cb - 6.0 w/o Cr - 2.5 w/o Al. Although a coating for this alloy was recommended for its use above 900°C.

8. The structural and chemical homogeneity of both γ/γ'-δ alloys, Ni - 19.7 w/o Cb - 6.0 w/o Cr - 2.5 w/o Al, and Ni - 21.75 w/o Cb - 2.55 w/o Al, directionally solidified at 3 and 38 cm/hr respectively in a high thermal gradient were found to be remarkably uniform along their 15 cm length for bars nominally 1.2 cm in diameter. This observation suggests that biphase lamellar growth in the presence of a boundary layer is being accomplished under a minimum of convection.

9. The Ni_3Cb phase of the γ/γ'-δ alloys plastically deformed by twinning on the {211} planes and slip on the (010) plane when a tensile stress was applied parallel to the $[100]_\delta$ over the temperature range 20 to ~1000°C. Above ~1100°C other twin planes were operable and broader twins were observed.

10. A great insensitivity of composite microstructure to growth rate and temperature gradient was exhibited for γ/γ'-δ alloys whose compositions resided on the Ni,Al-Ni_3Cb monovariant eutectic trough. A critical G/R ratio of $<5°C\ hr\ cm^{-2}$ was determined for the establishment of plane front coupled growth.

11. It was demonstrated that significant advances in obtaining a favorable combination of properties useful for gas turbine applications can be made by strengthening a gamma nickel chromium matrix hardened by gamma prime precipitates with an aligned lamellar Ni_3Cb phase.

V. ALLOY RECOMMENDATIONS FOR FURTHER EVALUATION

Even though there have been and continue to be concentrated research and developmental programs on other, more refractory materials, nickel-base alloys must still be considered as the dominant materials for present and near-term high temperature, load carrying applications such as those experienced in gas turbine engines. Toward this end, the new γ/γ'-δ family of directionally solidified eutectic superalloys may permit a 100-200°F increase in allowable metal temperature above current superalloys. One of these alloys, Ni - 19.7 w/o Cb - 6.0 w/o Cr - 2.5 w/o Al, was found to be superior to all advanced nickel-base superalloys in tension and creep. Although the longitudinal mechanical properties of this alloy are outstanding, further improvements in creep and shear strength together with gains in oxidation resistance are envisioned by optimization of quinary additions. These modifications, which would particularly benefit the projected utilization of this material in the gas turbine, form the basis of a recommended, further investigation. An evaluation of the effect of heat treatment and processing parameters on mechanical properties is also strongly recommended.

VI. REFERENCES

1. E. R. Thompson and F. D. Lemkey, "Structure and Properties of Ni_3Al (γ') Eutectic Alloys Produced by Unidirectional Solidification", ASM Trans. Quarterly 62, 1969, pp. 140-55.

2. E. R. Thompson, F. D. George, and E. H. Kraft, "Investigation to Develop a High Strength Eutectic Alloy with Controlled Microstructure", Final report on U.S. Navy contract N00019-70-C-0052, United Aircraft Res. Lab., July 1970.

3. E. R. Thompson, E. H. Kraft, and F. D. George, "Investigation to Develop a High Strength Eutectic for Aircraft Engine Use", Final report on U.S. Navy contract N00019-71-C-0096, United Aircraft Res. Lab., July 1971.

4. E. H. Kraft and E. R. Thompson, "High Temperature Eutectic Composite and Its Modification", Final report on U.S. Navy contract N00019-72-C-0192, United Aircraft Res. Lab., Nov. 1972.

5. F. D. Lemkey and E. R. Thompson, "Nickel and Cobalt Eutectic Alloys Reinforced by Refractory Metal Carbides", Met. Trans., 2, 1971, pp. 1537-44.

6. H. Bibring, G. Seibel, and M. Rabinovitch, "Nouveaux développements dans l'étude des superalliages a fibres obtenus par solidification dirigée", Mémoires Scientifiques Rev. Métallurg., LXIX, 5, 1972, p. 341.

7. M. G. Benz, et al, "Exploratory Development for Synthesis and Evaluation of Directionally Solidified Composites for High Temperature Application", Interim Technical Reports to Air Force Materials Laboratory from General Electric Co., Sept. 1972 and Dec. 1972.

8. E. R. Thompson and F. D. Lemkey, "Unidirectional Solidification of Cobalt Chromium-Carbon Monovariant Eutectic Alloys", Met. Trans., 1, 1970, p. 2799.

9. E. R. Thompson, D. A. Koss, and J. C. Chesnutt, "Mechanical Behavior of a Carbide Reinforced Cobalt-Chromium Eutectic Alloy", Met. Trans., 1, 1970, p. 2807.

10. P. R. Sahm and M. Lorenz, "Strongly Coupled Growth in Faceted-Nonfaceted Eutectics of the Monovariant Type", J. of Mat. Sci., 7, 1972, p. 793.

11. F. L. VerSnyder and M. E. Shank, "The Development of Columnar Grain and Single Crystal High Temperature Materials Through Directional Solidification", Mat. Sci. and Engr., 6, 1970, p. 213.

12. M. Gell, C. P. Sullivan, and F. L. VerSnyder, "Casting and Properties of Unidirectionally Solidified Superalloys", Solidification Technology, Syracuse University Press, 1973.

13. J. W. Weeton, "Design Concepts for Fiber-Metal Matrix Composites for Advanced Gas Turbine Blades", ASME Paper No. 70-GT-133, 1970.

14. M. J. Noone, "Development of Composite Materials for High Temperature Applications", Final report on U.S. Navy contract N00019-69-C-0310, General Electric Space Sciences Lab., June 1970.

15. J. Brennan, United Aircraft Research Laboratories, Private Communication.

16. F. D. Lemkey and E. R. Thompson, "Directionally Solidified Eutectic Type Alloys with Aligned Delta Phase", U.S. Patent Pending.

17. E. R. Thompson, F. D. George, and E. M. Breinan, "The Influence of Interlamellar Spacing on the Strength of the Ni_3Al-Ni_3Cb Eutectic", Proceedings of the Conference on In Situ Composites, Lakeville, Connecticut, Sept. 1972. Printing and Publishing Office, National Academy of Sciences, Washington, D.C.

18. E. E. Brull and G. S. Golden, "X-ray Emission Spectrographic Analysis of Iron, Nickel and Cobalt Base Alloy", Rep. UARL-L158, United Aircraft Res. Lab., Sept. 1972.

19. Annual ASTM Standards, American Society for Testing and Materials, Philadelphia, Pa., 1970.

20. E. R. Thompson and F. D. George, "Investigation of the Structure and Properties of the Ni_3Al-Ni_3Cb Eutectic Alloy", Final report on U.S. Navy contract N00019-69-C-0162, United Aircraft Res. Lab., July 1969.

21. W. R. Hoover and R. W. Hertzberg, "The Mechanical Response of the Ni-Ni_3Nb Eutectic Composite: Part I. Monotonic Behavior", Met. Trans., 2, 1971, p. 1283.

22. P. Annarumma and M. Turpin, "Structure and High Temperature Mechanical Behavior of Ni-Ni_3Cb Unidirectional Eutectic", Met. Trans., 3, 1972, p. 137.

23. F. Tamás and I. Pál, "Phase Equilibria Spatial Diagrams", Iliffe, Butterworths, London, 1970.

24. J. Cisse and R. G. Davies, "Nickel-Rich Portion of the Ni-Al-Cb Phase Diagram", Met. Trans., 1, 1970, p. 2003.

25. W. E. Quist, R. Taggart and D. H. Polonis, "The Influence of Iron and Aluminum on the Precipitation of Metastable Ni_3Cb Phases in Ni-Cb Systems", Met. Trans., 2, 1971, p. 825.

26. M. Hansen and K. Anderko, "Constitution of Binary Alloys", McGraw-Hill Book Co., 1958, p. 1011.

27. F. Shunk, "Constitution of Binary Alloys, 2nd Supplement", McGraw-Hill Book Co., 1969, p. 192.

28. R. Henricks and M. Gell, PWA, East Hartford, Conn., Private Communication.

29. W. G. Pfann, "Zone Melting", Wiley, New York, 1958.

30. Z. M. Rogachevskaya, "Structural Diagrams of Metallic Systems", Vol. 8, Moscow, 1962, p. 211.

31. J. Cisse and R. G. Davies, "Nickel Rich Portion of the Ni-Al-Nb Phase Diagram", Met. Trans., 1, 1970, p. 2003.

32. F. R. Mollard and M. C. Flemings, "Growth of Composites from the Melt - Part II", Trans. TMS AIME, 239, 1967, p. 1534.

33. R. M. Jordan and J. D. Hunt, "The Growth of Lamellar Eutectic Structures in Pb-Sn and Al-$CuAl_2$ Systems", Met. Trans., 2, 1971, p. 3401.

34. K. G. Davis and P. Fryzuk, "Growth of Off-Eutectic Composites by Zone Melting", Canadian Metallurgical Quarterly, 10, 1971, p. 273.

35. K. A. Jackson, "The Dendrite-Eutectic Transition in Sn-Pb Alloys", Trans. Met. Soc. AIME, 242, 1968, p. 1275.

36. K. A. Jackson and J. D. Hunt, "Lamellar and Rod Eutectic Growth", Trans. TMS AIME, 236, 1966, p. 1129.

37. R. T. Quinn, R. W. Kraft, and R. W. Hertzberg, "Structure and Elevated Temperature Mechanical Behavior of Unidirectionally Solidified Ni-Ni_3Cb", Trans. ASM, 62, 1969, p. 38.

38. L. M. Hogan, R. W. Kraft, and F. D. Lemkey, "Eutectic Grains", Advances in Materials Research, Vol. 5, John Wiley & Sons, 1971.

39. H. E. Collins, "Development of High Temperature Nickel-Base Alloys for Jet Engine Turbine Bucket Application", NASA CR 54507, June 1967.

40. B. J. Piearcy and F. L. VerSnyder, "A New Development in Gas Turbine Materials - The Properties and Characteristics of PWA 664", PWA Report No. 65-007, 1965.

41. R. P. Gangloff and R. W. Hertzberg, "Elevated Temperature Tensile and Creep Rupture Behavior of the Unidirectionally Solidified Ni-Ni_3Cb Eutectic Composite", Proceedings of Conference on In Situ Composites, Dept. 1972, National Academy of Science and Engineering Report, 1973.

42. F. D. Lemkey and E. R. Thompson, "Eutectic Superalloys Strengthened by δ, Ni_3Cb Lamellae and γ', Ni_3Al Precipitates", Proceedings of the Conference on In Situ Composites, Sept. 1972, National Academy of Science and Engineering Report, 1973.

43. Y. G. Nakagawa and G. C. Weatherly, "The Nature of the Interface Between Two Ordered Lattices - the Ni_3Al-Ni_3Cb Eutectic", Mater. Sci. Eng., 10, 1972, p. 223.

44. F. D. Lemkey, B. J. Bayles, and M. J. Salkind, "Research Investigation of Phase Reinforced High Temperature Alloys Produced Directly from the Melt", Rep. UACRL D910261-4, United Aircraft Res. Lab., July 1965.

45. C. Grossiard, G. Lesoult, and M. Turpin, "Slip and Mechanical Twinning in Ni-Ni_3Cb Directionally Solidified Eutectic Alloy", Proceedings of the International Materials Symposium, Univ. of California, Berkeley, 1971.

46. R. E. Reed Hill, "A Rapid Graphical Single Surface Orientation Technique for Face-Centered Metals", Trans. Met. Soc. AIME, 236, 1966, p. 1283.

47. E. M. Breinan, E. R. Thompson, and F. D. Lemkey, "The Effect of Thermal Cycling on High Temperature Eutectic Composites", Proceedings of the Conference on In Situ Composites, Lakeville, Conn., Sept. 1972, National Academy of Sciences Printing Office, Washington, D.C.

48. F. D. Lemkey, "Coupled Growth and Stability of Aligned Multicomponent Alloys Designed for Gas Turbine Application", Paper presented at AIME Spring Meeting, May 1973.

49. Hervé Bibring, "Mechanical Behavior of Unidirectionally Solidified Composites", Proceedings of the Conference on In Situ Composites, Lakeville, Conn., Sept. 1972, National Academy of Sciences Printing Office, Washington, D.C.

50. G. S. Giggins and F. S. Pettit, "Oxidation of Ni-Cr-Al Alloys Between 1000 and 1200° C", J. Electrochem. Soc., Nov. 1971, p. 1782.

51. M. P. Arbuzov and V. G. Chuprina, "Oxidation of Ni_3Al-Ni_3Nb Alloys", Izvestiya VUZ. Fizika, 12, 1969, p. 75.

52. E. J. Felten, PWA, Middletown, Conn., Private communication.

53. C. A. Barrett, NASA Lewis Research Center, Cleveland, Ohio, Private communication.

*U.S. GOVERNMENT PRINTING OFFICE: 1973-739-154/56

NATIONAL AERONAUTICS AND SPACE ADMINISTRATION
WASHINGTON, D.C. 20546

OFFICIAL BUSINESS
PENALTY FOR PRIVATE USE $300

SPECIAL FOURTH-CLASS RATE BOOK

POSTAGE AND FEES PAID
NATIONAL AERONAUTICS AND SPACE ADMINISTRATION
451

U.S.MAIL

POSTMASTER : If Undeliverable (Section 158 Postal Manual) Do Not Return

"The aeronautical and space activities of the United States shall be conducted so as to contribute . . . to the expansion of human knowledge of phenomena in the atmosphere and space. The Administration shall provide for the widest practicable and appropriate dissemination of information concerning its activities and the results thereof."

—NATIONAL AERONAUTICS AND SPACE ACT OF 1958

NASA SCIENTIFIC AND TECHNICAL PUBLICATIONS

TECHNICAL REPORTS: Scientific and technical information considered important, complete, and a lasting contribution to existing knowledge.

TECHNICAL NOTES: Information less broad in scope but nevertheless of importance as a contribution to existing knowledge.

TECHNICAL MEMORANDUMS: Information receiving limited distribution because of preliminary data, security classification, or other reasons. Also includes conference proceedings with either limited or unlimited distribution.

CONTRACTOR REPORTS: Scientific and technical information generated under a NASA contract or grant and considered an important contribution to existing knowledge.

TECHNICAL TRANSLATIONS: Information published in a foreign language considered to merit NASA distribution in English.

SPECIAL PUBLICATIONS: Information derived from or of value to NASA activities. Publications include final reports of major projects, monographs, data compilations, handbooks, sourcebooks, and special bibliographies.

TECHNOLOGY UTILIZATION PUBLICATIONS: Information on technology used by NASA that may be of particular interest in commercial and other non-aerospace applications. Publications include Tech Briefs, Technology Utilization Reports and Technology Surveys.

Details on the availability of these publications may be obtained from:

SCIENTIFIC AND TECHNICAL INFORMATION OFFICE

NATIONAL AERONAUTICS AND SPACE ADMINISTRATION

Washington, D.C. 20546